2014

A Novel Synergistic Model Fusing Electroencephalography and Functional Magnetic Resonance Imaging for Modeling Brain Activities

Konstantinos Michalopoulos
Wright State University

A NOVEL SYNERGISTIC MODEL FUSING ELECTROENCEPHALOGRAPHY AND FUNCTIONAL MAGNETIC RESONANCE IMAGING FOR MODELING BRAIN ACTIVITIES.

A dissertation submitted in partial fulfillment
of the requirements for the degree of
Doctor of Philosophy

By

KONSTANTINOS MICHALOPOULOS
MSc, Technical University of Crete

2014

Wright State University

WRIGHT STATE UNIVERSITY

GRADUATE SCHOOL

August 15, 2014

I HEREBY RECOMMEND THAT THE DISSERTATION PREPARED UNDER MY SUPERVISION BY Konstantinos Michalopoulos ENTITLED A Novel Synergistic Model fusing Electroencephalography and Functional Magnetic Resonance Imaging for Modeling Brain Activities BE ACCEPTED IN PARTIAL FULFILLMENT OF THE REQUIREMENTS FOR THE DEGREE OF Doctor of Philosophy

Nikolaos G. Bourbakis, Ph.D.
Dissertation Director

Arthur Goshtasby, Ph.D.
Director, Computer Science & Engineering Ph.D. Program

Robert E. W. Fyffe, Ph.D.
Vice President for Research and
Dean of the Graduate School

Committee on
Final Examination

Nikolaos Bourbakis, Ph.D.

Soon M. Chung, Ph.D.

Yong Pei, Ph.D.

Larry Lawhorne, M.D.

Michalis Zervakis, Ph.D.

ABSTRACT

Michalopoulos Konstantinos, Ph.D, Department of Computer Science and Engineering, Wright State University, 2014.

A novel Synergistic Model fusing Electroencephalography and functional Magnetic Resonance Imaging for Modeling Brain Activities.

Study of the human brain is an important and very active area of research. Unraveling the way the human brain works would allow us to better understand, predict and prevent brain related diseases that affect a significant part of the population. Studying the brain response to certain input stimuli can help us determine the involved brain areas and understand the mechanisms that characterize behavioral and psychological traits.

In this research work two methods used for the monitoring of brain activities, Electroencephalography (EEG) and functional Magnetic Resonance (fMRI) have been studied for their fusion, in an attempt to bridge together the advantages of each one. In particular, this work has focused in the analysis of a specific type of EEG and fMRI recordings that are related to certain events and capture the brain response under specific experimental conditions.

Using spatial features of the EEG we can describe the temporal evolution of the electrical field recorded in the scalp of the head. This work introduces the use of Hidden Markov Models (HMM)

for modeling the EEG dynamics. This novel approach is applied for the discrimination of normal and progressive Mild Cognitive Impairment patients with significant results.

EEG alone is not able to provide the spatial localization needed to uncover and understand the neural mechanisms and processes of the human brain. Functional Magnetic Resonance imaging (fMRI) provides the means of localizing functional activity, without though, providing the timing details of these activations. Although, at first glance it is apparent that the strengths of these two modalities, EEG and fMRI, complement each other, the fusion of information provided from each one is a challenging task. A novel methodology for fusing EEG spatiotemporal features and fMRI features, based on Canonical Partial Least Squares (CPLS) is presented in this work. A HMM modeling approach is used in order to derive a novel feature-based representation of the EEG signal that characterizes the topographic information of the EEG. We use the HMM model in order to project the EEG data in the Fisher score space and use the Fisher score to describe the dynamics of the EEG topography sequence. The correspondence between this new feature and the fMRI is studied using CPLS. This methodology is applied for extracting features for the classification of a visual task. The results indicate that the proposed methodology is able to capture task related activations that can be used for the classification of mental tasks. Extensions on the proposed models are examined along with future research directions and applications.

TABLE OF CONTENTS

List of Tables

List of Figures

ACKNOWLEDGEMENT

I would like to thank my advisor Dr. Nikolaos Bourbakis for giving me the opportunity to work on this exciting topic. His mentorship and directions helped me to overcome any obstacles and complete this dissertation. His guidance and continuous support were invaluable and greatly appreciated. I want to thank Dr. Zervakis for all the years of collaboration and work and his continuing support and help over the years. My gratitude goes to Dr. Deiber for sharing the dataset I used in this work. I would also like to thank the members of my doctoral committee Dr. Yong Pei, Dr. Soon Chung, Dr. Larry Lawhorne. They have positively contributed in this work with their constructive criticism and suggestions. I also want to thank my colleagues Adamantia Psarologou, Anna Trikalinou, Athanasios Tsitsoulis and Stavros Mallios. Especially, I want to thank Michail Tsakalis for the great discussions and collaboration.

I want to thank my family for their constant support and encouragement. My parents Nikos Michalopoulos and Stamatina Zouzia, my brother Aggelos Michalopoulos and my sister Maria Michalopoulou. Last but not least, I want to thank my dear wife Alexia for all her support and patience throughout this journey.

CHAPTER 1: **Introduction**

Study of the human brain is an important and very active area of research in an effort to better understand, predict and prevent brain related diseases. Studying the brain response to certain input stimuli can help us determine the involved brain areas and understand the mechanisms that characterize behavioral and psychological traits and will allows us to help people with related problems. Neuro-feedback applications that are used for training the brain to focus remember and respond under certain conditions is another important direction of research. Different tools and methods have been developed in order to monitor and study the living brain activity. Electroencephalography (EEG) is one of the first methods used for this purpose. EEG has proven a valuable tool in the study of the functional, behavioral and cognitive functions of the brain [1, 2]. The main drawback of the EEG is that we cannot directly attribute the underlying activity to a certain brain region and therefore, the spatial resolution of the EEG is poor. On top of that, since the individual electrical activity of each neuron is really small, EEG only records electrical activity produced by the coordinated activation of a large ensemble of neurons. The main advantage though is that EEG has the best temporal resolution of all other brain monitoring modalities and it is relatively inexpensive.

Functional Magnetic Resonance Imaging (fMRI) is a technique that can records the changes in oxygenation of the blood oxygenation due to brain activity [3]. It takes advantage of the paramagnetic properties of the hemoglobin, the molecule responsible for carrying oxygen in the blood. When a certain brain region activates then the metabolic needs of the neurons cause an increase in the oxygenated blood flow, in an attempt to transfer oxygen to the activated region [3]. Taking advantage of this phenomenon, fMRI monitors changes in the magnetic field due to the increased concentrations of the hemoglobin. FMRI provides the best spatial resolution when it comes in the localization of functional activities of the brain. The main problem is that the time scale of neuronal activation is measured in terms of milliseconds, while the oxygenated blood response takes a few seconds to pick up. This difference in time scales between the responses makes the interpretation of the fMRI response difficult and significantly reduces the activities that can be monitored by this modality. Another thing that should be taken under consideration is that fMRI is an indirect measure of the neuronal activity and any inferences regarding the neuronal activity should be made with caution.

1.1. Extracting information from the EEG signals

In this work, we study the fusion of the EEG and fMRI in an attempt to bridge together the advantages of both modalities. It is apparent that EEG contains a wealth of information regarding the underlying brain activity, since it is a direct measure of the neuronal activity. Therefore, there is the need to efficiently analyze the EEG signals and extract as much information as possible. Signal processing techniques have been extensively used in order to extract information regarding the brain activity. Such methods include spectral analysis tools like the Fourier transform or the

continuous wavelet transform, which are used for the identification of changes in the power, frequency and phase of the signal.

EEG signals are recorded from a number of electrodes attached in the human scalp, the number of which depends on the application and the available equipment. At any point in time we record the ensemble of many active brain processes activating in parallel. The electrical signals arising from these activities propagate through the brain tissue and scalp and get recorded in the channels attached in the scalp of the head. Therefore, each electrode records a different mixing of the underlying activity depending on its position on the top of the head. Recently, there has been an increased interested in multivariate techniques that can take advantage of the multichannel EEG. Such methods include Independent component analysis (ICA) and Principal component analysis (PCA)[4, 5]. These techniques have been applied in order to separate the useful brain related signals from the ongoing and probably irrelevant EEG activity.

An alternative view of the multichannel EEG is provided by the so-called microstate model [6]. In this approach the ensemble of channels are considered as a single feature vector (topography) and thus the recording is treated as a multivariate sequence [7]. Clustering techniques has been applied in this multivariate context in an effort to identify centrotypes or representative vectors that optimally represent the sequence. Under this context, analysis of EEG data revealed that the multivariate signal does not change randomly but rather maintains a rather stable configuration for a certain period before moving to another one. These stable configurations or in other words these vectors were considered to represent the atomic blocks of brain organization. Although these topographies do not uniquely characterize brain activity, under a certain context can reveal important information regarding the evolution of the brain activity.

Although this approach seems intuitive, in practice it is difficult to apply and most importantly to associate the results with already known correlates of neuronal activity. In this work, we provide a synergistic framework of methodologies for the study and exploitation of EEG topographic information. We propose new methodologies for the multivariate analysis of the EEG microstates and we demonstrate the effectiveness of this approach in the decoding of neuronal activity. On top of that, we demonstrate the usefulness of our methodology for the detection and characterization of abnormal brain activity. Using the proposed methodology we are able to discriminate between control and progressive Mild Cognitive Impairment subjects.

1.2. The need for fusion of EEG and fMRI

EEG alone is not able to provide the spatial localization needed to uncover and understand the neural mechanisms and processes of the human brain. Functional Magnetic Resonance imaging (fMRI) provides the means of localizing functional activity, without providing the timing details of these activations. Although, at first glance it is apparent that the strengths of these two modalities, EEG and fMRI, complement each other, the fusion of information provided from both of them is a challenging task. Recently, numerous approaches have been proposed for the fusion of such information. Each of them exploits different aspects and properties of one modality or the other. Initial approaches took advantage of the good spatial resolution of the fMRI to efficiently solve the inverse source localization problem of EEG [8]. Active regions, as identified by FMRI were used as hard or soft constraints to reduce the solution space of the source localization problem. A different perspective is to use the time course of activation of EEG features in order to predict regions that the BOLD signal co-varies with the EEG

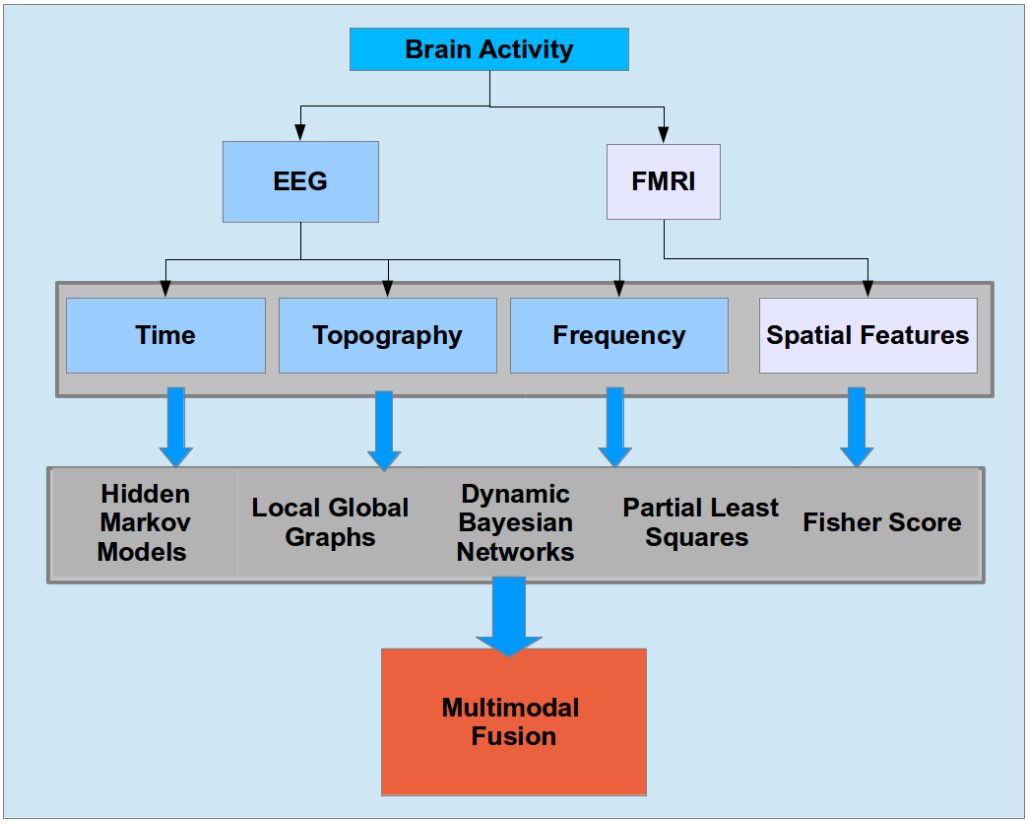

Figure 1.1: General overview of the methods used in this work for the analysis of EEG and the multimodal fusion of EEG and fMRI.

features. These approaches have found significant applications in the detection of the epileptic focus and on experiments that lack a distinct experimental stimuli or event [8].

Symmetric approaches try to take advantage of both EEG and fMRI using both modalities equally [8]. The majority of these methods incorporate some sort of data-driven technique that decomposes the two datasets into corresponding components. Methods such as Joint Independent Component Analysis and Canonical Correlation Analysis have been employed successfully and revealed correspondences between features of the EEG and the underlying fMRI activity. Decomposition and cross-decomposition techniques have been also used in the pattern recognition

field for extraction of interesting patterns and reduce the dimensionality of the problem. Therefore, they are good candidates to be used in multivariate analysis of neurophysiological data. Thus, using these techniques in a new synergistic way, will allow us to take advantage of pattern recognition and machine learning techniques in order to fuse the modalities together.

This directly leads to the concept of ensemble classification and fusion where the final decision regarding the assignment of a measurement into one category or the other is decided by using the output of multiple classifiers. The final decision is based on the ensemble of individual scores which are used to draw the final decision. There are different architectural to study this subject and it is an interesting field with a lot of researchers working on this topic.

In this dissertation, Chapter 2 presents the main approaches and methodologies for the analysis of EEG and fMRI. The chapter continues with a survey on the approaches for EEG-fMRI fusion and the future directions that are currently shaping. Chapter 3 introduces and describes a new descriptor of the EEG topography based on the Local Global Graphs (LG graphs). Here, a new similarity measure is developed, based on this descriptor and it is applied on the average Event Related Potential derived from an auditory experiment. A hierarchical algorithm has been used for the derivation of the microstates and the results are compared to prior analysis on the same data.

On Chapter 4, a novel modeling of the EEG microstates based on Hidden Markov Models and LG graphs is introduced. This novel modeling of the EEG topography captures the spatiotemporal dynamics of the EEG signals on all electrodes. The properties of the derived model are used in order to extract useful statistics regarding the duration of the microstates and the syntactic patterns between these microstates. This is a novel approach in the study of the microstate model and results indicate that it is capable to effectively characterize the temporal evolution of EEG topography.

In Chapter 5, a methodology for fusing EEG features and fMRI features, based on Canonical Partial Least Squares (CPLS) is presented. The HMM modeling approach is used in order to derive a feature based representation of the EEG signal. In this case, we use the HMM model in order to project the EEG data in the Fisher score space and use the Fisher score vector in order to describe the sequence of the EEG topography. Then the correspondence between this new feature and the fMRI using CPLS is studied.

Finally, in Chapter 6, we discuss possible extensions of HMM work, using more complex Dynamic Bayesian Networks. Using this formulation, it is possible to include more features in the analysis and provide a unified model of electrodes, frequency and time, that can be used for classification effectively. In Chapter 7, we conclude this work and summarize the major findings and results.

CHAPTER 2: **Current trends in ERP analysis using EEG and EEG/ fMRI synergistic methods.**

2.1. Introduction

The human brain is the most complex organ known. It consists of millions of neurons interconnected to each other, forming a large network capable to store and process information from the environment. Towards understanding how the brain works different techniques have been developed and various methods have been employed in an effort to capture, analyze and understand the complex brain activity.

Electroencephalography (EEG) is one of the first techniques used to study the living brain by measuring the electric current produced by the neuronal activity [1] by using electrodes attached in the head scalp. The measured electrical oscillations have been associated with different brain functions or cognitive states and provided useful insight on the brain organization. Additionally, EEG allows the characterization of different brain pathologies and a lot of effort has been devoted in the research of markers that can characterize a brain disorder and help the diagnosis [2].

Different studies have been conducted in search of discriminant features for diseases like epilepsy, Alzheimer disease and schizophrenia [2]. In Section 2 of this chapter, the advantages and disadvantages of EEG for the analysis of brain activity will be presented, along with measures and techniques that allow us to analyze and detect specific brain activations.

Magnetic resonance Imaging (MRI) is an imaging technique that takes advantage of the magnetic properties of hydrogen and the way it interacts in the presence of an external magnetic field to produce detailed images of the tissue under consideration. Functional Magnetic Resonance Imaging (fMRI) is an imaging technique that measures the change in blood oxygenation that occurs as a byproduct of neuronal activation. There exist different techniques that enable the measurement of changes in the brain flow like blood oxygen-level dependent (BOLD) measurements [3], arterial spin labeling [9] and injected contrast agents techniques [10]. Regardless the method used, fMRI provides an indirect measure of neuronal activity and lacks the temporal resolution of EEG. Since mostly the BOLD technique, is being used in conjunction with other modalities, we are going to focus mainly in BOLD studies for the remaining of the chapter. The properties of BOLD fMRI along with its strengths and limitations are presented in detail in Section 2.3.

Combining information obtained from different modalities seems really promising, since Functional MRI and EEG (or MEG) seems to be complementary in nature and are ideal candidate modalities for such integration. EEG provides excellent temporal resolution of neural activations and MRI/ fMRI provides structural and spatial accurate information about metabolic changes in different brain regions - that can be attributed to neural activation. The focus will be on a specific category of experiments, known as event related, that involve repetition of a specific input or test, multiple times in order to infer information about the EEG/fMRI response under certain conditions. These experimental conditions can be correlated with specific mental states or cognitive functions

and this procedure has been proven extremely useful in clinical and physiological research. The elicited brain response due to the stimulus is known as Event Related Potential (ERP). There exists a rich literature about the functional meaning of the different peaks of ERP in EEG (such as the P1, N1 and P3), which are thought to reflect different aspects of information processing in the brain.

In this chapter we are going to present methods and techniques used for the analysis of EEG and fMRI. We will focus in methods for analysis and characterization of event related experiments in EEG as well in fMRI. Then, we will discuss the different approaches to EEG-fMRI integration and fusion along with their strengths and limitations. The last section is devoted in methods used for the integration of the individual brain activations in terms of a distributed network and attempts that try to integrate EEG and fMRI in the so-called network space.

2.2. Event-related experiments using EEG

The unmatched feature of EEG over other brain imaging techniques is its temporal resolution. EEG measures the electrical activity of the brain and it presents excellent temporal resolution, of the millisecond scale. This electrical activity is measured by attaching electrodes on the scalp of the head (Figure 2.1). However, the electrical signature of single neurons is too weak to be recorded

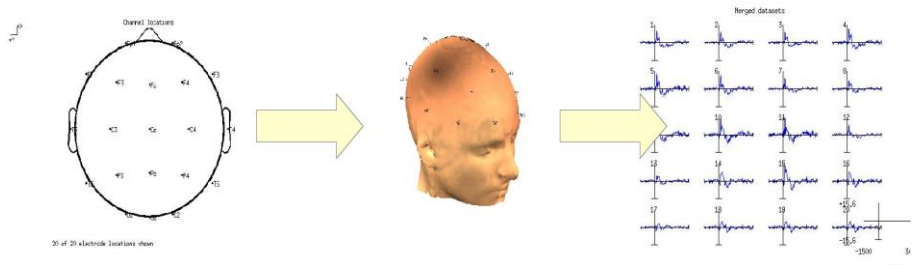

Figure 2.1: Graphical illustration of the electrode configuration in the scalp of the head.

in the scalp. The electrical signal we capture with EEG is the combined, synchronous firing of large group of neurons, mainly large pyramidal neurons oriented perpendicular to the scalp [11].

Being a direct measure of neuronal activity with great temporal resolution, EEG is used for studying the temporal dynamics of neuronal activity. The main drawback of EEG is that it presents poor spatial resolution and we cannot directly attribute EEG features to a certain brain area accurately without prior knowledge. More specifically, as the generated electrical potentials from a certain brain region have to travel through brain tissue to scalp, the recorded signal consists of the spatially dispersed mixing of concurrent electrical activations of other nearby regions. The mixing effect due to the transmission process of the generated electromagnetic field is known as volume conduction effect. As a result, the final recorded signal captures the sum of multiple activations propagated to the scalp from nearby regions. The problem of recovering the unknown sources from the observed EEG signal in the electrodes is an ill-posed problem known as the EEG/ MEG inverse problem [12].

2.2.1. Analysis and characterization of Event-related potentials in EEG

The ERP represents the brain response under a specific input and it has been proven extremely useful in clinical and physiological research. There are a lot of studies about the functional meaning of the different characteristics of the ERP such as peaks and valleys of the time signal or increases/ decreases of a specific band relative to stimulus onset. Such characteristics are considered as manifestations of specific aspects of information processing in the brain [1]. Based in this modular view of the processing that takes place in the brain, ERPs were considered to be generated by fixed latency, phase-locked responses [1]. The underlying assumption is that a certain task will evoke a specific brain response and therefore, repeating the same experiment multiple times it will be able

to detect this response by averaging the recorded signals over trials. The averaging will enhance the fixed response and will increase the signal-to-noise ratio (SNR) in the average signal [13].

Induced activities are expressed through the increase or decrease of energy in a specific band post-stimulus, denoted as event related synchronization (ERS) or desynchronization (ERD), respectively [14]. Induced activities are oscillations non phase-locked to the stimulus and have been associated with a variety of different functions related to perception and different types of cognitive processes [15]. Studies on induced oscillations put the classical, modular ERP paradigm into question. In [16], authors correlate alpha energy and alpha phase on stimulus onset with the ERP amplitude, indicating that the ERP and ongoing EEG oscillations interact and relate to each other. Evoked and induced oscillations may be considered as coupled processes with different spatial origins and partially overlapping frequency content [17].

Nevertheless, there is an ongoing debate regarding the generative model of ERP activations and there is no definite answer on the generating mechanism of the ERP. The models that have been proposed can be grouped in two categories. The additive model considers the evoked response as completely independent from the ongoing background EEG, whereas the phase reset model suggests a phase re-organization of ongoing EEG oscillations as the generative mechanism of the ERP. Although this debate has attracted a lot of attention, there is not enough evidence which point of view is more probable. The evoked model has enabled the extraction of useful information about the neurophysiologic origins of ERP, mainly through averaging over trials. Underlying the evoked model approach is the assumption that the event itself gives rise to certain brain processes at fixed latency and with similar phase, independently from ongoing EEG. This activation serves the response to the event and then vanishes. Averaging of the single trials and inspection of the characteristics of the resulting ERP waveform results in a significant increase of the signal-to-noise

ratio, so that useful information can be easily extracted about the brain process and its characteristic markers.

On the other hand, the phase-resetting model assumes that the phase-locked phenomenon is not different from the induced activations that appear to be time-locked but not phase-locked. This model states that the different ongoing oscillations either synchronize in phase or time modulated by the stimulus. This model reflects a more dynamic approach on how the different brain regions are synchronizing in order to respond to the given input.

Until now there is not a single answer to this ongoing debate. Indications that show the validity of one or the other model have been reported in many cases and each is strong enough to rule the other model out. On top of that there exist cases that demonstrate the validity of both models where different activations with the aforementioned characteristics occur simultaneously. In the next section, we will present measures that try to quantify such events.

2.2.2. ERP analysis Measures and methods based on EEG analysis

A variety of methods and measures have been employed, to characterize the nature of EEG activity in terms of its major time/frequency activity and topographic origin [5], [18]–[20]. EEG is a highly non-stationary signal and time-frequency transforms have been employed in order to examine the time evolution of its power spectrum. Short time Fourier transform and the wavelet transform is two of the most widely used time-frequency transforms for EEG analysis [20], [21], [4], [22].

The number of brain activations that are recorded simultaneously at the electrodes is generally unknown. The spatial mixing of these activations by volume conduction and the need to distinguish brain activity from signals originating from other parts of the human brain, brought into the

foreground techniques for the decomposition or de-mixing of the multichannel EEG. The most prominent techniques include Principal Component analysis (PCA) and Independent Component Analysis (ICA) [23].

Principal Component analysis operates in the multichannel EEG signal and transforms the data into uncorrelated mutually orthogonal components. PCA is a well known technique for dimensionality reduction and has many applications in the field of pattern recognition. It has been used in this context as a preprocessing step before the application of ICA. Independent component analysis (ICA) is increasing in popularity in the field of EEG signal processing. ICA is a statistical signal processing technique which tries to solve the so called blind source separation problem (BSS). In the BSS problem the goal is to recover/ estimate the original sources by using only the information available from the observed mixed signals without having any information about the mixing process or the sources. In general, the classic blind source separation model where we observe k signals which are generated by the linear mixture of m source signals can be described as:

$$x(t) = As(t) \ , \tag{1}$$

Any approach used to solve this kind of problem has to make some assumptions about the source signals the mixing process or both. The main assumption of ICA is that the source signals are statistically independent. ICA has been used successfully in the decomposition of many natural signals and the main factor of this success is that the assumption of independence seems to apply well on many natural signals, rather than other mathematical constraints, like orthogonality.

One of the first applications of PCA and ICA was the de-noising of the multichannel EEG signal. PCA was the first technique employed for artifact correction and removal from EEG recordings [24, 25] but thorough studies demonstrated that ICA was more efficient for this purpose

[26]. PCA is commonly used for reducing the dimensions of the problem before applying ICA or for data reduction and summarization of time-frequency transformed data [5], [27].

ICA has been proven very successful in the analysis of EEG data and especially in the exploration of the dynamics of ERP data. It is being used for removal of artifacts from the EEG recordings with success without losing relevant information. Also, it has been successfully applied on continuous or event related EEG to decompose it into a sum of spatially fixed and temporally independent components that can lead in different spatial distribution patterns, which in turn may be directly attributed to underlying cortical activity.

2.2.3. Time Frequency features

The EEG signal is known to be a highly non-stationary signal and the classical spectral analysis of the EEG using the Fast Fourier transform is not able to describe the evolution of the frequency EEG content. Short time Fourier transform was one of the first techniques used to alleviate this problem by operating on windows of appropriate length. The main disadvantage with this approach is that for every frequency the same window was used and therefore the same resolution in time and frequency was achieved for all points. Wavelet approaches overcome this limitation by using varying window lengths depending on the frequency under consideration. Scaled and translated versions of a basis function are used to decompose the signals into the corresponding translation-scale ranges. The notion of scale corresponds to different frequency ranges while the notion of translation to the different time-windows on the signal. There exists a the tradeoff between frequency and time resolution and small scale (high-frequency) transforms of the function have shorter time windows while large scale versions (low-frequency) are evaluated with longer windows. Higher frequencies have better time resolution and lower frequency resolution while

lower frequencies present the reverse effect. The wavelet transform has been used extensively in the analysis of EEG data with good results. The basis that has been mainly used is the complex Morlet function.

The classical procedure for quantifying evoked responses is through averaging over trials. This procedure enhances the task related response and filters out the irrelevant background EEG. As noted earlier, this approach assumes that background EEG behaves as random noise and that the task related response is approximately identical from trial to trial. Phase relevant measures as intertrial coherence (ITC) have been used to characterize the phase consistency of the detailed time frequency content throughout trials [22]. ITC can be expressed as following:

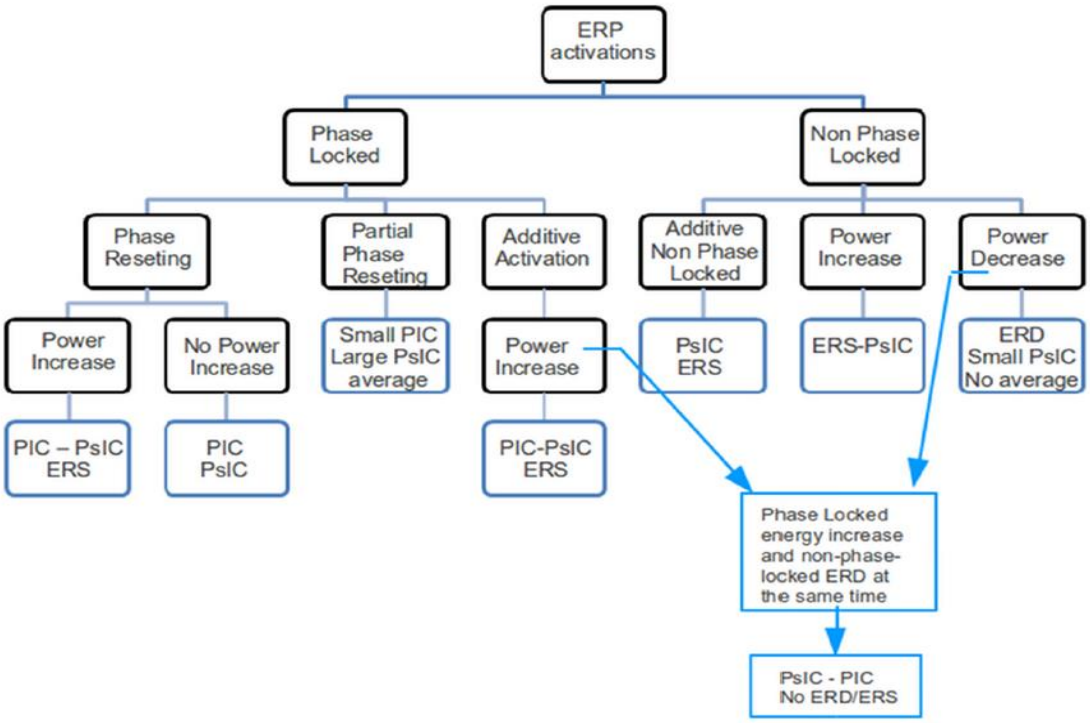

Figure 2.2: Summary of the different ERP activations and how they are reflected in the measures. We can see that the measures discussed above cannot sufficiently characterize the nature of the activations.

$$ITC[k,n] = \frac{1}{T}\sum_{i}^{m}\frac{X_i[n,k]}{|X_i[n,k]|} \tag{2}$$

In [20] a similar measure for quantifying phase-locked activity in ERP trials called phase intertrial coherence (PIC).

$$PIC[k,n] = \frac{\sum_i X_i[n,k]}{\sum_i |X_i[n,k]|} \tag{3}$$

Though the two measures are similar, PIC measure takes under consideration the amplitude of the measured signal and not only the phase [20]. The first measure for quantifying event related oscillations is the Event-related desynchronization (ERD) and event-related synchronization (ERS) which measures increase or decrease in the power of specific bands relative to some baseline pre-stimulus power. Event related spectral perturbations (ERSP) are an extension of these measures in the time frequency domain, enhanced with tests for significance [4]. In [20] a measure for the evaluation of consistent oscillations across trials is introduced under the term Phase-shift intertrial coherence (PsIC) which is defined as following:

$$PsIC[k,n] = \sum_{i}\frac{|X_i[n,k]|^2}{\max(|X_i[n,k]|^2)} \tag{4}$$

This measure cannot be directly compared with the other two since it does not take into account variations in the power of a certain band but rather examines whether a narrow band oscillation is present in single trials, in a consistent manner.

In Figure 2.2 the representation in the measures of the different assumptions about the generation of the ERP covering the spectrum between the two models, is presented. We can see that even though we can distinguish evoked from induced activations through the PIC measure, the underlying generative model cannot be distinguished using only these measures. Further research is needed in order to shed light in this complex debate.

2.3. Methods for FMRI analysis.

The main goal of fMRI is to identify and map brain regions to certain brain functionalities. We will focus in fMRI using BOLD, as the majority of fMRI related studies are based on this approach. It is important to describe the basic principles behind fMRI since it will allow us to better understand the nature of the measured signal and will allow us to identify the level at which the two modalities can be combined.

BOLD fMRI takes advantage of the magnetic properties of the hemoglobin which are used as a natural contrast agent. Hemoglobin is the protein responsible for the transport of oxygen from the respiratory organs (lungs) to the rest of the body. The oxygenated hemoglobin presents different magnetic properties than the de-oxygenated one. Deoxygenated hemoglobin is paramagnetic while the oxygenated presents diamagnetic properties. In practice, this means that the magnetic field is distorted around blood vessels containing deoxygenated hemoglobin and this distortion results in reduced relaxation time [3]. The tissues around blood vessels with different concentrations of (de)oxygenated hemoglobin will have different relaxation times and therefore different intensities in the final MR image. We will not go into details about the process of image formation since this is beyond the scope of our study.

BOLD FMRI measures the flow or the change in flow of the oxygenated blood in the brain. Increased blood flow occurs as the brain requires energy, in the form of glucose, to be delivered in areas involved in some sort of processing. An active area requires more energy, which translates to increase of the oxygenated blood arriving in this area. Therefore, fMRI measures blood oxygenation levels, which change with increased metabolic demands of active brain areas and form a sort of indirect measure to neuronal activity [28].

In order to observe physiological or pathological changes in functional activity using fMRI an experiment has to be set up that will help reveal and identify such activities. MRI images are obtained while a subject is performing a motor, cognitive or sensory task, designed to elicit specific brain activity. Using the obtained images, the next step is to find patterns of activity that correlate with the performed task. Voxels whose intensities over time present significant correlation with the time evolution of the experiment are considered as related to the task and marked as active. The effect of noise and the need to perform complex experiments has led to the development of complex preprocessing and analysis methods.

The design of the experiment can be categorized into two distinct categories depending on the way that the stimuli are presented to the subject: block and event -related designs. In block designs the stimuli of a certain class are presented continuously for a certain period/ block of time [29]. Usually, periods of rest are alternating with periods of task. The idea behind this type of design is to increase the signal to noise ratio of the hemodynamic response by requesting continuously the same response and therefore a steady level of BOLD signal. This comes in the expense of completely disregarding the temporal evolution of the hemodynamic response.

On the other hand, event-related designs alternate the order of presented stimuli, which are presented in random order separated by a short period of rest. The response to each stimulus is measured and the hemodynamic response (HRF) function can be estimated. Event-related designs allow the execution of more complex experiments in the expense that it is not always possible to detect these activations due to low signal to noise ratio [30].

2.3.1. FMRI data preprocessing

Analysis of Functional MRI data involves a series of preprocessing steps necessary before the actual statistical processing. The series and order of such steps are also known as preprocessing pipeline [31]. This section does not describe preprocessing steps taken in k-space, only methods used in the image space.

These preprocessing steps involve temporal and spatial registration of the acquired MR signals in order to compensate for noise and variations due to the measurement process [31]. Noise in fMRI can be introduced due to MR signal strength fluctuations throughout the session known as thermal noise [28]. This kind of noise is due to thermal motion of the electrodes in the scanner or the tissue under examination. Thermal noise increases as the temperature and the strength of the magnetic field increases. Another source of noise originates from the system itself and is related with inhomogeneities of the magnetic field and variations of the gradient fields used to spatially target the measurement [32]. Thermal and system noise are unavoidable under a particular setup and do not relate with the experimental task and their effects can be easily mitigated.

A different source of noise is due to subject movements. The subject under consideration cannot remain still throughout the whole session. Head movement is a major source of noise in fMRI studies and excessive head motion during an experiment may render the data unusable [32]. Since the whole procedure relies in radio frequency pulses, in order to localize the recorded activity, even small movements will have the effect of transferring activation from one location to nearby ones resulting in blurring of the obtained signal.

An additional problem with head movement is that sometimes is related to the task and its effects can influence the final result. This effect is mostly apparent in visual tasks where the subject has to guide its gaze to various presented targets. Even though it is required only to move its eyeballs, most of the time this movement is accompanied by a small involuntary displacement of

the head. Also, even small movements due to breathing or heart beating introduce noise. The effect of breathing and heart beating on the results is rather complex since they make the brain inside the skull to move and expand [33].

In order to compensate for noise and cancel any non-task related influences the preprocessing of the data includes noise correction, slice-timing correction, motion correction and registration [31]. The final pipeline sequence depends largely on the experiment design, the strength of the magnetic field and the pulse sequence used for acquiring the k-space data.

Slice-timing correction adjusts the data of each slice as each slice was sampled at the same time. This procedure tries to correct the fact that each slice is sampled separately at a slight different time interval than the previous one. Slices can be collected either sequentially, one adjacent slice after the other or interleaved, odd slices first, then the even ones. If the time needed to collect the whole brain volume is TR, then depending on the manner that the slices are collected the last slice is collected TR or TR/2 from the first one. Interpolation between voxels of the same slice acquired in adjacent time frames is used to estimate the signal for the specific acquisition time [34]. Different interpolation techniques have been proposed for slice-timing correction like linear, cubic and spline [35]. Usually slice timing correction is used as the first step since it simplifies next steps in the preprocessing procedure [31].

Due to system inaccuracies or subject movement, voxels are displaced and therefore an alignment step is needed so that the time series of each voxel represents the BOLD signal from the same brain region throughout the session. Usually, rigid-body registration is used in order to correct head motion and a large number of techniques have been proposed [31]. We can classify the algorithms into those that use intensity based measures and those that use landmarks in order to register the slices together. The algorithms used in order to calculate the rigid body parameters and

the interpolation method are other factors that differentiate the different algorithms. Many algorithms have been proposed and almost all fMRI analysis packages include their own implementation of algorithms like mutual information based algorithms, normalized correlation and AIR automated image registration just to name a few [36]–[39]. All of these algorithms assume that all the slices of a single stack have been collected at the same time and they consider a rigid movement of the whole brain volume. This is one of the main reasons why slice timing correction usually precedes head motion correction.

Most of the fMRI studies use multiple subjects to infer information about activating regions. Since the size and shape of brains of different subjects vary along with the relative location of several anatomical brain structures a sort of normalization and registration has to be performed before inferring conclusions from the results. This preprocessing step is achieved by bringing the different volumes in the same coordinate system and then some linear or non-linear registration to a common brain atlas is applied, so that their shape, size and direction are the same [30], [40].

2.4. FMRI Analysis approaches.

After a series of preprocessing steps have been carried out, the data are ready for statistical analysis. The data that we have to work with include brain captions in different time points. Alternatively, we can consider our data as the time evolution of the intensity of each pixel in the captured brain slices. A typical fMRI dataset consists of thousands time-series; if we consider that we have 32 slices with each slice being a 128x128 matrix. Typical fMRI analysis involves the detection of changes in the mean signal intensity of the MR data during different behavioral conditions. Different statistical methods have been employed to accomplish this task, ranging from simple correlation analysis to more complex models that take under consideration the temporal and

spatial correlations of the data [34]. The final output is an activation map generated for each condition or experimental task. Voxels, which present increased activity during a certain condition, are marked as active. An example of the performed steps can be seen in Figure 2.3.

An approach for detecting significant changes is to use Student's t-test. T-test is commonly used in fMRI analysis due to its simplicity and easy interpretation of the results. Since we have multiple recordings in time an alternative approach is to use the Kolmogorov-Smirnov (K-S) test to compare the distribution of the MR signal intensity between the two conditions [42]. This test can be used to detect changes in the variance along with changes in the mean [43] Split-half test is another option that has been used to determine significantly different voxels [44]. Many studies have extended in these techniques by adding spatial or other constraints. A well-known and popular approach, that uses multiple linear regressions in order to take under consideration the time course of the fMRI signal, is the General Linear Model [45], [46].

The formula of the general linear model is

$$Y = X\,b + n \tag{5}$$

where Y is the response, X is the matrix of predictors and b the unknown coefficients of the predictors. The error n is assumed to have normal distribution with zero mean and variancess_2. In our case, Y represents the time course of the fMRI signal in the voxels; X represents the design matrix of the experiment under which we obtained the measurements. Under the assumption that each measurement and each voxel is independent, the parameters b can be obtained by least squares. The GLM model is a more general model that encompasses t-test and correlation approaches. GLM makes some assumption about the data as that the voxels and their time courses are independent and that the same model as described by the design matrix is sufficient for all voxels. These

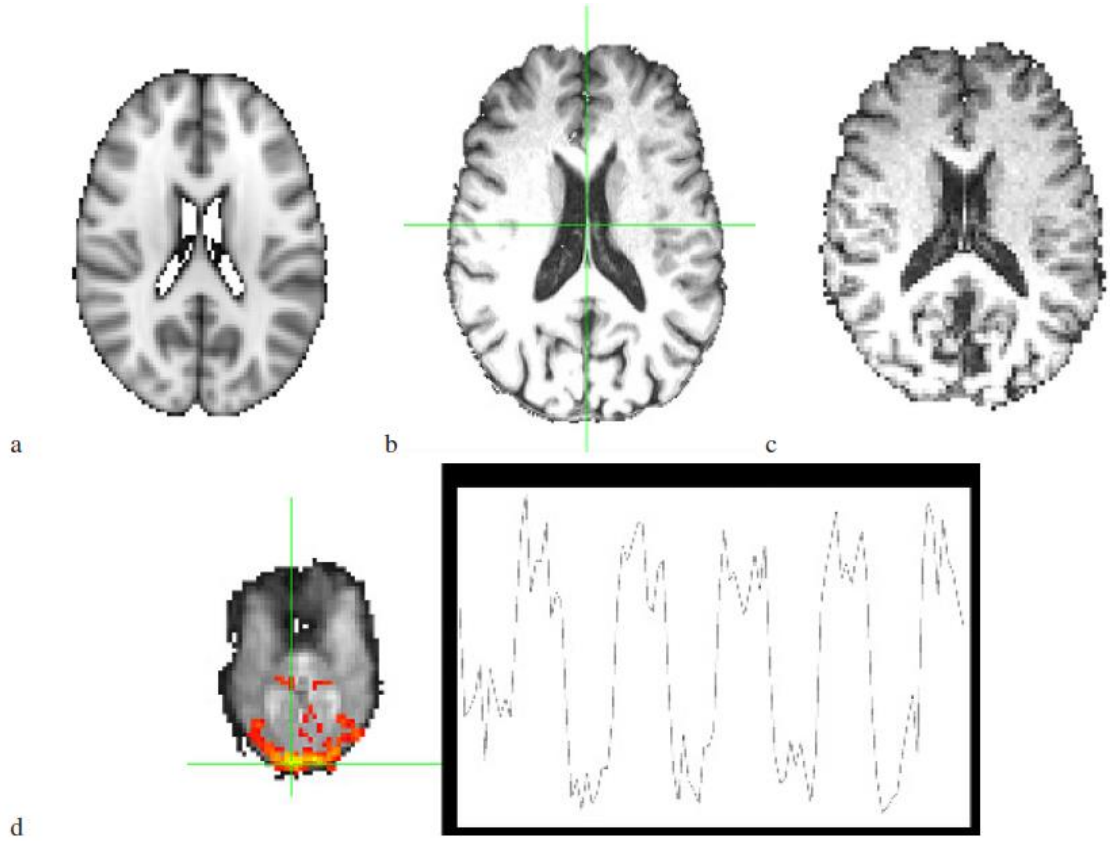

Figure 2.3: First row: Example of affine registration using the FSL toolbox [41]. Figure a, is the template brain we want to register to. Figure b is the brain we want to register and in figure c we can see the registration result. Affine registration is used as a first step before applying non linear techniques. Second row shows the time course of a specific voxel with high correlation with a block experimental design.

assumptions do not hold in reality and a lot of efforts have been devoted to the extension of the GLM.

The design matrix incorporates the different experimental conditions and is a matrix containing the BOLD response for each experimental stimulus. The bold response can be modeled as Linear Time Invariant System (LTI), where the stimulus is the input and the Hemodynamic Response Function acts as the impulse response of the system [42]. A LTI system can be fully characterized

by its impulse response or transfer function. If the brain is treated as an LTI system, finding the transfer function of this system would allow us to predict the response of the brain in different conditions and under complex inputs. Of course this is an approximation, but it has been shown that an LTI approximation can characterize quite well the behavior of many systems.

The GLM formulation is the most popular technique for detecting active regions in an fMRI experiment. The main drawback is that it is a very strict model and any mis-modeling will result in an increase of the false positive rate. Also the way that the HRF is calculated plays a significant role to the final result. Non-linear models like the Balloon model [47] that models changes in the flow and volume and how these changes affect the BOLD response are more realistic but they require the estimation of a lot of parameters and they are sensitive to noise. The linear model is very popular mainly due to its simplicity and interpretability.

A different approach is to use the information of the data without imposing any strict, specific model. This kind of techniques are very popular since they allow the execution of experiments with complex stimuli that makes it difficult to estimate the time of activation and therefore makes the use of models not practical. Data-driven approaches have been used in psychological studies involving emotion, motivation or memory. These techniques have found many applications in the study of resting state fMRI experiments.

Popular component decomposition techniques include Principal Component Analysis (PCA) and Independent Component Analysis (ICA). These have already been described the basic principles behind PCA and ICA in the EEG section. In the fMRI context, there exist two different approaches, mathematically equally. PCA or ICA can be either temporal or spatial [48]. In the first case we are looking at the temporal structure of the data in order to find voxels/ regions that present the same time evolution while on the other hand we are looking in the spatial structure of the data

and we are looking for similar spatial patterns through time. PCA was one of the first techniques to be employed in the voxel time series in order to extract spatial regions with similar temporal evolution, allowing exploration of the functional connectivity of brain regions.

ICA is more popular and has numerous applications in all kind of studies, from event-related to resting state studies. Temporal and spatial ICA have been used extensively, although spatial ICA is more often encountered in studies. For the spatial case the ICA model is

$$X = As \tag{6}$$

where X is a $t \times n$ matrix where t represents the time points and n the voxels, A is $t \times t$ temporal mixing matrix for the txn spatial independent components/ images of the matrix S. Temporal ICA presents the symmetrical configuration where X is a $n \times t$ matrix and A is a $n \times n$ spatially mixing matrix for the $n \times t$ independent time courses. Since the number of voxels is much larger than the number of time points, temporal ICA is much more computationally intensive than the spatial one.

The problem with ICA is that since it is a stochastic method, different runs would produce different results [49]. Before using the calculated independent components in our analysis we have to evaluate the reliability of those components. Different methods have been proposed for evaluating the consistency of the results. The most popular technique runs ICA multiple times in bootstrapped data and then clusters the independent components. Components that belong to clusters with small inter-cluster and high intracluster distance are considered reliable for further evaluation [49]. In contrast to PCA where the significance (variance explained) of each principal component is already known, in ICA each component has to be evaluated separately in order to distinguish task related ICs from noise. In spatial ICA [50] was directly compared to the GLM and

is used as a way to solve the GLM problem without using a fixed design matrix; it is directly computed by the ICA.

Analysis and evaluation of Independent components can be distinguished into two approaches. The one is inspired from the extensive work in the EEG Event related experiments where independent components are separated into task related and noise [18] and thus ICA is treated as a filtering procedure. In a different context, the filtering aspects of ICA were used in order to remove task related activity in order to study the state of the brain at rest [51].

Other methods that have been applied to fMRI data and not presented here include Canonical Correlation Analysis [52] with extensions to accommodate group analysis like in [53]. These approaches led to new algorithms that were able to incorporate not only data from multiple subjects but also from multiple modalities [54].

2.4.1. Multivariate Pattern Analysis

Analysis of FMRI data considers the activation of each brain voxel and uses the General Linear Model in order to evaluate the degree of co-variation of the task response of each voxel to the theoretical BOLD response. In essence, mass univariate tests of significance are performed, one for each voxel under consideration. This type of analysis answers the question regarding the brain regions that present significant correlation with the BOLD response induced by the experimental paradigm.

The complementary question regards the patterns of activation. This means that we can test whether certain pattern of activation can be used in order to predict which task or condition produced them. This type of analysis requires considering the ensemble of voxel activity in order to effectively characterize the task activation. In a seminal paper [55] first introduced this approach

in order to identify whether there exists a specific brain area responsible for the processing of faces. This problem is also known as the decoding problem and has been an active area of research lately. The term multivariate pattern analysis refers to fact that the neural response is treated as the total pattern of activity rather than each voxel separately.

Under this context, machine learning techniques have been applied in order to extract patterns that best characterize certain tasks [56]. One of the most interesting implications of using machine learning techniques is that we can use the trained classifier in order to learn more about the features/ voxels that contribute to the classification result. Therefore, we can localize the most informative features and use them to further evaluate and interpret the result. Multivariate pattern techniques have been proved to be more informative than the GLM model and provided answers to a different set of questions regarding as the states that a given area may be involved and the functional organization of different areas under a given task.

This work is related to the MVPA approach regarding the means for decoding the EEG and fMRI activations patterns. The main idea is to use machine learning techniques to integrate information from both modalities in order to enhance the accuracy of the classification. At the same time we can evaluate the relation between coupled features from the two modalities. This allows us to either localize in time fMRI activations or localize in space EEG features that contribute significantly to the classification result. In the next section we present the method used for the integration of the information between the two modalities. Another advantage of this approach is the flexibility that it provides in the analysis of the datasets. It allows evaluating the effect of different features without altering the whole model.

2.5. EEG-fMRI

Combining information obtained from different modalities seems really promising especially in the study of the brain. Functional MRI and EEG (or MEG) seem to be complementary in nature and forms an ideal candidate pair of modalities for such integration. EEG provides excellent temporal resolution of neural activations and MRI/ fMRI provides structural and spatial accurate information about metabolic changes in different brain regions - that can be attributed to neural activation.

It is apparent, that the two modalities describe and represent different phenomena that there is no assurance that they are directly and uniquely associated/ correlated. The most promising results supporting EEG-fMRI integration come from studies that combine fMRI with implanted electrode data [57]. These studies show significant correlations between the time course of activations of fMRI and electrophysiological signals.

On the other hand, there exist several studies that suggest that such integration is not as straightforward as it seems. A one-to-one correspondence between Event Related Potential (ERP) peaks with fMRI activations cannot be assumed as underlined in [58], [59]. In [60] simultaneous recordings from a single subject are used in order to demonstrate that EEG significant features, as peak amplitude, are not likely to be correlated with BOLD signals.

Nevertheless, there are different views regarding the relationship between the local neuronal activity captured by the EEG and related changes in the cerebral blood flow. Another point that needs attention is how to treat the absence of any relation or correlation between the two modalities. This could be attributed in algorithmic limitations, meaning that we can categorize this absence as a false negative. The most difficult question is, though, what if a failure to associate the two

modalities is by itself a significant finding or an indication of pathology. There are no straightforward answers in this problem and there is an ongoing research regarding these questions. In general, we can assume that EEG activity is not necessarily co-localized with fMRI activations and also certain fMRI activations do not correlate with EEG. An illustrative model to describe the overlap of EEG explained activations and fMRI ones is described in Figure 2.4. It is obvious that parallel analysis of the two modalities will help us to understand better the activations reflected by these modalities. In this section we are going to discuss methods for identifying and characterizing brain activations using information from both modalities.

Towards this goal, several methods have been employed in order to take advantage of the extra information that each modality provides to the other. On the one hand we have the methodologies that use information from one modality in order to constrain or explain results derived from the other. This approach is known as information integration [8] and includes the methods that we will discuss in the next two sections. The other approach tries to find common patterns of activation in the two modalities in parallel. This approach is characterized as information fusion [8] and includes data-driven and model-based methods. We are interested mainly in the data-driven techniques that have been employed towards this direction.

2.5.1. 4.1 EEG Localization through fMRI constraints.

One of the first attempts for EEG-fMRI integration was to use the fMRI spatial information in order to constrain the problem of EEG source localization. Early attempts used dipole modeling to solve the source localization problem [61] and then regions extracted from the fMRI were used to constrain the dipole location inside the head [62], [63]. This methodology assumes that the possible EEG dipoles express hemodynamic changes reflected in the fMRI. As we mentioned earlier this is

an assumption that does not hold in general. On the other hand, dipole modeling localization assumes that the observed EEG is created by a couple of dipoles which seems to be an unrealistic assumption.

In order to overcome the limitation of dipole modeling, current density modeling approaches were employed for the source localization of the EEG [64]. LORETA [65] is the most popular technique for localization through current density modeling. A major disadvantage of the proposed methodologies is that in order to compare the sources calculated from the EEG we have to collapse the EEG in time, either by calculating the sources using the average over time or by using the average LORETA source estimations, thus canceling the temporal advantages of EEG. An important aspect was highlighted by the findings in the study of [64]. In this study, it was shown that fMRI regions and LORETA sources were matching when the groups mean data was used. On the individual level though, only half of the subjects presented significant correspondences. The group finding shows that such relations can be established but the individual results stress the fact that caution should be exercised when trying to combine the two modalities.

Despite the fact that EEG source localization is an ill-posed problem and the obtained results should be treated with a certain degree of uncertainty, a lot of efforts has been dedicated to this kind of analysis that extends beyond functional characterization and extends to works that try to asses functional integration [66], [67]. Nonetheless, there still exist major issues in the application of this approach that seem difficult to be transcended soon.

2.5.2. FMRI prediction using EEG information.

A different approach to the problem of EEG-fMRI integration is gaining grounds lately, primarily due to technology advances that allow simultaneous recording of EEG and fMRI. This approach uses EEG features in order to infer fMRI activity.

The work in [68] was the first to display that using fMRI activations we can localize EEG bands without the use of complex and ambiguous methods of source localization. In this work, authors used the alpha band power as a predictor in order to identify regions that changed with alpha band power modulation [68]. Following works extended the study in other bands [69], [70]. This technique has been extremely useful in the analysis of the brain rest state or in complex experiments without a specific stimulus or task. An important application is the pre-surgical evaluation of pharmaco-resistant focal epilepsy where the accurate localization of the epileptic region is needed [71]–[73]. Actually this clinical application was the driving force behind the development of the needed hardware that allowed simultaneous recordings [74].

A different application is based on the examination of EEG-fMRI event-related single trial co-variation. The goal is to identify brain regions that the BOLD response shows the same modulation as a specific single trial ERP component (peak). The basic idea is to use features of the single trial ERPs and use them as predictors for producing fMRI maps related to each single trial feature [75], [76].

2.5.3. Data-driven fusion approaches

The approaches described above use one modality in order to constrain or predict the other. Models that use a common generative model, explaining the data of both modalities would be the ideal solution to the fusion problem. There have been made efforts towards this direction, without any model reaching a sufficient maturity level [77]–[79]. On top of that, the complexity of these

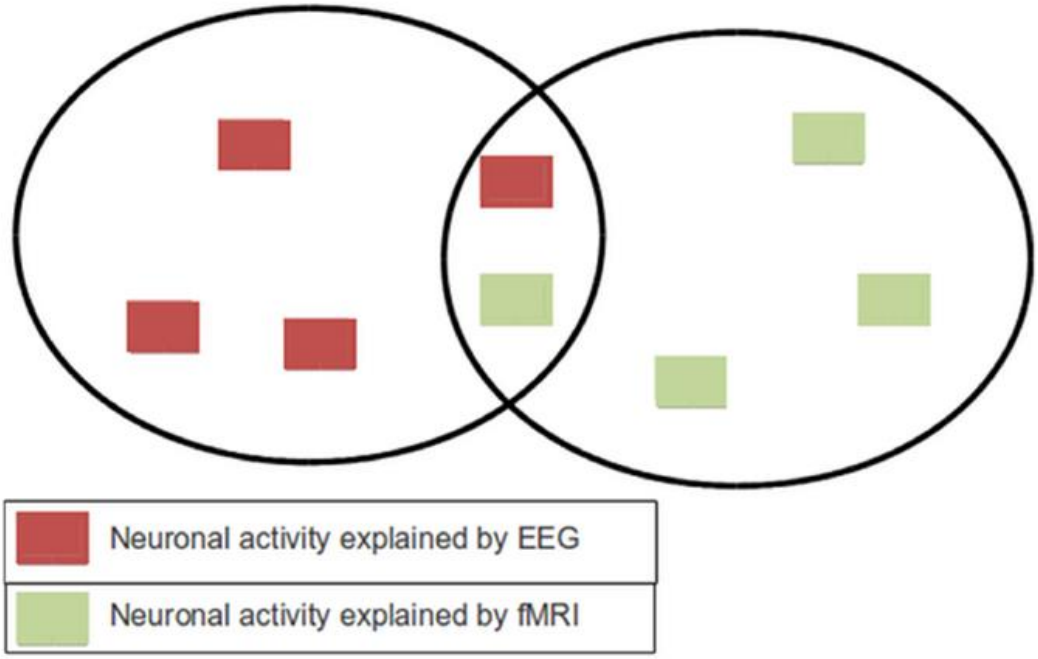

Figure 2.4: Illustration of activities explained by each modality. Activities in the cross-section are reflected in both modalities and are the ones that we can use in fusion. Illustration is based in [8]

models renders their application difficult and therefore many models exist only in the theoretical domain or have found limited applications.

Recently, inspired from the advances in the application of multivariate methods in EEG and fMRI, data-driven fusion is gaining a lot of attention. A lot of effort has been geared towards methods that extend application of ICA to multi-modal data. In this category we have a series of ICA-based methods developed for this end [54], [80]. Other methods include multi-set canonical correlation analysis [81], [82], which has been applied to single trial ERP and fMRI. The application of these methods has been focused primarily in the analysis of ERP data, in an effort to explore and exploit trial to trial variations.

Based on the success of ICA in analyzing EEG and fMRI separately, there has been an effort to extend ICA for the fusion of EEG and fMRI. There are studies that use ICA to decompose EEG data and extract useful features that can be used to predict the fMRI activation [75], [83]. Other studies used ICA to extract distributed regional networks from fMRI and the BOLD signals where correlated with power fluctuations in different EEG bands [84]. The aforementioned approaches use ICA in one or the other modality and then use an asymmetrical approach as the ones described earlier. We will to focus algorithms that operate in both modalities and offer a symmetric approach to the problem.

In this context joint ICA was proposed in [85]. The joint ICA algorithm assumes that EEG and fMRI features share the same mixing matrix. In joint ICA we assume that the modalities are jointly temporal or spatial independent and therefore increased BOLD activity will be reflected in increased amplitude of a certain ERP peak. Joint ICA operates in the space defined by the features of both modalities. In order to avoid bias we need to transform EEG and fMRI data and bring them in the joint space so that we can recover the common mixing matrix and independent sources that explain the features. Usually the ERP data from selected channels are used as features while the fMRI activations maps extracted in a previous step (using GLM for example) are the corresponding features for fMRI. The ERP data used are up sampled in order to match the number of fMRI voxels and the data from both modalities are normalized and concatenated into a single matrix, in which joint ICA is going to be applied.

The problem with joint ICA is that the assumptions regarding the generation of the observations are too strict and possibly are not physiologically plausible. A method proposed for relaxing these assumptions and to provide a more flexible estimation is parallel ICA [80]. This method identifies components in both modalities simultaneously and constraints the solution so that maximum

correlation is achieved between the mixing matrices of the two decompositions. The correlation constrain is defined by the maximally correlated components in each iteration. The number of constrained components is allowed to vary from one iteration to the other. The correlation threshold is chosen manually and prior knowledge about the experiment is required for choosing the appropriate threshold. Parallel ICA has been reported to provide stable results and has been used extensively for the fusion of other modalities as well [86].

One of the first attempts of EEG-fMRI fusion was proposed in [87], using N-Partial Least Squares (N-PLS) [88]. N-PLS is a general multi-way extension of Partial Least Squares regression. N-PLS describes the covariance of both the independent and dependent variables. This is achieved by fitting the multi-linear models for the independent and dependent variables simultaneously, constrained by a regression model relating the two models. A three-way model was used for the EEG data, having spectral, temporal and spatial atoms and a linear model was used for fMRI with spatial and temporal atoms. N-PLS was used to find correlations between fMRI time courses and spectral components of the EEG. The problem with this approach is that each modality is decomposed separately and then, each decomposition is correlated to the other, a procedure that does not guarantee that the optimal relations will be discovered [89].

Canonical Correlation Analysis (mCCA) [81] assumes a different mixing matrix for each modality and transforms the data so that the correlation in the trial to trial variation between the two modalities is maximum. It has been proposed for group analysis of fMRI data and it has been used for feature based multimodal fusion [81]. An extension of mCCA is multi-set CCA, which extends CCA to incorporate more than two modalities. In order to work with the two modalities a series of preprocessing steps are needed in order to transform the data for common analysis. fMRI data are preprocessed (motion corrected, slice timing correction, etc) and regions of interest are

extracted based on an anatomical automatic labeling atlas. The normalized mean of each ROI is used as input for the mCCA algorithm. It has been observed that the rate of stimulus presentation and subsequent learning of the stimulus appearance pattern modulate the amplitude of certain components of the single trial ERP. The amplitude of the single trial ERP from selected channels is used to calculate the modulation function that will be used in conjunction with the fMRI. The resulting signals over trials are convolved with a standard HRF function and then averaged over the channels and down sampled to reduce the dimensionality of the data. Multi-set canonical correlation analysis provides a flexible framework for information fusion. It can be used for multimodal and group analysis using raw or featured based inputs. Unlike the ICA methods that promote sparsity of the results M-CCA produces component maps that may not be as sparse, thus making the interpretation of the results difficult.

An in depth review of these methods can be in found in [89] where their performance is evaluated in simulated scenarios, although there is not any absolute conclusion about the adequacy of each method. This is somewhat expected if we consider that the success of each method depends on the plausibility of the underlying assumptions and the application.

The main drawback with the majority of these approaches is that all the methods described above consider a generic HRF function with its parameters like undershoot and peak latency to be fixed across regions and subjects. This is in contrast with studies that show that there exists variability in the HRF response not only between subjects but also between regions of the brain [90], [91]. In order to reduce bias and increase sensitivity, it is important to incorporate subject and region specific hemodynamic functions in the methods. A recent work that is moving in that direction, using a model of neurovascular coupling as a constraint for the Parallel ICA can be found

in [92]. Nevertheless, data-driven methods provide a flexible framework for exploring EEG-fMRI fusion with many directions that require further investigation.

2.6. Connectivity, EEG and fMRI

The methods presented earlier try to identify relationships and common patterns in the data or features extracted from them. So far, the methods presented were considered for the identification of brain activations for EEG or active brain areas for fMRI and the subsequent functional characterization of such regions or activities. This approach is known as functional segregation and its goal is to identify brain activations and assign a specific functionality to them [93]. The complementary task is to describe the functional interactions of the different brain activities that together form large functional networks [93]. It is known as functional integration and it is the subject that we are going to discuss in this section and how fusion of EEG and fMRI can be achieved in this context.

Functional integration involves the study of networks formed between brain areas in the case of fMRI [94] or between EEG bands if we are dealing with EEG [95]. Such networks are thought to play significant role in information processing of the brain [20], [95]. Brain networks are studied using the functional connectivity (FC) and effective connectivity (EC) of brain activities [93], [96]. Functional connectivity is defined as the temporal correlations between remote brain activations. On the other hand effective connectivity is defined as the causal influence of one system to another [96], [97]. Functional connectivity captures the correlation between remote brain activities; in essence identifies the nodes of the network while effective connectivity reveals the integration and hierarchy inside the network.

2.6.1. Functional Connectivity

Functional connectivity in EEG has been applied to identify interactions between single electrodes, predefined groups of electrodes or between independent components of the data [98]–[100]. In order to assess Functional connectivity in EEG different signal analysis techniques have been proposed. The earliest is through the calculation of the autocorrelation between signals captured in selected electrodes [101]. Magnitude squared coherence (MSC) is another measure that it is used to measure linear connectivity in the frequency domain [14]. Coherence captures the variations in the relation of power and phase between two signals and takes its maximum value of one when the power and phase of the two signals are stable. A direct extension in the time-frequency domain is the wavelet coherence, which can quantify time varying time-varying coherence [102]. Non-linear techniques include phase synchronization measures as the Phase Locking Value (PLV) [96], [103] and generalized synchronization (GS) [96], [104]. Finally, information based techniques like Cross mutual information and Minimum description length have been applied [96].

Functional connectivity in fMRI allows the characterization of interactions between remote brain regions during a certain task. The earliest methods used to identify interacting regions relied on cross-correlation of initial seed voxels and voxels in other brain regions [105], [106]. In [107], authors indicated that this procedure is biased since the results depend in the initial choice of seed and completely ignore any relations between the voxels.

In order to avoid such biases, Principal Component analysis was used in order to decompose the BOLD time-series into orthogonal components which represent spatial patterns with the greatest amounts of functional connectivity in descending order [94]. Spatial ICA as we saw earlier can decompose the data into independent maps which can be used to evaluate functional

connectivity between brain regions [48], [50]. ICA has also been used to find and characterize functional networks (FN) in the data.

A natural extension of this approach was to examine the functional relation between FN networks instead of voxels or regions in the brain, a technique known as Functional Network Connectivity (FNC) [108]. This technique could provide insight in complex relationships between remote cerebral sites.

2.6.2. Effective Connectivity

The methods described do not provide any information about the temporal precedence of the different brain activations and therefore cannot efficiently describe the dynamic interactions between brain activations in order to accomplish a certain mental task. This synchronization can be expressed as phase alignment between two remote neural assemblies or as the influence of one system to another [94].Methods for assessing effective connective include Dynamic causal modeling (DCM) [109] and Granger Causality (GC) [110].

Dynamic causal modeling employs a generative forward model explaining how the data were caused. DCM treats the brain as an input-state-output system where the deterministic inputs correspond to experimental stimulus that evokes brain responses. It was first introduced for analysis of effective connectivity in fMRI and later was extended to EEG [111].

Granger causality is a data-driven technique and is based on the concept that cause precedes its effects. Quantification of this effect is achieved by using the notion of cross-prediction. If incorporating past values of a time series s1 improves future predictions of time series s2, then we can say that s1 has a causal influence in s2 [97]. Since this relation is not reciprocal the relations depicted from this measure can be efficiently represented as a directed graph. The Granger causality

concept has been generalized to multivariate signals by techniques as the Directed Transfer Function (DTF) [112] and Partial Directed coherence (PDC) [113].

For the estimation of effective connectivity in fMRI, Dynamic Causal modeling and Granger causality are the most widely used techniques. Dynamic causal modeling was originally developed for analysis of effective connectivity in fMRI. The main problem with the application of DCM is that it requires an a priori definition of the anatomical network and its computational complexity restricts its inference capability to a limited number of networks [114].

Granger causality has been applied in fMRI data using more or less the same methodologies used for functional connectivity. For example it has been applied to calculate effective connectivity of a target region to the other voxels in the brain [115], [116]. A promising approach, inspired from FNC, uses Granger causality in order to quantify effective connectivity between derived Functional Networks in patients with Schizophrenia and provides a different point of view in the fusion of EEG and fMRI [117].

2.7. Fusion in the network Space

Measures of functional and effective connectivity, as described earlier, can be used to construct directed or undirected graphs between brain regions or electrode sites. Individually in each modality, there exists a number of studies that use graph theoretical approaches in order to describe the underlying networks [95]. The extracted networks from each modality cannot be directly compared, though. Regardless the differences in their temporal scale, the nodes of the extracted network in each case represent different things. For the fMRI the nodes of the network are brain regions while in the EEG case the nodes are mapped to electrode sites. Although, a direct

comparison is not possible, the general topologies can be used to combine information from the micro to the macro level.

Few studies exist that attempt to fuse EEG and fMRI in the context of functional integration. The majority of studies presented, are calculating functional or effective connectivity in only one modality. An early attempt to study EEG and fMRI under the light of functional integration is presented in [62]. In this work, fMRI was used to inform and constraint the inverse source localization of the EEG. The time courses of the EEG were used to calculate causality using the Direct Transfer Function. Nevertheless causality was computed based only in the EEG data and information from fMRI is used only to constrain the source localization solution.

Recently, the work presented in [118], proposes the fusion of EEG and fMRI in network space. They use the term multimodal FNC (mFNC) to describe their methodology. They use spatial ICA to decompose both modalities into independent components and extract FNs from each modality. Then, Granger causality is calculated between independent components of each modality. Source localization is used in order to localize the EEG independent components and test whether can be associated with a fMRI FN.

Matched EEG-fMRI FNs are assumed to represent the same neuronal populations. This approach is consistent with the model that explains the neuronal activity as expressed by fMRI and EEG, presented in Figure 2.4. Figure 2.5, presents an illustrative description of the concept of FNs in EEG-fMRI integration.

The problem of how to correspond network nodes between modalities is solved using source localization in order to map the scalp surface EEG activity to brain regions. This is an active field and the use of networks and graph theory for fusing information between modalities looks promising.

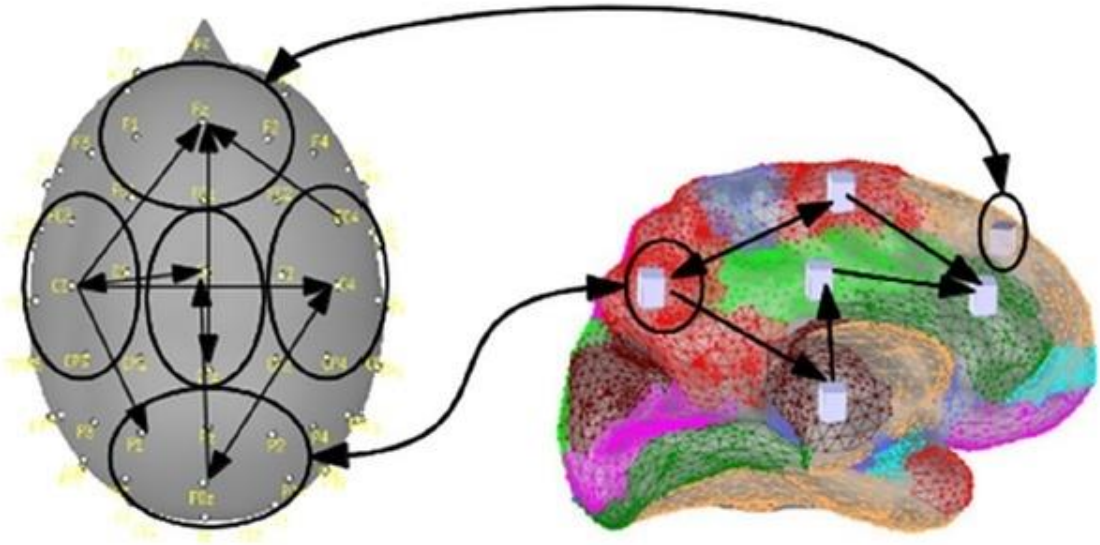

Figure 2.5: Illustration of the explained activations and their connectivity. Notice that the activations related to only one modality can now be indirectly linked.

2.8. Discussion

Illustration of the explained activations and their connectivity. Notice that the activations related to only one modality can now be indirectly linked. We described methods and measures used for the analysis of Event Related Potentials and discussed the complex activations that take place and the debate about their generating mechanism. The excellent temporal resolution of the EEG allows the study of the different brain activations in the millisecond scale and new techniques and methodologies enhance our knowledge and understanding of how brain works. Moving beyond isolation and connection of specific EEG features to specific cognitive processes, functional

integration as expressed by functional connectivity and effective connectivity will help to solve or clarify how the individual brain components work together and synchronize in time.

Analysis of fMRI has made great advances toward identifying brain regions activating in response to a task and provide supplementary spatial information that EEG cannot provide. The advances in fMRI depend not only in the accuracy of the system or the magnetic strength but also on the tools for analysis. Independent component analysis allowed the performance of complex experiments which would be difficult to model under the GLM and allowed the exploration of complex mental states and perhaps more significantly, the exploration of the so-called rest-state.

Fusion between EEG and fMRI looks very promising since the strong feature of the one is the weak of the other. Reality though, proved more complex and EEG and fMRI fusion is still an open area for research. The main problem is that there is not a one to one correspondence between active fMRI regions and EEG activations. Data-driven techniques that look for common pattern between the two modalities look very promising and provide a different view in the single trial analysis which could help solve open problems in both fields.

Of course, there is room for improvement especially in the part of the EEG where a lot of information has been left unexploited. In contrast with the wealth of information revealed in the single trial analysis of EEG data the majority of studies of the EEG-fMRI fusion seem to use only a portion of the available features, disregarding a lot of information and in a sense, canceling the advantages gained by the analysis of EEG. Finally, the emerging trend of fusion of the two modalities in the network space seems promising and will allow for a more in depth understanding of the underlying mechanisms.

CHAPTER 3: **LG graph representation of EEG topography**

Electroencephalogram (EEG) records the electrical activity of the brain and has been widely used for the study of brain functions and pathologies [119]–[121]. Since the isolated electrical activity of a single neuron is too weak to be captured by the electrodes in the surface of the head, the measured electrical activity recorded is the combined activation of large group of neurons, synchronously activating. The produced electrical current propagates through the brain structures and the scull to the head scalp. Due to volume conduction the recorded electrical activity in the electrode is the summation of multiple sources activating at the same time. Therefore, we cannot directly derive the part of the brain that produced the recorded activity.

Event related potentials (ERP) are brain activities recorded as a response to a specific stimulus or event, as we saw in previous chapters. In order to identify the activity associated with the given stimulus the experiment is repeated many times and the individual trials are averaged. The resulting waveform is examined at a specified electrode or electrodes and features like amplitude and latency of different peaks are extracted. ERP allows us to associate such EEG features with physiological features or processes [1]. Over time advanced signal processing techniques have been utilized to extract information from the averaged waveform as well as the single trials [121], [122]. Often, the

analysis is restricted in a certain time window and electrode, where the appearance of the brain response is expected. Different algorithms have been proposed in order to identify the optimal electrode and/or the most interesting segment of the EEG in time [123]. The problem with this approach is that these measures are dependent to the experimental setup. The choice of the reference electrode affects the amplitude and phase of the signals in the different electrodes and significantly impacts the statistical outcome of the analysis and its interpretation. Additionally, the a priori selection of an electrode and/ or time interval introduces bias in the analysis and may ignore other related components lying outside the predefined spatial and temporal regions.

Although, this approach has been proven to be quite successful and has provided useful insights in the brain functionality, there is still the need to take full advantage of the provided EEG information. Towards this goal, an alternative methodology has been proposed that moves the EEG analysis from the temporal to the spatial domain and considers the electrical field in the electrodes at each time point [124], [125]. The main advantage of this approach is that the distribution of the electrical activity in the electrodes is independent of the reference electrode [124]. Topographic analysis of the EEG offers a different view in the EEG data and has been proven capable to offer new insights on the brain functionality [126]–[128].

The basic idea is that a certain topographic configuration at a certain point in time is caused by a number of active sources in the brain [7] and subsequently certain topography reflects a distinct brain functional state. In order to describe such functional states, information from all electrodes should be used in an equal way. It has been shown that the topography of the electrical field does not vary randomly with time but rather displays short periods (50-100 milliseconds) of stable topographical configurations followed by a period of instability before moving into a new stable configuration [124].

These stable topographic configurations known as microstates are considered the basic elements that reflect the brain state over the given time interval that the EEG was recorded. Although the same topographic organization is result of the same underlying sources, it is reasonable to assume that different distributions of the electrical field in the scalp represent different brain states.

At each time point the functional state of the brain is represented by the topological configuration of the electrical field. Each state can be mapped into the N-dimensional sensor space and then apply machine learning techniques in order to find formed classes of spatial maps in this N-dimensional space [127]. With denser electrode configurations and taking under consideration the volume conduction effect, the dimensionality increases without a necessary increase in the descriptive power of the topographic map.

In this chapter, a new method for characterizing stable topographic maps in the EEG is presented. The derived methodology uses the Local Global graph in order to model and represent the topographic activity at each time point of the EEG, while at the same time reducing the complexity of the problem. In the next section, we present methods for the characterization of the spatial EEG information. Then, the building blocks of our methodology are described and their application in the analysis of ERPs. Finally, results of this methodology in real EEG data are presented.

3.1.1. EEG microstates

The microstate model takes under consideration the spatial distribution of the electric field in the scalp also known as topographic map. It has been observed in [124] that a certain topographic map remains stable for a period of time before it changes abruptly to a new configuration. These

time segments can be interpreted as functional states of the brain that reflect basic elements of information processing. So a change from one stable microstate to another indicates an alteration of the functional state of the brain. Such microstates have been considered as the atomic elements of higher cognition [6]. The information carried by the sequence of microstates does not imply that the information processing in the brain is strictly sequential, but rather captures the dominant processes, active at the given moment [6].

Initial approaches for the identification of the dominant microstates, involved the extraction of a set of distinct features that characterize the map. Such features are the locations of the different peaks and the amplitude and/or the polarity of these peaks. Analysis is often limited to the values of maximum positive and negative peaks of the map as preprocessing step to simplify the analysis and interpretation of the results. This choice is also inspired by the dipole like modeling of EEG sources and reflects the anticipation of a single active brain source.

Several other metrics have been proposed that attempt to quantify and describe the different configurations of the topographic map. Global Field Power (GFP) is a measure of the power of the electric field in all electrodes and is formulated as the standard deviation of the electrodes at a single time point [7]. It is defined as follows:

$$\mathrm{GFP} = \sqrt{\frac{\sum_{i=1}^{N}(v_i - \hat{v}_i)^2}{N}} \tag{7}$$

where the v_i is the voltage in each electrode ian $\hat{v}_i$ is the mean over all electrodes N. This measure is independent of the reference electrode and quantifies the flatness and hilliness of the map. It has been used in order to normalize the electrode amplitude before comparing the various topography maps.

Based on GFP, a measure of the distance between two maps has been defined as:

$$\mathrm{GDM} = \frac{1}{N}\sum_{i=1}^{N} \frac{(v_i - \hat{v}_i)}{\sum_{i=1}^{N} \frac{(v_i - \hat{v}_i)^2}{N}} - \frac{(u_i - \hat{u}_i)}{\sum_{i=1}^{N} \frac{(u_i - \hat{u}_i)^2}{N}} \tag{8}$$

where v_i and u_i are the potentials of the electrodes of the two maps [7]. This measure is known as Global Dissimilarity Measure (GDM) [7]. Based on these measures statistical tests have been developed in order to identify significant differences between conditions or groups of subjects [7].

Different techniques have been developed in order to identify the microstates present in an EEG recording [129]–[131]. A series of preprocessing steps, common in most methods, are carried out before the actual analysis. Each topographic map is centered to the mean over all electrodes and the maps are normalized by dividing with the standard deviation of the measurements [7]. Since the electric field oscillates at different bands, the polarity of the electric field also varies while the overall relation between the channels remains the same. Examining the power or the absolute values of the map allows the identification of microstates regardless their polarity.

The first attempts for the identification of microstates were based on sequential algorithms comparing the position of the negative and positive extremes of the topography in two successive maps. This approach was able to identify periods of stable topography were the difference between the maxima remained small, under a certain threshold [124]. More recent methods treat the problem using clustering approaches [127], [7]. In [127] a modified version of the k-means algorithm was employed for the segmentation of the EEG into microstates. Agglomerative clustering algorithms have also been employed for this purpose. The temporal continuity is either enforced in the clustering procedure or a post-processing step reassigns maps to clusters based on the constraint that nearby (in time) maps must belong to the same microstate [130].

These techniques have been applied in on-going EEG recordings and ERP data as well. There has been an effort to identify basic microstates that represent the sequence of information processing under different conditions. The majority of these studies identified four to five microstates as capable to explain the dynamics of the electric field topography over time [132]. Specifically, in ongoing EEG studies four microstate classes have been identified with their duration and frequency changing with age [6]. The microstate duration has also been associated with sleep states and wakefulness [133]. Different pathologies have been also related with differences in the number of identified states, their duration and their variance [134]–[136].

3.2. The Local Global Graph

3.2.1. Local Global Graph

Local Global Graph (LG graph) is a well-known technique with many applications in computer vision. In general, a graph can be represented in different ways like the Voronoi Tessellation [139] and Delaunay Graph [140]. Graphs have been used successfully for image segmentation [141], object recognition and image understanding applications [142].

The main property of graph modeling is the application of distance constraints in the defined nodes and it can be used to model the relation between pixels for image segmentation, relation between regions for part based object detection and relations between segments for context based image understanding. It is obvious that the aforementioned tasks have a hierarchical relationship, as we are moving from objects to scenes. The LG graph takes advantage of this hierarchical nature and combines the local information of the object along with the global information of the image, which is the relationship between objects.

The LG graph extends the information that the graph holds by attaching information about each node. We can describe each segment of the image as a graph describing the shape of the region. Other information such as the color of the region and geometric properties of its shape can be retained in the graph of its region. Along with the centroid of each region, this local graph can be considered a node of the greater graph representing relations between segments of the image.

In the LG graph, the nodes of the Global graph are considered to be the segmented objects of the image. In this case, the relationship between the nodes represents the geometrical relationship between segments in the image. Connection between the nodes can be calculated using the Delaunay triangulation. We want to further simplify the relationships between the regions of the image and for this reason a node can be arbitrarily chosen and only connections to this node to be taken under consideration. The idea behind this simplification is that we can full characterize the geometrical relations between nodes by keeping only their relations to a common reference and discard redundant information. This step is not necessary and depends on the specific application.

3.2.2. LG graphs for modeling of the EEG topography

Segmentation

The first step is to obtain the topographic maps for each point in time from the multichannel EEG. We remove the mean from each channel and then for a given time point we colorcode the values in the electrodes, representing minimum with blue and maximum with red and the natural neighbor interpolation method is used to interpolate the values in the space between the electrodes [143].

Our goal is to group channels into regions that present similar activations. The watershed segmentation algorithm uses the local minima in the image as initial points (seeds) and then the

regions are growing from each seed, until the borders of one region reaches the limits of another [144].

Since we are interested in the spatial structure of the electric field, we normalize each map by its GFP. The main advantage of this algorithm is that it creates compact regions that represent similar activity without using any prior knowledge about the number of regions that we expect to produce. The segmentation step provides a natural way to reduce the dimensions of our problem and still remain in the sensors space. Next we present the Local Global Graph and its application for the spatial analysis of the EEG.

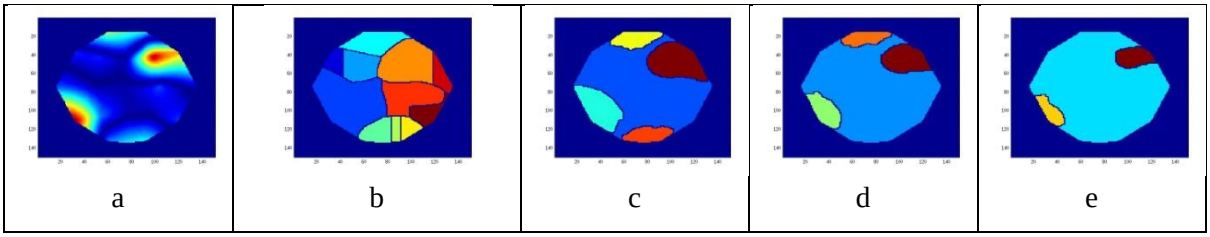

Figure 3.1: Different levels of segmentation obtained by the marked watershed algorithm. Image b displays the original watershed algorithm which results in over-segmentation of the topography. In C, D and E, results of the marked watershed approach are displayed, using different levels for the background.

3.2.3. Modeling using the Global Graph

The Local Global Graph (LG graph) as we already noted, is a method for modeling the structural (global) information in images while preserving the local characteristics of the individual nodes [145]. In essence is an attributed graph that holds local information in each node. The general idea is that we can fully characterize the geometrical relations between nodes by keeping only their relations to a common reference and discard the redundant information.

In our case we model each topography map using the LG graph structure. Our goal is to extract the significant features of the topography map (the peaks and valleys) and use them as nodes of the

global graph. For this purpose, we treat each topography map as an image and we perform a segmentation step in order to extract the major peaks.

As a preprocessing step, we remove the mean from each channel and normalize each channel by the standard deviation of the individual map. We arrange the electrode values in a Cartesian grid according to their given coordinates and we color code the values in the electrodes, representing minimum with blue and maximum with red. The natural neighbor interpolation method is used to interpolate the values in the space between the electrodes [146]. This is a popular interpolation technique that has been used extensively [147].

Our goal is to group channels into regions that present similar activations. The marked watershed segmentation [148] creates compact regions that represent similar activity without using any prior knowledge about the number of regions that we expect to produce. The threshold for background identification can be adjusted depending on the application and the data at hand. The result of the watershed algorithm is equivalent as taking the iso-contours of the electric field for defining peaks and valleys in the map [149].

The centroids of the segmented regions of the map (excluding the background) will be used as the nodes of the LG graph. The centroid is defined as:

$$\mathrm{centroid}(x, y) = \left(\frac{\sum_{x,y} x * I(x, y)}{\sum_{x,y} I(x, y)}, \frac{\sum_{x,y} y * I(x, y)}{\sum_{x,y} I(x, y)} \right) \tag{9}$$

where I(x, y) is the value at the point (x, y) belonging to the region R of the map. The centroid is directly affected by the field distribution in the given area and is representative of the underlying field. Therefore, changes of the field inside a region will be reflected in the centroid.

In each node we attach set of attributes that characterize the region. These attributes are the mean amplitude and power of the region, the channels contained there and the number of pixels

that the segmented region contains. These attributes define the local information of the LG graph. We can use this information to compare regions for changes and provides a compact local descriptor of the topographic map.

3.3. LG graph similarity

The problem of defining the distance between two topographic maps can be seen as calculating the distance or similarity between two LG graphs. In order to compare two graphs, the first step is to find the nodes that match between the two graphs. This is achieved by using the local attributes of each node. The similarity between two nodes is defined as the overlap of the two regions. The Jacard similarity measure is used for this purpose as following:

$$S_{i,j} = \frac{r_a^i \cap r_b^j}{r_a^i \cup r_b^j} \tag{10}$$

In this case r_a^i, r_a^i represent the regions of the two topographies under consideration.

This measure displays the degree of overlap between two regions and is calculated for each region in graph A versus all the other regions in graph B. Nodes are assigned together, starting from the pair with maximum similarity and moving in descending order to the other nodes that present a degree of overlap. This measure is used to establish node correspondence between the two graphs.

Once we have the matching nodes we can proceed with the calculation of the global similarity between the two graphs, based on the amplitude of the region's electrical field. For calculating the global similarity of the two graphs we define the following quantities:

$$S_{field} = \frac{\sum_{i=\{M_{i,j}\}} \sum_{j=\{r_a^i \cap r_b^i\}} \left| r_a^i(j) + r_b^i(j) \right|}{\sum_{i=\{r_a\}} \sum_{j=\{r_a^i\}} \left| r_a^i(j) \right| + \sum_{i=\{r_b\}} \sum_{j=\{r_b^i\}} \left| r_b^i(j) \right|} \tag{11}$$

$$S_{centroid} = 1 - \frac{\sqrt{(r^{i}_{centroid_a} - r^{i}_{centroid_b})^2}}{d} \quad (12)$$

In equation 11 r_a and $r_b$represent the regions of graph A and B respectively, while$\{M_{i,j}\}$ is the set of matched regions between the two graphs. In equation 12, $r_{centroid_a}$and $r_{centroid_b}$ represent the locations of the corresponding centroids. Parameter d is the maximum distance between two points in the topographic map.

The final similarity between the two graphs is defined as the product of these three quantities and qualifies as a metric since it has an upper limit with maximum value of 1, it is symmetric and takes the maximum value only when the two graphs are identical. Using the distance between the centroids ensures that the maximum value is achieved only when we have identical graphs. Finally, the sign of the similarity is determined by comparing the polarities of the matched regions.

Using this methodology we are able to robustly represent topographic maps and compare them together efficiently, even in the presence of noise. We can use this metric to quantify the similarity of consecutive topographies of the single trial activations.

3.4. Results

We applied the LG graph methodology in an ERP data set obtained from a single healthy subject performing an auditory oddball experiment. 27 channels were used to record the EEG and the data were sampled at 1024Hz. Each trial has1300 samples and the auditory stimulus occurred at 600ms. We used 40 trials that correspond to the target stimuli in order to generate the average ERP in each channel. A detailed description of the full dataset can be found in [122].

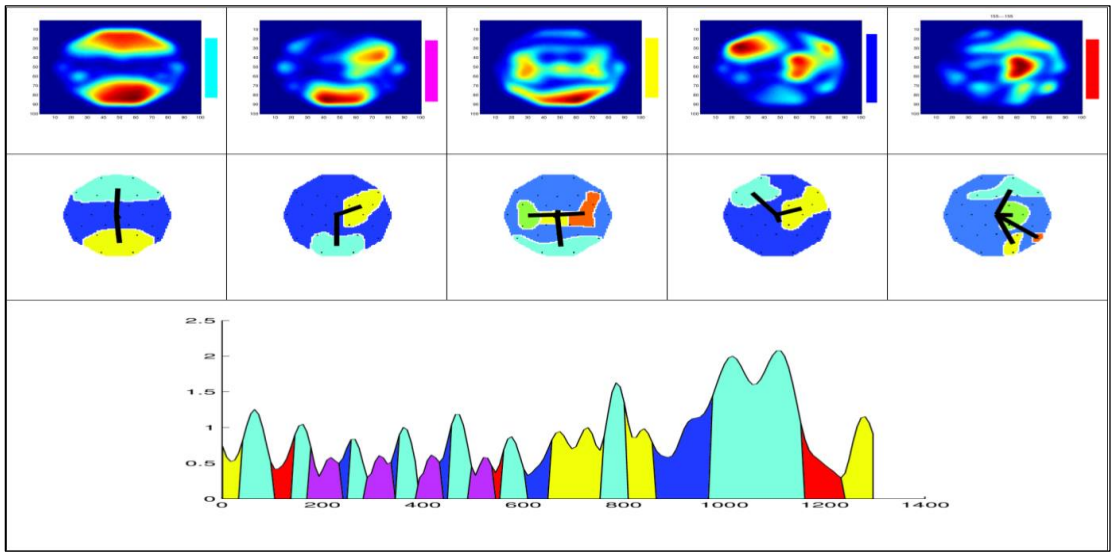

Figure 3.2: Row a. Four stable maps identified in the average ERP. The bar next to each map represents their label. These maps correspond to the 88% of the total time points. Row b displays the corresponding LG graphs. Row c displays the distribution of the microstates in time.

We calculated the average ERP of the wideband signal and for each time point, we applied the LG graph methodology. A simple sequential algorithm was employed in order to find stable topographic maps and perform a first evaluation o our methodology. The LG graph of the first point in time formed a cluster and the distance from all the other graphs was calculated. The graphs that presented high similarity (>0. 8) with the initial, were considered as part of the same cluster and were labeled accordingly and removed from the set. The next ungrouped graph was used to form the next cluster and the same procedure continued.

Finally, when all the clusters where formed a merging procedure was applied and clusters that presented high similarity were merged together. Following this procedure we extracted 4 major microstates which account for the 88% of the total activity in the average ERP. The extracted graphs

and can be seen in Figure 3.2 (row a and b), where the maps and the resulting graphs are displayed, accordingly.

Table I

Microstate Properties for pre and post stimulus periods

Variance explained	**Microstate 1**	**Microstate 2**	**Microstate 3**	**Microstate 4**
Prestimulus	27.7	20.2	31.1	21
Poststimulus	38	27.8	16.2	18

In Figure 3.2-row c, the explained GFP from each microstate is presented in time. We can see that the different microstates stay active for a short duration in time. All four microstates occur equally and interchange rather rapidly. In contrast, the green and red microstate dominates the post stimulus. As can be seen in Table I, the two microstates present increased duration compared to their prestimulus behavior.

3.5. Conclusion

Modeling each segmented map using the LG graph methodology, we transform the problem from the channel space to a LG graph matching problem. We take advantage of the hierarchical properties of the LG graph and we simplify the matching procedure significantly, without sacrificing the descriptive power of our features. A major advantage of this methodology is that the LG graph is flexible enough to incorporate different local and global measures at the same time, a fact that allows for different queries and views in our data.

CHAPTER 4: **Modeling EEG single trial microstates using Local Global graphs and Discrete Hidden Markov Models**

4.1.1. Introduction

EEG recordings provide a wealth of information regarding the underlying brain activity in the millisecond scale. Event related potentials (ERP) are EEG recordings that take place under a certain experimental setup in an effort to elicit a specific brain response to a specific stimulus or event. As we saw, in order to identify the activity associated with the given stimulus the experiment is repeated many times and the individual trials are averaged. The resulting waveform is examined at a specified electrode or electrodes and features like amplitude and latency of different peaks are extracted. ERP allows us to associate such EEG features with functional processing of the stimulus and other cognitive functions [1].

A variety of techniques have been developed and applied to EEG recordings in order to extract descriptive features from the multichannel EEG. The majority of studies are geared towards the exploration of the time and frequency characteristics of the multichannel EEG signals. This approach usually entails the selection of a single channel on which the analysis of signal properties

is performed [120]. The selection of the electrode is mainly subjective and aims to specify electrodes that maximally represent certain features considered important in the experimental setup [120].

Choosing the right electrode or sets of electrodes is not a trivial problem, with many different factors to be taken under consideration. Due to volume conduction, the recorded electrical activity forms the summation of multiple sources that activate in coordination. In this context, choosing a single electrode for analysis seems to be rather problematic, since various electrodes may capture different aspects of the underlying brain activity. Multivariate techniques as Principal Component Analysis (PCA) and Independent Component Analysis (ICA) have been employed in an effort to alleviate this problem [13], [24], [119], [149].

PCA has been used in order to summarize the correlated activity of the different electrodes into a few principal components that can capture the variation of the multichannel EEG. Unfortunately, the orthogonality constraint imposed by PCA seems to be quite strict and it is difficult to associate the individual components with meaningful physiological activity [23]. ICA has been used in order to decouple the multichannel recordings into independent components in an effort to alleviate the mixing effect of volume conduction [119]. The main problem with this approach is that the resulting independent components have to be inspected in order to distinguish the ones that capture related brain activity and therefore a similar problem to the electrode selection rises again.

The traditional ERP analysis follows a similar procedure and considers the different trials of the experiment and averages them together in order to amplify the task-related activity over the ongoing background EEG activity. A certain electrode is identified and analyzed for the extraction of features of the average waveform. Efforts to use single trials in order to extract features usually betake to ICA or PCA in order to enhance the related activity from noise.

A different problem that affects this kind of analysis is that the derived measures and features are dependent on the experimental setup. The EEG recordings are taken in reference to some ground electrode that provides the baseline over which the measurements are made. This electrode is considered to be unaffected from brain activity. Unfortunately, this assumption is not valid and the choice of the reference electrode affects the amplitude and phase of the signals in the different electrodes and significantly impacts the statistical outcome of the analysis and its interpretation [127]. Additionally, the a priori selection of an electrode and/ or time interval introduces bias in the analysis and may ignore other related components lying outside the predefined spatial and temporal regions defined for analysis.

Nevertheless, despite its limitations, this approach has provided results that gave useful insights regarding brain pathologies or functionality [118], [150]. An alternative view on the collected EEG data has been proposed focusing on the spatial properties of the multichannel EEG and considering the electrical field in the electrodes at each time point. The main advantage of this approach is that the distribution of the electrical activity in the electrodes is independent of the reference electrode [121] and therefore the results remain unaffected by a change in the reference electrode.

In the previous chapter, we introduced a new measure used for this type of analysis, also known as topographic or microstate analysis. The microstate approach has been proven capable to derive new insights on the brain functionality [136]. The assumption is that a certain topographic configuration at a certain point in time is generated by a number of brain sources [127]. Therefore, it is reasonable to assume that certain topography reflects a distinct brain organization or functional state, at that time. The relationship between the observed topography and the active sources is not bi-directional, since different brain sources may produce the same topography, but one can claim that a change in topography certainly reflects a change in the active brain sources. Furthermore, it

has been shown that the topography of the electrical field does not vary randomly with time but rather displays short periods (50-100 milliseconds) of stable topographical configurations followed by a period of instability before moving into a new stable configuration [121], [127], [136].

These stable topographic configurations known as microstates are considered as the basic elements that reflect the brain state over the given time interval of EEG recording. At each time point the functional state of the brain is represented by the topographical configuration of the electrical field. Each state can be mapped into the N-dimensional sensor space and pattern recognition and machine learning techniques can be employed in order to find formed classes of spatial maps in this N-dimensional space [126]. Different studies have shown that there exist relations between the pre-stimulus microstates and the post-stimulus response [136] and also provide evidence that the temporal relations of the sequence of microstates includes important information.

Nevertheless, little effort has been devoted to the application of the microstate analysis on the single trial ERP [151], [152]. The main problem is that the single trials are inherently noisy and thus it is difficult to identify the major microstates. Another problem with the analysis on single trials is that after each trial has been segmented into microstates it is difficult to assess and interpret the result in a meaningful way.

A methodology for the identification of EEG microstates that uses the Local Global (LG) Graph structure as a means to describe and characterize the EEG topography at each time point was presented in the previous chapter. Local Global graph are attributed graphs that have found many applications in computer vision and image understanding problems. In our case, the LG graph provides a structural representation of the EEG topography and provides a robust comparison between the structural configurations of different topographies. Based on the LG graph descriptor

we present similarity and distance measures that can be used for the comparison of the extracted LG graphs in the presence of noise. This chapter is structured as following: In the next section the overall methodology, definitions and methods for microstate segmentation are presented. Next described the Hidden Markov model approach to microstate segmentation of the signal is described and this chapter closes with the application of the aforementioned methodology in data from normal and Progressive Mild Cognitive Impairment subjects.

4.2. The overall methodology

The overall methodology is illustrated in Figure 4.1. For each time point in the multichannel

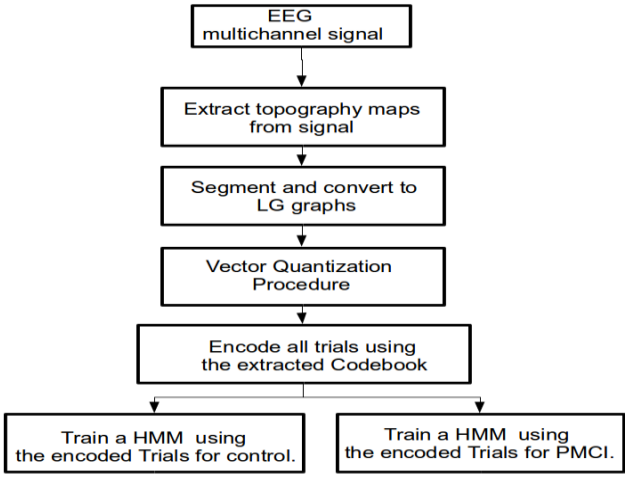

Figure 4.1: The overall procedure used for the estimation of HMMs from single trial activity

EEG signal we extract its topography map and we apply image techniques for the extraction of important features.

Segmentation is applied in order to get the dominant activated regions and from the segmented image we extract the Local Global graph (LG graph). In order to extract the various microstates a quantization step that allows characterizing the different topographies by a compact codebook. Each cluster is treated as a single state and we model the transitions from one state to the other,

using Hidden Markov models (HMM). This way we are able to capture the spatio-temporal evolution of microstate configurations in the single trials. The details of the LG graph methodology, clustering and HMM modeling is presented in the Methods section.

Under this formulation the single-trial microstates, instead of being conceived as periods with quasi-stable topography, are rather considered as periods with stationary distribution of topographies. Recent studies [153] investigated the transition between identified microstates and compared these interactions between groups of normal, subjects with schizophrenia, Alzheimer and Frontoteporal dementia and found differences in the syntactic patterns, as they called them. In this study, the HMMs serve a dual role; on the one hand to segment the single trials into microstates under the assumption of stationary distribution of the topographies. On the other hand, the estimated HMM describes effectively the transitions between the microstates or in other words the syntactic patterns that can be observed in single trials.

We use the aforementioned methodology in order to train HMM from normal and Progressive MCI subjects and use these models to distinguish between the two groups. Discussion on the results and the interpretation is following in the discussion section.

4.3. Identifying EEG microstates

Different techniques have been developed in order to identify the microstates present in an EEG recording [128]–[130]. Most of them include some common preprocessing steps. Each topographic map is centered to the mean over all electrodes and the maps are normalized by dividing with the standard deviation of the measurements [127]. Since the electric field oscillates at specific bands, the polarity of the map of the electric field also changes while the overall relation

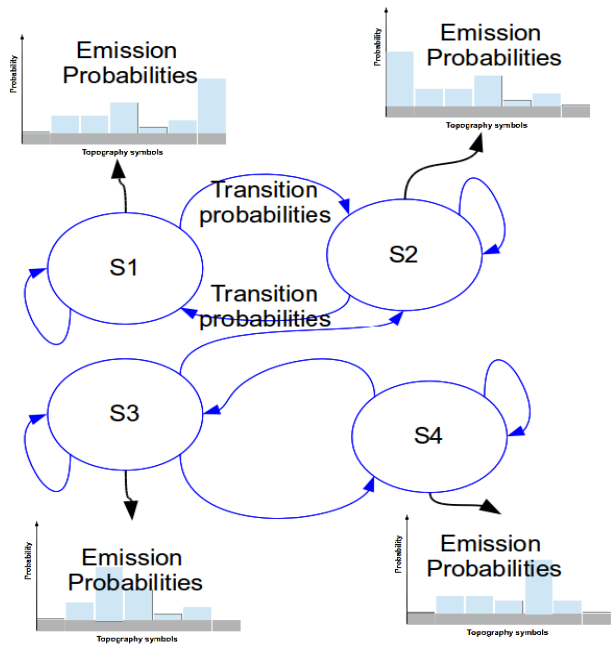

Figure 4.2: The HMM model. Each hidden state represents a microstate under which the probabilities of the observed topographies follow a certain distribution.

between channels remains the same. Examining the power or the absolute of the map allows the identification of microstates regardless their polarity.

The first attempts for the identification of microstates were based on sequential algorithms that were using the position of the negative and positive extremes of two successive maps. This approach was able to identify periods of stable topography were the difference between the maxima remained small, under a certain threshold [121].

Recent methods are treating the problem as a clustering one [125], [127]. In [125] a modified version of the k-means algorithm was employed for the segmentation of the EEG into microstates. Agglomerative clustering algorithms have also been employed for this purpose. The temporal information is either embedded in the solution and usually a final post-processing step reassigns

maps to clusters based on the constraint that nearby (in time) maps must belong to the same microstate [129].

4.4. Application of the microstate model

Such clustering approaches have been applied on ongoing EEG recordings and data collected from Event Related Potentials (ERP). The main goal is to identify microstates that represent the information processing taking place under different conditions. The majority of the studies consider four to five microstates as capable to explain the dynamics of the electric field topography over time [154]. Specifically, in ongoing EEG studies four major microstate classes have been identified that their duration and frequency is affected and changes with age [123]. The duration of microstates has also been associated with sleep states and wakefulness [132]. Different pathologies have been also related with differences in the number of identified states, their duration and their variance [133]–[135].

Application in ERP data revealed that different microstates characterize the brain processing associated with the various types of stimulus. Microstate patterns have been identified for visual, auditory and somatosensory stimuli in different studies [135], [136]. The majority of ERP analysis is based on the analysis of the average ERP and little effort has been devoted in the analysis of single trial ERPs. A major problem that held back the exploration of the microstate model in the single trial domain is that the single trial ERP is characterized by low signal to noise ratio and therefore it is difficult to identify stable microstates. Another problem with the analysis of the single trials is that the volume of data to analyze becomes quite large, making the interpretation of the results difficult.

In this work we introduce an alternative methodology for the analysis of the topography of single trial ERPs. We will use it to identify common topography patterns appearing in the single trial data. Instead of trying to directly segment the signal into periods characterized by a single topography map, we explore a different approach that uses clustering as an intermediate step to perform quantization of the data and build a vocabulary of topography maps. These maps can be used to approximate the single trials topography in a compact, yet detailed manner.

Using the quantized codebook, we segment the signal into spatially stationary states using Hidden Markov Models (HMM) [137]. The main idea is that we can train a Hidden Markov model using the single trial sequences of topography maps and use it to predict the underlying microstates of the signal. The trained model effectively summarizes the transitions between the states and can be used in order to distinguish between pathological conditions or functional states. In the next section we will describe the distance measure between topography maps used and the HMM methodology for modeling single trial EEG microstates.

4.5. Methods

The first step for microstate segmentation is to define an appropriate measure of distance or similarity between two topography maps. Most of the measures proposed, treat each point in time as a multidimensional vector and under this formulation well known distance measures between vectors can be applied. As we mentioned earlier, GMD is such a measure and it the equivalent of the Pearson correlation coefficient between two vectors. Other measures that have been used are the cosine similarity [130]. These measures provide an objective estimation of the distance between two maps.

The main problem with the vector approach is that it disregards the spatial information of each channel and therefore it is sensitive to noise and spurious activity in isolated channels. On the other hand, maxima based measures are too coarse to fully characterize the map and missing important peaks due to noise significantly affect the result.

4.6. Local Global Graph

The Local Global Graph (LG graph) is a method for modeling the structural (global) information in images while preserving the local characteristics of the individual nodes [144]. In essence is an attributed graph that extends a graph by letting it hold local information in each node. The relationships between the nodes represent the geometrical relationship between regions of the image. To further simplify the representation, a node can be arbitrarily chosen and only connections to this node can be taken under consideration. The general idea is that we can full characterize the

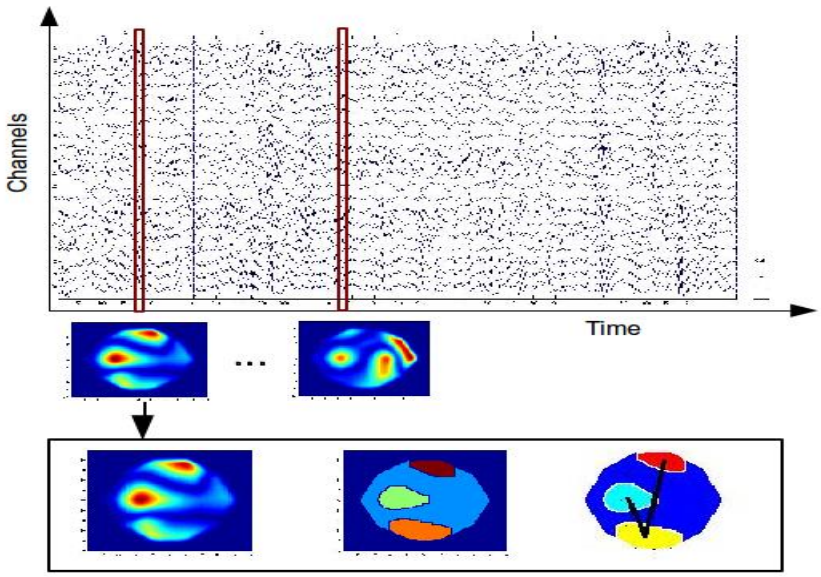

Figure 4.3: Illustration of the LG graph modeling procedure. From the multichannel signal we extract the topography map. The dominant features of the map are used to create the LG graph.

geometrical relations between nodes by keeping only their relations to a common reference and discard the redundant information. The methodology for modeling using the LG graph is described in detail in Chapter 3.

4.6.1. Modeling Single trials using HMM

The next step is to identify the dominant microstates and segment the signal into a sequence of quasi-stationary topographic maps. Different unsupervised learning techniques have been used that treat the ensemble of topography maps in the feature space. This approach disregards the temporal dependencies between neighbor topography maps and considers them as independent samples.

Hidden Markov models are a class of bivariate discrete-time stochastic processes that have no memory properties in the sense that the future depends only on the present state and is independent for any past states. Hidden Markov models have been used widely in the modeling of temporal sequences, with applications in speech recognition [137], pose estimation [155] and bioinformatics applications [156]. A hidden Markov model consists of an unobserved/hidden discrete Markov chain {Xn}, which describes the transition probability between states and the state-dependent observation variables {Yn}. The observation variables are conditionally independent given the current state and their distribution depends only on the current state. If the observation variables are discrete then the model is called a Discrete Hidden Markov model. The model can be described using a set of parameters $\lambda=\{\pi,A,B\}$ where π denotes the initial state probabilities, A is the transition matrix and B the matrix of the probabilities of the observable symbols.

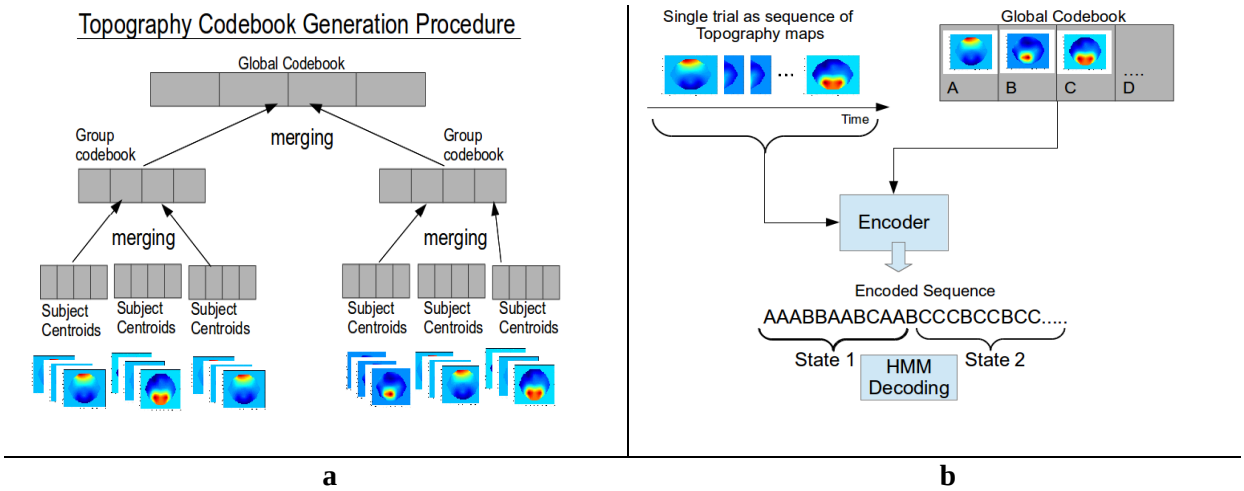

Figure 4.4: a) Illustration of the procedure used for extraction of the overall codebook. B) The resulting codebook is used for encoding the data and feed the encoded sequence to a HMM for training.

HMM have been used for modeling EEG data in terms of modeling the sequence of specific EEG features over a single or multiple channels [157]. In our approach we are using the series of topography maps as symbols emitted from a certain microstate. Each microstate is defined as periods with stationary probability densities for the emitted topographies.

Using this approach we can consider the microstate model as defined above in terms of states of a Hidden Markov model. The observations in our case are the series of topography maps and the distribution of the observed topographies depends on the current state. Figure 4.2 illustrates the model. This model takes under consideration the dependency of the topography over some time period and can effectively segment the multichannel signal into the sequence of states (microstates) without the need of further preprocessing or temporal smoothing.

An important aspect of this approach is the modeling of the observations' conditional distributions. In [158], HMMs were applied in intracranial EEG recordings and the conditional probabilities were modeled by a Gaussian mixture, treating the observation variables as continuous

ones. In our case, we consider a discrete model where the different topography maps are treated as discrete variables. This means that the observation sequence has to be transformed into a series of discrete values drawn from a single codebook. Next, we discuss the creation of this codebook and the implications on the model.

4.6.2. Topography Quantization

Our objective is to create an efficient codebook that can represent the different configurations of the electric field in the single trial, subject and group level. The motivation comes from the results in [153] that present results and conclude in differences by identifying a set of classes among different groups of subjects. Our goal is to transform the different maps of a sequence S to a discrete sequence of codebook indices drawn from the generated codebook.

We are using the LG graph methodology that we presented in Chapter 3 in order to model the topography maps. Using this LG graph representation we calculate the pair-wise distances between all graphs of a subject and build the proximity matrix. We use the single-link hierarchical agglomerative algorithm in order to merge graphs that are close together into a cluster. The single link algorithm is a well-known method, which has been applied many times for vector quantization with good results [159]. Using this procedure we can use a distance threshold to control the number of extracted clusters at each step.

We follow a hierarchical procedure for the extraction of the codebook moving from the subject level, then to the group and finally between group level. For each level, we extract from each cluster the graph that has the minimum mean distance in his group. These centrotypes are passed to the next level where the same procedure is followed between subjects and between groups until the global codebook is extracted. We illustrate this procedure at Figure 4.4b. The final codebook has

the centrotypes against which, the single trial data are going to be encoded by assigning the LG graphs to the symbol that minimize their between distance, as defined in equation 11.Using this scheme we create a finite set of topography maps, which can be used to transform the sequence of topography maps to a sequence of codebook indices. Each single trial, for all subjects, is encoded based on the global codebook extracted.

The fidelity of the quantization process depends on the number of symbols of the final codebook. The more symbols the better the reconstruction of the original sequence but in expense of increased computational cost introduced for encoding and estimating the emission probabilities. Therefore, the overall cost for estimating the Hidden Markov Model increases significantly. Another problem is that in such cases, in order to estimate the emission probabilities efficiently, a larger training set is required. There exists a trade-off between the error reconstruction and the computational cost involved. Using a small number of representative topographies will under-fit the data and, potentially mask differences between the microstates. On the other hand, using too many symbols increases the training time and the data needed for robust estimation of the parameters. This is a problem that can be solved analytically by trying different values of parameters and select the model based on certain cross-validation criteria. In our case, in the different levels we keep as many clusters as indicated by the given reconstruction error and this way we control the clustering procedure so that similar topographies merge together in order to reduce redundancy.

4.6.3. Classifying single trials using HMMs

The final step involves selection of the model structure, training and the estimation of the parameters for the Hidden Markov Model. Following the literature on microstates [134], [153] we

decided to test a Hidden Markov Model with four states. No other constraints were used in the structure of the model. We used the Baum-Welch [137] algorithm to estimate the parameters of the model.

Data were split into three sets, train, validation and, the test set. The train and validation sets are of equal sizes and 20 trials out of nine subjects were used for each. The test set had 10 trials per subject and there were no overlaps between the sets. The Baum-Welch algorithm is an Expectation Maximization algorithm and as such, convergence to a local minimum is not always guaranteed. Also, initialization of the algorithm plays an important role in the final result. We constructed multiple random initializations of the model parameters and trained the model using them. The trained models were evaluated on a disjoint validation set. The model that presented the highest log-likelihood on the validation dataset was kept for further consideration.

The discriminant function, used for classifying a sequence to one group or the other is based on the likelihood that the data sequence S is generated from the given model derived from normal or pathological subjects respectively. The discriminant function is then defined as:

$$D = \log\left(\frac{P(S|M_n)}{P(S|M_p)}\right) \geq e \tag{13}$$

Varying the threshold e, we can construct the Receiver Operator characteristic curve for the models under consideration.

4.6.4. Evaluation of the model

Besides classification we want to evaluate the learned HMM as a mean to extract the microstates from the observations. In this context we want to associate the Hidden states of the model with specific, physiologically interpretable microstates.

Each hidden state is characterized by the emission probabilities of the observed symbols. In our case these symbols are the distinct topographies used to construct the codebook and quantize the signal. Although these topographies are not the same, they certainly share common active regions. We can alternatively consider the emission probabilities of the HMM on the region level and interpret them as the probability that a given region will be active in the current state.

The emission probabilities reflect the probability that a certain map will appear at a given state. Therefore, in order to calculate the probabilities for each region we multiply the symbol probability with the normalized amplitude of the corresponding local regions. Adding these products together, for each state, results in a parametric map that characterizes the state and can be interpreted as the topography map of the hidden state. In vector notation the parametric map of each state is defined as:

$$\boldsymbol{m}(\boldsymbol{i}) = \sum_{\boldsymbol{j}=\boldsymbol{1}}^{\boldsymbol{symbols}} \boldsymbol{E}(\boldsymbol{i},\boldsymbol{j}) * \boldsymbol{C_j} \tag{14}$$

where$E(i,j)$ is the emission probability of symbol j for state i and C_j is the jth symbol map. The result is a topography map where each region is weighted by the total probability of activation in the current state.

Using the estimated transition matrix, useful statistics can be calculated regarding the modeled process. The time invariant probability of the underlying Markov chain represents fraction of time that a microstate is expected to be active during a large number of transitions. Using the limiting

probability we can calculate the average number of transitions from one state to the other in order to estimate the bias between state transitions. These quantities characterize the features modeled by the estimated HMM model and can be used in order to explore the differences between models.

4.7. Results

4.7.1. Data Description and preprocessing

The dataset was provided by the Clinical Neurophysiology and Neuroimaging Unit, University Hospitals of Geneva (Switzerland). All elderly individuals in the control group were screened with extensive neuro-psychological testing to confirm the absence of cognitive deficits [160]. The elderly control group used in this analysis consists of 12 subjects. MCI cases were recruited in a large acute and intermediate care geriatric hospital [160]. The final progressive MCI group consisted of 14 subjects. EEG data were recorded using 20 surface electrodes, according to the 10–20 international system. Subjects performed a visual detection task where background patches (non-target) and patches containing letters (target) were sequentially displayed in the screen. Detailed description of the experimental conditions and data acquisition can be found in [160].

We considered all trials from the visual detection task (detection of rare targets among standard stimuli), and from each trial we analyzed a portion starting 1500ms before stimulus presentation and lasting for 3500ms after the stimulus. Data were filtered in the 0.5 to 20Hz range. Trials that presented significant artifacts or noise were discarded from the dataset. After the rejection of trials with artifacts, a set of 70 trials was used from each subject.

4.8. Extracting the codebook

The LG graph was calculated for each map and the pair wise LG graph distance between the graphs of a subject was derived. The single-link hierarchical clustering algorithm was applied in order to extract the representative vectors at the subject level. The methodology described earlier was followed for the identification of among-group and between-groups representative topographies. Gathering the centroids of all subjects in each group a subsequent hierarchical clustering was performed and the representative graphs were extracted at the group level. Finally, the global codebook was constructed using the group level centroids in a final clustering step.

In order to test the effect of codebook length in the result we calculated the Receiver Operator Characteristic curves for different codebook lengths and for different HMM models. The results can be seen in Figure 4.5.

4.1. Training and classification results

Using this setup, we tested HMMs using different configurations. Since we are interested in correspondences with the classical microstate models, we tested our approach for four, five and six states, since the majority of the results in the literature have identified 4 to 5 microstates to be most prominent.

We used a leave-one-label-out cross-validation scheme. In this procedure, we calculated the codebook from a total of 11 control and 11 PMCI subjects, leaving one out from each class. From each subject 30 trials were used for training and a disjoint set of 20 trials per subject for the validation set. We trained the model of each class using 10 random initializations of the starting parameters on the training set.

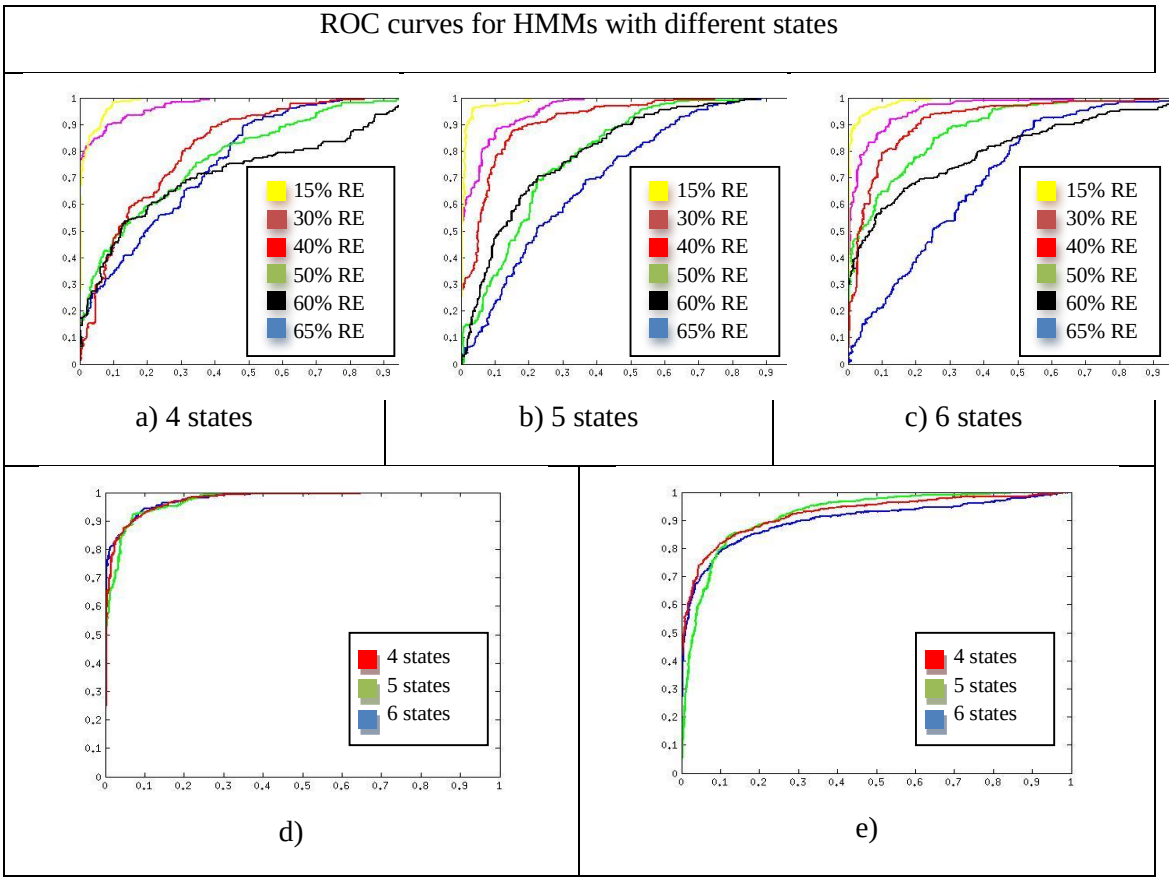

Figure 4.5: Figures a), b) and c) represent the results for different reconstruction errors for each state correspondingly. The ROC curves for HMMs with different numbers of states. We can see that the Figures d) and e) display the mean ROC curve for reconstruction errors >30% and <30% for 4, 5 and, 6 states. It is apparent that the number of hidden states does not affect significantly the classification results.

The validation set of 20 trials per subject was used to select the best fitted model. Finally, 30 random trials from the left out set were used to construct the test set and evaluate our classifier. We examined the results using the trials of the subjects not included in the training procedure. The mean ROC curve from the leave one subject out iterations was calculated along with the mean area under the curve (AUC) for each model and each reconstruction error. Each trial in the test set was decoded using the controls and one for the PMCI models respectively. Using the log-likelihood ratio between the posterior probabilities of the two models as in equation 13, test trials were

assigned to one or the other group. The results can be seen in Table II along with the ROC curve in Figure 4.5.

Table II. Receiver Operator Characteristic results
For the Test set

Reconstruction error	**4 States Model**	**5 States Model**	**6 States Model**
	AUC	**AUC**	**AUC**
15%(120 symbosl)	0.955	0.964	0.9675
30%(60 symbols)	0.905	0.914	0.9082
40%(20 symbols)	0.774	0.833	0.9046
50%(10 symbols)	0.661	0.764	0.7426
60%(5 symbols)	0.652	0.725	0.7655
65%(4 symbols)	0.586	0.557	0.6080

For each model we examined the results using codebooks of different lengths. The resulting ROC curves can be seen in Figure 4.5(row a). We can see that the accuracy of the system increases with the number of symbols used or alternatively with decreasing reconstruction error. This is something expected since the quantization error is smaller when using larger codebooks. We have to notice though that we found no significant difference when using number of symbols resulting in reconstruction errors below 30%, indicating that below that threshold we are probably capturing transient/noisy activity that adds little information in the distribution of topographies. It also indicates that a small number of topographies cannot sufficiently explain the variability of the single trial activations giving only a rough approximation that may mask important differences in brain response.

As we increase the number of states, we obtain better results for fewer symbols (Figure 4.5, first row). This was expected since as we increase the number of parameters of the HMM model, we get a better fit of the data. However, the computational cost increases significantly with the number of parameters and as we can see in Figure 4.5 the results do not justify selecting a higher order model. A different problem, although unrelated to the classification task, relates to the physiological interpretability of the hidden states which is discussed in the next section.

4.1. Discussion

4.1.1. Differences in duration and occurrence between controls and PMCI

Using the estimated models, we decoded the single trials using the Viterbi algorithm and we examined the statistical effect of different microstates parameters. Based on the decoded single trial sequences, we calculated the microstate duration and number of occurrences per group. The states of the two trained models were realigned so that a correspondence between the states of the two models is achieved. In Table III we present the mean duration and occurrence of the microstates per group.

Table III: Duration and Occurrence statistics

Mean duration			
	Controls	**PMCI**	**Significant difference(p<0.05) Simultaneous intervals Bonferroni corrected (p < 0.00625)**
A	20.238	14.810	*p= 12.86 10-6(Control)
B	18.425	19.000	*p= 0.000467 (Control)
C	20.012	18.847	*p= 6.86 10-6 (Control)
D	20.943	20.579	p= 0.00783 (Control)
Mean number of Occurrences / trial			
	Controls	**PMCI**	**Significant difference(p<0.05) Simultaneous intervals, Bonferroni corrected (p < 0.00625)**
A	35.200	28.344	-
B	30.949	39.757	*p= 0.0036 (PMCI)
C	25.713	28.272	-
D	36.014	39.981	-

We compared the two groups using two sample Hotelling's t^2 test. We are using this multivariate statistical test since it is clear that the parameters of one microstate affect the other. The Bonferroni correction has been applied in order to evaluate which parameter was responsible for rejecting the hypothesis. We can see that the duration of microstates A, B and C differ significantly between control and PMCI subjects. We can see that the PMCI subjects are expected to spend less time in microstate A and B and more time in microstate C compared to the normal subjects. On the other hand, only microstate C displayed significant difference in the number of occurrences between the two groups, with many more occurrences in PMCI subjects. In

conjunction with the duration results, microstate C appears to be the dominant state in PMCI along with microstate D.

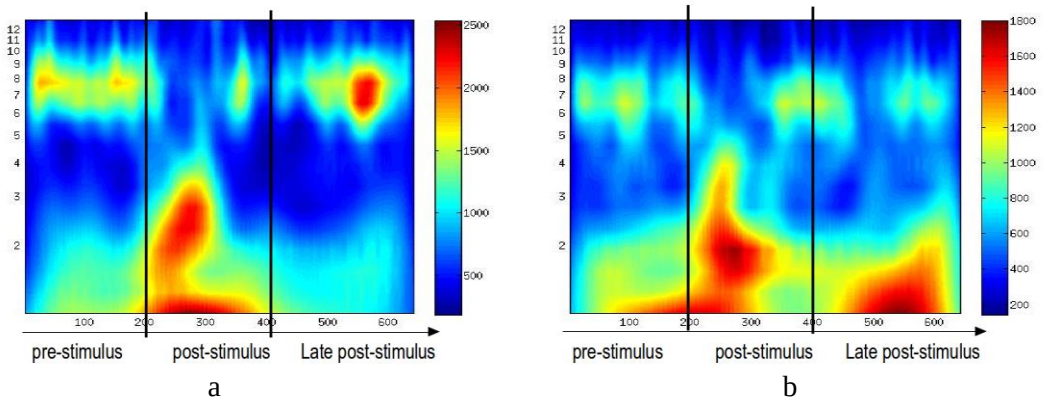

a b

Figure 4.6: Representative mean time-frequency power for bands delta to alpha for one normal and one PMCI subject. The periods used for the statistical analysis of the extracted HMM states can be observed in the figure. PMCI subjects present reduced alpha activity compared to controls [161].

4.2. Discussion on the functional role of hidden states

Regarding the physiological evaluation of the HMM modeling, we examined the four-state model on the training data in order to evaluate the results in conjunction with other studies that reported four dominant microstates. We assign a distinct topography to each hidden state using the approach described earlier. The resulting topographies for control and PMCI subjects can be observed in **Error! Reference source not found.**. We cannot directly associate these topographies with specific EEG activations as identified from the time-frequency analysis of the same dataset [161], since they appear repeatedly over the duration of the trial.

In an attempt to associate the estimated states with specific functional processing states, we divided the single trial into three periods of activation for the specific task: a) the pre-stimulus period, b) the post-stimulus period where the main response component is expected and the c) late post-stimulus period where alpha activity is present [162]. We measure the duration and occurrence of the identified states and we assess these characteristics for the different periods of the experiment.

Within each group, and for the microstate duration and occurrence separately, we applied a one-way multivariate analysis of variance (MANOVA), testing the effect of the period of activation. The data were tested for normality using the Shapiro-Wilk multivariate test for normality. The MANOVA test rejected the null hypothesis that the mean difference in duration among the three periods is zero. On the other hand, the hypothesis that the mean difference in microstate occurrences among periods is zero cannot be rejected, for both groups. Thus, the statistical tests suggest differences in the duration but not the occurrence of microstates among the three EEG periods. The individual confidence intervals were calculated using the Bonferroni correction and the results can be seen in Table IV along with the individual variables that contribute to the rejection of the null hypothesis. We can see that both groups display similar patterns of activations between the three periods.

In the post-stimulus period, the duration of state and C is increased compared to pre-stimulus, in both groups. More specifically, state A presents increased duration during the first post-stimulus interval. During the late post-stimulus interval the duration of state A decreases compared to the post-stimulus and presents no significant difference to the pre-stimulus period. Overall, we can see that the duration of state A increases during the first period after the stimulus and returns to pre-stimulus levels later.

Table IV: Within Group comparison of mean duration and occurrence between periods

	Controls			
	A	**B**	**C**	**D**
Pre	19.745	18.322	19.234	20.584
Post	20.734	18.732	20.543	21.286
Late Post	19.718	18.850	20.021	20.752
Pre-Post	Post > Pre (p = 0.00016)	-	Post > Pre (p = 5.4 10-5)	-
Pre-Late Post	-	-	L.Post> Pre (p=0.00089)	-
Post–Late Post	Post >L.Post (p = 9.77 10-5)	-	-	-
	PMCI			
	A	**B**	**C**	**D**
Pre	14.588	18.513	18.658	20.412
Post	15.121	18.657	19.129	21.018
Late Post	14.537	19.069	18.714	20.925
Pre-Post	Post > Pre (p = 0.00032)	-	-	-
Pre-Late Post	-	-	L.Post>Pre (p=0.0048)	-
Post - Late Post	Post >L.Post (p = 0.00010)	-	-	

State C on the other hand displays increased duration during the whole post-stimulus period in the control group. It presents significant difference, compared to the pre-stimulus, in the post-stimulus and in the late post-stimulus period. It does not present though significant difference

between the post-stimulus period and the late post-stimulus one. This indicates that the hidden state C reflects a sustained, stimulus related activation.

In conjunction with the time-frequency analysis (Figure 4.6) the duration of microstate A varies along with the occurrence of evoked activity, mainly related to theta and delta bands [161], which are dominant during the first period. On the other hand state C in controls can be related to induced activity which is apparent in the early and the late post-stimulus period. The fact that class C's duration remains increased in the late post stimulus period could be related to the alpha power rebound that is observed at the corresponding period [161, 162].

The main difference that can be observed between the two groups is the behavior of microstate C. In the PMCI group, state C presents increased activity only in the late post-stimulus period. Therefore, in the PMCI subjects only state A increases its duration in the early post-stimulus period. This behavior can be compared to the reduced phase-locked activity presented in the PMCI subjects; at the same period. In comparison to other studies the methodology presented provides increased classification performance and can be used to infer significant features of the topographic sequence. Recently, a method using a Gaussian Mixture Model (GMM) was proposed in order to tackle the single trial classification problem. This study clusters the topographies of the single trials using the GMM technique. The number of clusters is determined at the training stage and this technique has been applied for the discrimination between two tasks. The methodology is applied within each subject. In our case, using a HMM allows us to also account for the temporal evolution of the topographies, which plays an important role as the results indicate. We also describe an effective strategy for using this approach among subjects. As future work and directions it would be interesting to combine the two approaches for building and evaluating a continuous Hidden Markov model and compare the results.

4.3. Conclusions

We presented a methodology for modeling single trial EEG activations using Hidden Markov models. A flexible distance measure inspired by the image processing field was used that allows the robust estimation of the distance between two topography maps. Using this measure, we quantize the space of topographies and create a symbol codebook that characterizes the different topographies of the single trial activations. The length of the codebook is determined by the level of the reconstruction error and reflects the fidelity of the constructed codebook. In order to deal with the noisy single trial recordings, we define the notion of quasi-stable topography in terms of segments with stationary probability distributions. Modeling the sequence of topography maps using discrete HMMs allows us to identify periods with such stationary distributions. At the same time, we are able to describe the numerous transitions between states in a compact and effective way.

Applying this modeling approach on real data, we attempt to differentiate the structure of single-trial responses between control and progressive MCI subjects. Our results indicate that the classification accuracy of our methodology depends mainly on the level of the reconstruction error. This is expected since the codebook length determines the generalization capability of our system. The results indicate that we can discriminate between control and progressive MCI using single trials from a simple detection task. The number of hidden states did not affect the final result, although further studies would provide more conclusive results on the role of hidden states. Using the trained models we studied properties as the duration of the hidden states in the single trials. The findings of our approach are in line with other studies that found significant differences in features of general microstate classes between subjects.

The detection accuracy at single-trial level indicates that there exists an alteration in the pattern of information processing that is reflected in the topography maps. Such higher-level interpretation of EEG can reveal important information regarding the functional organization of the brain, but these aspects require far more extensive consideration.

CHAPTER 5: **Fusion of EEG topographic features and fMRI using Canonical Partial Least Squares**

Combining information from EEG and fMRI has been a topic of increased interest recently. The main advantage of the EEG is its high temporal resolution, in the scale of milliseconds, while the main advantage of fMRI is the detection of functional activity with good spatial resolution [86], [163]. The advantages of each modality seem to complement each other, providing better insight in the neuronal activity of the brain. Although, fMRI provides an indirect measure of neuronal activity different studies have established that there exist common neural generators that explain both, EEG activation patterns and the fMRI BOLD response [53]. The main goal of combining information from both modalities is to increase the spatial and the temporal localization of the underlying neuronal activity captured by each modality.

Initially, limitations of the recording technology did not allow for the simultaneous use of both modalities. Recent advancements though, in the EEG technology made possible the recording of EEG inside the fMRI scanner [65]. This technique renewed the interest in the combination of these two modalities and allowed the development of new techniques for their integration and fusion [51], [86], [164]. Decomposition techniques such as Canonical correlation analysis [79] and partial Least Squares [84] have been used for the analysis of such datasets.

Independent component analysis (ICA) was extended and modified in order to decompose simultaneous recorded datasets, resulting in the Joint ICA [51] and parallel ICA methods [77]. Simultaneous EEG and fMRI recordings allow exploring the direct correspondence between EEG and BOLD variability, either in task related or resting-state experiments. One major drawback of the concurrent recordings is the severe contamination of the EEG recordings with scanner artifacts that seriously degrade the signal quality.

Initial attempts for EEG and fMRI integration, before these technology advancements, involved separate recordings of the same experiment in an effort to identify common sources of the explained brain functionality. The main drawback of separate multimodal recordings is that it is no longer possible to establish direct correspondence between fMRI and EEG trials and therefore it is no longer possible to directly exploit the response variability in the trial level. It is apparent that some transformation of the data in a common space and the extraction of representative statistics is needed for the effective analysis of such recordings. In the analysis of such datasets the main

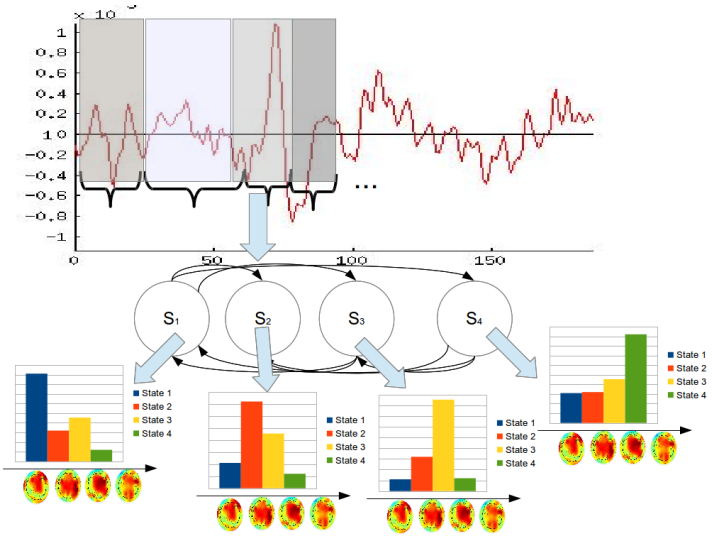

Figure 5.1: Illustration of the Hidden Markov formulation for the modeling of the ERP topography. Hidden states of the HMM represent periods with quasi-stationary distribution of topographies.

assumption is that the response to a given stimulus remains the same when recorded in different time points and different methodologies have been applied for the analysis of separate recordings [115], [165]–[167]. The main idea is to align the two modalities together and work on the estimated response elicited from the task presentation.

On the other hand, the main advantage is that separate recordings do not suffer from signal quality degradation due to scanner interference. The majority of the studies in separate recordings have been focused in solutions in the source space, where source localization techniques are used in order to estimate the brain regions that are more probable to generate the observed EEG. In this context fMRI is used for evaluation of the result or for restricting the search space of the localization algorithm. In order to study significant features of the EEG and fMRI, analysis of separate recordings exploits the common subject to subject variations under a group analysis setting. Canonical Correlation analysis has been used for this purpose with significant results [79]. In this chapter a novel feature, exploiting the properties of the HMM formulation is used for the characterization of the average ERP with applications for the decoding of EEG. We are using EEG and fMRI data that are separately recorded in order to identify common sources of co-variation between the datasets and work on their common subspace in order to exploit information from both modalities.

5.1. Feature Extraction

5.1.1. EEG as sequence of field topography maps

Recently, there has been an increased interest in methods that exploit information carried by the topographic configuration of the electrical field in the scalp electrodes [132], [168]. Initially,

this approach was introduced in [121] where it was first observed that the topography of the electrical field does not change randomly, but rather follows certain patterns, depending on the task at hand. It was though that these distinct topographies reflect the underlying sequence of brain activation and constitute a higher representation of the activation sequence of brain functions needed to complete the task.

In order to recover the dominant topographies from the EEG signal different methodologies have been applied either in the average or the single trial Event Related Potential (ERP) [125], [168]. The main approach followed is to first define a measure of similarity between topographies and then apply a clustering algorithm in order to represent the set of topographies using the cluster centroids. In [169], we introduced a new measure of similarity based on the Local Global Graph (LG graph) which was applied for the segmentation of the average ERP. This measure treats the topographic map as an image and uses segmentation in order to extract the LG graph. The segmentation step provides the additional advantage that reduces the dimensionality of the problem and reduces the co-linearity of the measurements of nearby channels, by grouping neighbor channels together. The similarity between topographies is measured in a hierarchical way, starting from the nodes of the local graph and then taking under consideration the spatial relation of the nodes.

5.1.2. Modeling using Hidden Markov Models

Different algorithms have been applied for clustering the topographies. A modified k-means algorithm has been applied in [125]. Also hierarchical clustering algorithms and soft clustering algorithms as Gaussian mixture models [168], [169] have been successfully applied for the identification of dominant topographies. Some implementations incorporate temporal filtering of

the results in order to remove isolated topographies in time and create a smooth temporal segmentation. In this study, we model the topographic sequence using Hidden Markov Models (HMM) as presented in Chapter 4.

HMMs are bivariate random processes consisting of a random variable modeling the observed processes and a hidden Markov chain which describes the transition between the different states. The probability of the current hidden state depends only on the previous state [137]. The distribution of the observations depends only on the current state and is independent of previous observations and states. In our case, we consider the sequence of the topographies as the observed variable and the different and the underlying hidden states as periods that present stationary distribution of topographies, similarly to the approach presented in Chapter 4. The HMM seems to be a good fit in the microstate model, since it allows to model both the spatial and temporal relationships of our data. Initial results, in a work to appear, on single trial activations of healthy and Progressive Mild Cognitive Impairment subjects indicate that we were able to distinguish between the activations of the two groups using a generative classifier build from the HMMs.

HMMs can be considered in the more general framework of Dynamic Bayesian Networks (DBN). HMMs are the simplest DBN models we can build. In [170], we extended the modeling of the topographic sequence using Dynamic Bayesian Networks. This extended approach is discussed and presented in Chapter 6. Summarizing, the trained networks were used for the binary classification between two tasks with good results and confirmed that the topographic sequence carries valuable information about the underlying brain processes complementary to the time-frequency analysis approach. The main problem with this approach is that using these generative models it is difficult to assess the impact of each parameter of the model and therefore it is difficult to associate the model parameters with other features and well known descriptors of the brain

response. In an effort to combine the strengths of generative models with the strengths of generative ones, we introduce the Fisher score for the analysis of EEG.

The procedure for building the HMM is to apply a vector quantization step and then learn the model parameters on the encoded sequence. Specifically, we use the k-means algorithm on the multichannel vectors of the average ERP from all subjects in order to extract the observed symbols. The encoded sequence is used to learn the parameters of the discrete HMM using the Baum-Welch algorithm [137]. We apply this methodology on the wideband average ERP signal for extracting the topography codebook and learning the model parameters.

5.1.3. Mapping to Fisher Score space

The Fisher score space was introduced in [171] in an effort to bridge generative and discriminative models. The main motivation was to map variable length sequences into fixed length feature vectors, a problem often encountered in bioinformatics [171]. Fisher score uses the derivative of the parameters of the HMM given a certain sequence. Using the derivative of each parameter for a sequence we are able to build a feature vector of length equal to the number of parameters of the model. These vectors can be used to form the so-called Fisher kernel which has been used with kernel classifiers and methods [172] .The Fisher score has been very popular and have found many applications in classification of protein sequences [172], text, speech recognition and images for face recognition, shape/texture recognition and activity recognition [173].

The Fisher score maps a sequence to fixed length vector using the parameters of the generative model. The gradient of the parameters for a given sequence are used to accomplish this. In the case of HMM the gradient of the parameters of the trained HMM is computed for a sequence. The derived gradient describes how the parameters of the model must change in order to adapt to the

new sequence. Therefore, the derived features can be used to evaluate how well the given sequence fits the model parameters and we can evaluate the deviation from a given parameter explicitly. The Fisher vector for each parameter is defined as:

$$F_i = \nabla_{\Theta_i} log\, P(O|\Theta_i) \tag{15}$$

Regarding the modeling of the EEG topography, the Fisher score of a sequence provides useful insight for which parameter deviates most for a given sequence. The gradient of the parameters of the diagonal of the transition matrix A reflect the difference in the mean duration of the given states while the gradient of the off-diagonal entries of the matrix reflect the difference in the mean frequency of transition from a state to another. The same applies for the emission parameters with respect to the topography distribution. For the discrete case the gradient indicates a change in the distribution, where a certain representative topography may appear more often than expected in a given state. The gradient of the emission parameters is easier to interpret in the continuous case though, were the emission distribution is modeled using a Gaussian distribution or a mixture of Gaussian distributions [155, 159]. This study presents results for the discrete case, although the derivation for the continuous is straightforward. The gradient of the transition matrix can be calculated using the sufficient statistics of the HMM. The sufficient statistics of the HMM (the forward and backward probabilities) can be derived by the forward-backward algorithm [137].

5.2. Methods

5.2.1. Partial Least Squares for multimodal fusion

Different methods have been employed for fusing data from different modalities. Joint ICA and parallel ICA are two of the most popular algorithms used for this purpose. The main problem

with these approaches is the strong assumption of independence imposed to the latent variables. CCA on the other hand has been used successfully for the fusion EEG and fMRI data [79]. CCA uncovers latent components that are maximally correlated between datasets. The main problem of the CCA method is that it maximizes the correlations between latent variables of the two sets and operates on the cross-correlations matrix. Therefore, CCA is vulnerable to outliers and it is often the case that CCA solution to fail to summarize the variance of the two datasets [173].

On the other hand Partial Least Squares (PLS) methods have been used successfully for the analysis of neuroimaging data [174] and have found applications in different problems [175]. Multiway PLS has been applied in the analysis of simultaneous recorded EEG and fMRI data in [84]. In general, it seems though that PLS methods have been neglected in this context, partially due to the success of ICA methods in the analysis of EEG and fMRI. In general, there exist different formulations of the partial least Square method for the analysis of two sets of variables. The one known as Canonical Partial least squares (CPLS) tries to uncover the shared information between two sets of variables. It also known as Canonical Two Block Mode A PLS (PLS-C2A) [176]. The main advantage of CPLS methods over CCA is that CPLS maximizes the covariance between the latent variables of the two datasets and therefore avoids the poor summary of variance problem of CCA, by directly trying to maximize the cross-covariance between the two sets. Although the formulation of CPLS looks similar to that of CCA, the computational details of CPLS make the solution numerically stable and the results are easier to interpret than CCA [176].

In general, CPLS tries to find two sets of latent variables (one for each set) that maximally co-vary. More formally we assume that we have two sets of variables X, Y, where the columns are the different variables and the rows are the paired samples. We also assume that variables of X and Y have zero mean and are scaled to unit variance. The main assumption is that the variables of X are

generated by the same number of latent variables as the variables of Y. Suppose that we have two paired sets of latent variables L_x, L_y for each set. We are interest to uncover these pairs of latent variables and CPLS does so by working on the cross-covariance of the two datasets. CPLS calculates pairs of latent variables defined as:

$$\{L_{X_i}, L_{Y_i}\}, i \in \{1, .., r\} \tag{16}$$

so that latent variables $\{L_{X_i}\}$ and $\{L_{Y_i}\}$ represent the most interesting subspaces (in the least square sense) of the cross-covariance matrix R. R is defined as:

$$R = X^T Y \tag{17}$$

We want to find linear combinations $\{L_{X_i}\}$ and $\{L_{Y_i}\}$ such that:

$$Cov(L_{X_1}, L_{Y_1}) = max\{Cov(Xu, Yv)\} \tag{18}$$

where u, v are the coefficients that maximize (18). It is well known that the solution of equation (18) can be obtained by solving the singular value decomposition of the cross-covariance matrix as:

$$R = UDV^T \tag{19}$$

Therefore we can recover the linear combination weights for each set, which for set X are the singular vectors U and for the Y set the singular vectors V. The latent variables can now be calculated as:

$$L_X = XV \tag{20}$$

$$L_Y = YU \tag{21}$$

Using this method, we are able to describe, using a linear combination, the features from X that maximally co-vary with features from Y. Working with the covariance matrix guarantees that the

latent variables will sufficiently describe the cross-covariance structure of the data, in contrast to CCA that may provide a poor summary of the datasets variability.

5.2.2. Dimensionality reduction using PCA.

The main problem in the analysis of fMRI data is the large number of features compared to the sample size. A single scan of the head usually involves hundreds of thousands of voxels. Several feature selection techniques have been applied in order to reduce the amount of features and allow us to work with a smaller subset of features. Choosing an appropriate region of interest and working with the corresponding voxels is such a technique. Another approach is to first solve the General Linear Model and based on the solution choose the voxels that differ significantly among tasks. This way we can select only the most informative features for our analysis.

Despite these approaches that significantly reduce the number of features, most of the time it is beneficial to reduce even further the dimensionality of the problem. Principal component analysis is a well-known method that allows us to transform our data to a lower dimensional space while retaining the as much of the original variance as possible. PCA projects the data into the lower subspace as follows:

$$Y = XU \tag{22}$$

where U is the matrix of the eigenvectors of the covariance matrix of X. By choosing the k eigenvectors that correspond to the largest eigenvalue we can map our original variable X to a lower space Y' which corresponds to the k largest eigenvalues as follows:

$$Y' = XU' \tag{23}$$

PCA is well known technique and has been applied extensively for reducing the dimensionality of the initial problem. We apply PCA to the processed EEG and fMRI feature sets separately as a preprocessing step before the analysis of the cross-covariance of the two sets.

5.3. Application

Our goal is to couple information from both modalities in an effort to generate new features that capture the variation between subjects. The main idea is that instead of producing features that summarize the variance of each set independently, we use PLS in order to describe the structure of the cross-covariance matrix in an effort to capture the features that present task related behavior between the two modalities. Therefore, in contrast to PCA which operates in the covariance matrix of each set to reduce the dimensions of the problem, we are taking into consideration the modulation of features across modalities in order to recover the task related features.

5.3.1. Data Description

The data come from the study [177] and have been made publicly available from the authors. We used the EEG and the fMRI part of the dataset only. In this dataset, 16 subjects were asked to perform a visual task where faces of famous persons, unfamiliar faces and scrambled faces where presented to them. The complete description of the dataset can be found in [177]. The EEG data were recorded in separate sessions several days apart from the fMRI session.

There were 300 faces and 150 scrambled faces in total. The scrambled faces were created by taking the Fourier transform of a group of 150 images of faces [177]. The phases of the transformed images were permuted and then inverse transformed in the original space. Finally, the new

scrambled image was masked using the outline of the original face [177]. For the MEG/EEG data each subject completed 900 trials over six sessions, while for the fMRI each subject completed 900 trials over 9 sessions [177].

5.3.2. EEG preprocessing and Fisher score calculation

The data were examined for artifacts and Independent component analysis was used in order to remove eye-blink artifacts [23]. Trials that were heavily contaminated were excluded from further analysis. The data were band-pass filtered in the range 0.5-31Hz using a linear Finite Impulse response filter and the average over all trials per task was calculated for all subjects resulting in 3 average ERPs for each subject.

Using the averages we extracted the discrete HMM as described in section II. We tried different number of states and number of symbols. The number of symbols were chosen so that the reconstruction error of each sequence to be less than 30%. The resulting codebook consisted of 15 topographies. We used 6 hidden states for the HMM. The model with the given parameters was selected over other models based on the maximum log-likelihood achieved by the model given the data.

We followed a simple strategy for calculating the Fisher score for the average sequences. We trained the HMM, on the trials of the scrambled faces and then the Fisher score of all ERPs was calculated based on this HMM. The Fisher score of each ERP reflects the deviation of the sequence from the HMM parameters learned using the scrambled faces and therefore we expect smaller deviations for ERPs of the same class and larger for the other classes. We treat famous and

unfamiliar faces as the same stimulus and the gradient of the parameters reflect the change in the model depending on the stimulus.

5.3.3. fMRI preprocessing

The fMRI volumes consisted of 33 T2-weighted transverse echoplanar images. Each session consisted of 210 volumes with a repetition time (TR) of 2000ms. FMRI data were preprocessed as in [177]. We used SPM5 [178] in order to register the slices of each subject together. A T1-weighted image of each subject was segmented to gray matter, white matter and Cerebrospinal fluid and the segments were registered to the corresponding segments of an MNI template in Tailarach space [178]. The slices of each run were first co-registered and then time corrected. The co-registered volumes were then registered and normalized to the processed T1 volume of the corresponding subject.

5.3.4. Feature Extraction

Since we want to take advantage of information from both EEG and fMRI using CPLS, we have to work with paired datasets. Trials from EEG and fMRI were recorded at different times and therefore we cannot have a direct correspondence between trials of the same subject. For this reason we are going to work across subjects. For the EEG we will use the average ERP on a single channel. A channel located in the occipital area was selected that presents strong ERP peaks after the stimulus. The ERP peaks that we anticipate to observe from this type of stimulus, is a positive peak at 100ms (P100) and a negative peak at 170ms (N170) after the stimulus.

For the fMRI data we are going to work with the beta maps of each subject. We model the HRF response of each subject using a canonical HRF, build from two gamma functions [178]. Using the General Linear model we model the activity of each voxel as:

$$Y_i = Xb_i + e \tag{24}$$

where Y is the activity of a given voxel and X is the design matrix of the experiment (derived using the convolution of a Dirac function with the HRF function). We estimate, for each voxel the beta value and use the corresponding maps to build the fMRI dataset. The final fMRI dataset consists of sixteen subjects and 3 parametric maps per subject, one for each task.

5.4. Results

5.4.1. Evaluation using the average ERP and fMRI.

We performed CPLS using the features from EEG and fMRI. We constructed two EEG datasets. The first consists of the average of each subject. In this case the samples of the average ERP are the features that we are going to use. The dimensionality of the fMRI data was reduced before applying CPLS. Initially, we selected voxels that differ significantly between tasks, as indicated by an ANOVA test. We set a threshold of 0.05, uncorrected. The resulting dataset was further reduced using principal component analysis.

We applied CPLS in the set consisting of the average ERP dataset and the reduced fMRI and to the set consisting of the ERP Fisher scores and the reduced fMRI. The results can be seen in Figure 5.2. An EEG component that corresponds in the N170 peak is presented along with the corresponding fMRI component. We can see that the EEG component characterizes well the activity around the N170 peak. On the other hand, the fMRI CPLS component reveals areas that

co-vary with the EEG component and are in agreement with other studies regarding the areas involved in the generation of N170 [179]. Significant areas of activations were calculated by thresholding the Z transformed loadings of the fMRI component. We can observe that the N170 component is mostly associated with activations in the occipital and lingual gyrus (marked with yellow rectangle), the left superior Occipital cortex (red rectangle), the middle temporal gyrus (blue rectangle) and the precentral gyrus (green rectangle). These regions match the ones reported by other studies [179] and confirm that results of the decomposition. These initial results indicate that CPLS is able uncover meaningful components that co-vary between the two datasets.

5.4.2. Evaluation using the Fisher score and fMRI

In this case we used the EEG dataset containing the features derived by taking the gradient of the HMM parameters. The parameters of interest are the transitions between the states of the HMM model. In order to localize the activity in time, we use three windows around the peaks of interest. The first period starts right after the stimulus onset and includes the P100 peak. The second period includes the negative peak N170 and the last period covers the late period of the trial up to 650ms after the stimulus onset, as can be seen in Figure 5.2(second row).

We applied CPLS in the fisher score datasets and in this case, we searched for components that present significant differences among the stimuli. We performed Student's t-test and three components displayed significant difference between the two tasks. We used the loadings of these components to map the contribution of the components to the original variables. The loadings were reformatted into the corresponding transition matrices for each window and the transition weights were Z normalized. In this case, we found components whose loadings significantly differ between tasks, in contrast to the previous case (using the average ERP). In total 3 components were

identified that presented significant differences. These components are presented in Figure 5.5 along with the states with dominant loadings for all periods and the corresponding fMRI activations. In Figure 5.2 bottom, the most significant states and fMRI activations of these components are presented along with the average activation for comparison.

For each time period, we identified the most important entry in the transition matrix of the component. For all the windows the entries represent the transition to the same state and therefore can be translated as differences in the mean duration of the state. This result is expected since we are working with the average signal and we don't expect significant differences in the rate of transition from one state to the other. The transitions in the same state can be explained as the mean duration of the state at the given interval. In Figure 5.2 bottom, the mean topographies, as calculated by the emission probabilities of the identified state, are presented for the P100 and N170 periods along with the corresponding fMRI component. Two of the identified components (components A and B) presented loadings that strongly projected in the periods of P100 and N170. The third component (component C) projected strongly in all periods with activations corresponding to the transition rate between states. For the period of the ERP component P100 the states that presented the higher loading were state 1 and state 4 identified by component B, while score for component C is higher for state 2 at the same period. Component A had significant score at state 4, for the N170 period. For this evaluation, the scores corresponding to parameters of transitions between states were not taken under consideration.

The results present similarities with the ones for the ensemble of components for N170 of the average set. We can observe significant fMRI activations located in the occipital lobe (yellow) and

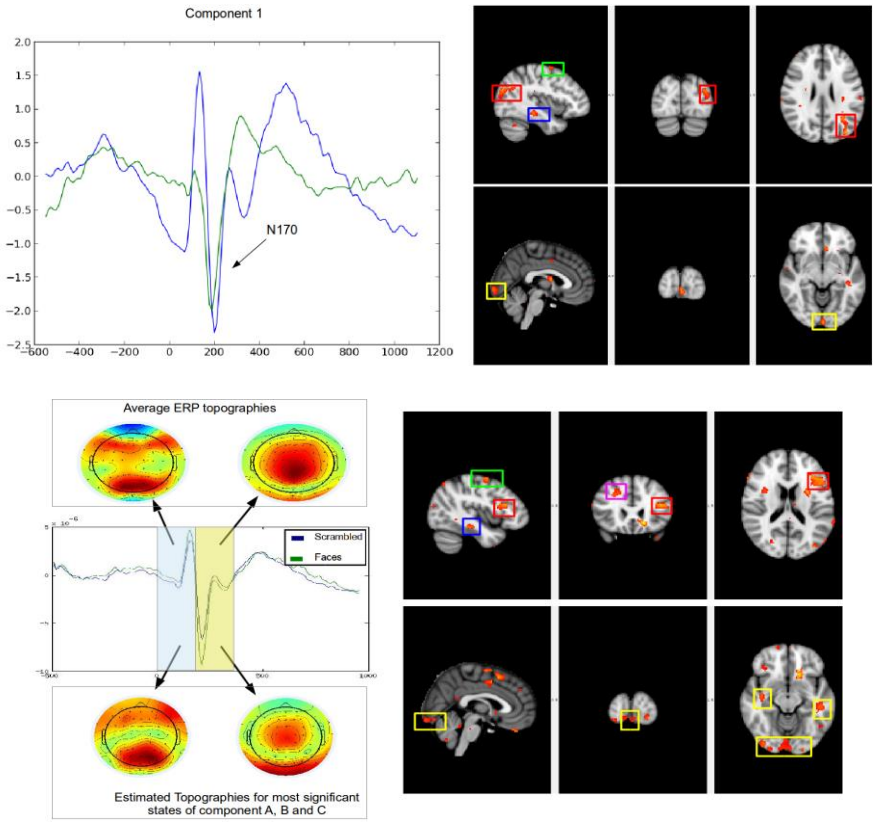

Figure 5.2: CPLS Components related to the N170 peak and the corresponding fMRI activation. Top, a component that captures the activity around the N170 peak and the corresponding component for the fMRI. Bottom, a component that presents significantly different activation between the tasks, using the Fisher score feature dataset for the EEG. We can see that we have common activations for the fMRI activity between the two components. Relevant activity to the N170 is marked with colored rectangles. Yellow rectangle marks the area in the Occipital gyrus, while green and blue mark the middle temporal gyrus (blue rectangle) and the precentral gyrus (green rectangle), respectively. For the average ERP case with red is marked the lateral superior Occipital cortex. For the Fisher score case red and magenta mark the inferior and superior frontal gyrus, respectively.

the occipital fusiform gyri (yellow) and the post central gyrus (green). In this case, the component projects significantly to all three periods and therefore is expected to have more active regions than

in the case of the average ERP. The additional activations are located mainly in the inferior and superior frontal gyri (red) and are related to ERP components that appear later in time (as the P600) [179].

5.5. Evaluation of CPLS for classification fusion

There has been increased interest in Brain Computer Interface systems that try to decode patterns of brain activity to the corresponding input. Significant research has been devoted for such systems and various algorithms have been developed for this task. The majority of these studies are using EEG as the main modality for this purpose. The main reasons are the ease of use and setup of EEG and the low cost of the required equipment, especially when compared to other alternatives.

Despite these advantages and the very good temporal resolution of the EEG it is apparent that it would be beneficial to combine information from other modalities in order to increase the performance of the system. The most common approach is to use features from different characteristics of the brain response. These approaches to BCI systems, also known as hybrid systems, take advantage of different aspects of the brain response and combine them to increase the accuracy or reliability of the system under consideration [180], [181]. In a multi modal setting, combination of EEG with EOG, EMG and NIRS data are the ones most commonly encountered [181]. These studies have proposed the information fusion of NIRS and EEG in order to increase the accuracy of the system.

In this work, we study the use of CPLS in order to borrow information from fMRI for increasing the classification accuracy using information from both modalities. In the next section we discuss the general strategies employed for classification fusion and the present initial results of this methodology.

5.1. Classification Fusion

In general, the fusion problem can be divided into two large categories: early feature fusion and classification score level fusion. In the first case, the idea is to combine different features together in order to build a better and more informative feature set. Different methods have been applied for feature fusion that vary depending on the application. The simplest approach is to concatenate the different features of data sources into a single vector and apply machine learning techniques using the ensemble of features. The main problem with this approach is that the dimensionality of the problem increases and so does the number of samples needed to learn the feature space. Decomposition techniques have been proposed in order to reduce the problem of dimensionality ranging from Principal component analysis performed on each feature set separately, to cross-correlation [182]–[184], tensor decomposition techniques and Bayesian approaches.

The second approach operates on the estimated scores of each sample derived from multiple classifiers on each feature set separately. The fusion in this case happens at the last stage of the procedure and the goal is to increase the accuracy and reliability of the classification by combining the individual results [185]. The main assumption behind this approach is that modalities are independent and therefore we can use the partial scores in order to improve the result. The most common combination techniques are by taking the sum of scores, the product or using the minimum or maximum of the individual classifier scores. Extension of this approach leads to classification trees and Random Forests [186], where classifiers are built from random subsets of the data and their results are used in a majority voting procedure. Finally, in this case we can also categorize the

decision level fusion techniques, where we consider the final prediction of each classifier and then apply some sort of voting scheme for the final decision [187].

An initial study of the effectiveness of multi-modal feature fusion using CPLS for the classification of a visual task using EEG and fMRI is the goal of this work. The main idea is to take advantage of the fMRI information in the training phase in order to enhance the prediction of EEG in the test phase. For this study, the Fisher kernel feature derived in the previous sections is used.

5.1. Evaluation of Canonical Partial Least Squares for classification.

Evaluation of CPLS method is performed on the data derived from the average ERP of all subjects. Selected windows of the average ERP are transformed into the equivalent Fisher score using the procedure described previously. The feature vector for each subject and task is used for the classification procedure. Initially, the performance of CPLS as a dimensionality reduction method is compared to Principal Component analysis. Using PCA for comparison has the advantage that the results of the comparison are easier to interpret, since both methods rely on the singular value decomposition and produce orthogonal projections. The other advantage is that since PCA operates on the global variance of the modality can be used as ground truth and compare the information retained by CPLS which operates on the common EEG-fMRI variance.

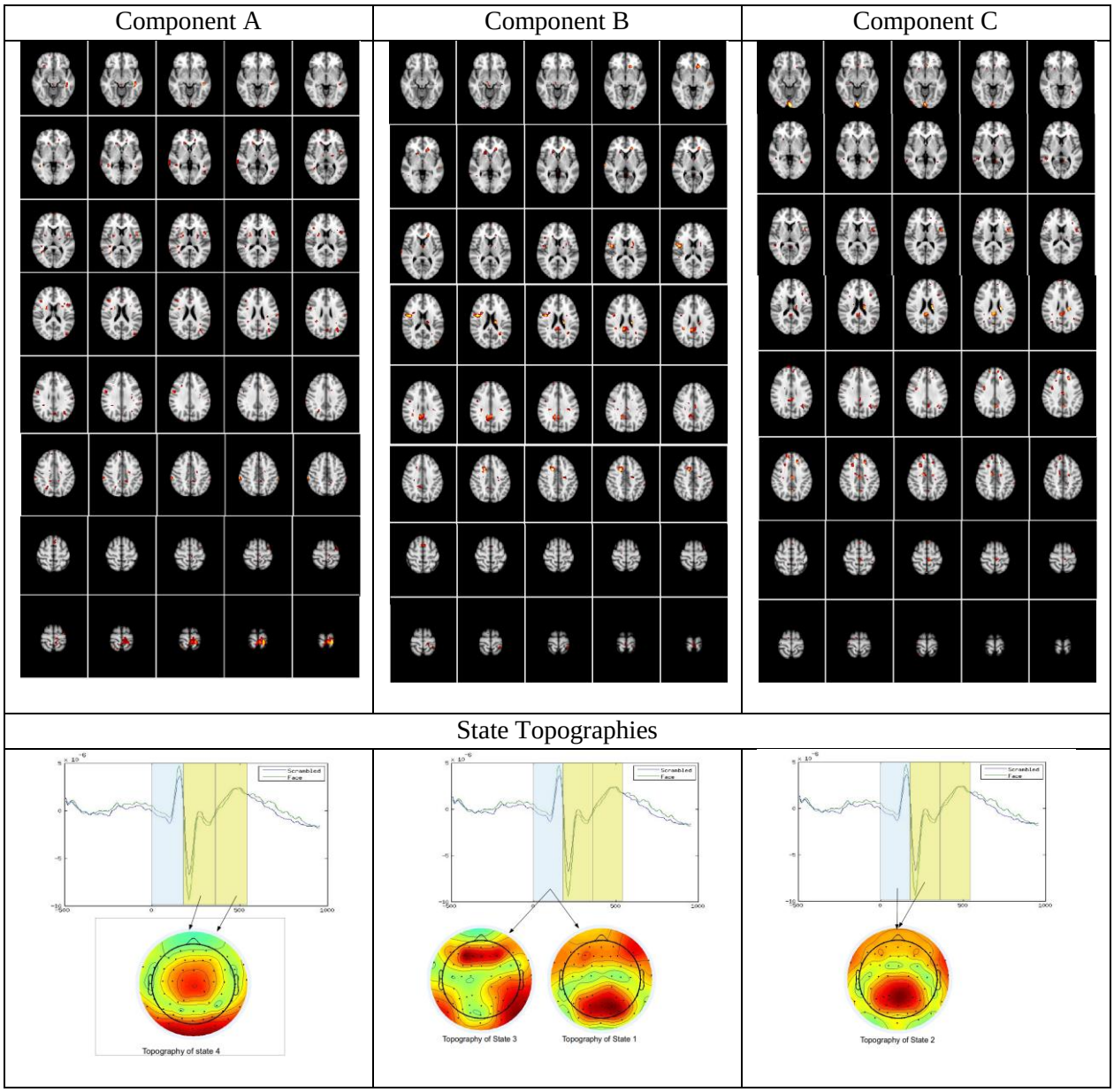

Figure 5.3: CPLS components that presented significant difference between states. The fMRI activations of the three components are displayed in the first row. Second row displays the states that correspond to features that the component present significant score. Only the parameters that represent within state transitions have been taken into consideration.

5.1.1. Classification procedure

The main problem with the current experimental setup is that the number of features/variables, greatly exceed the number of available samples. This makes the application of any classification algorithm prone to over-fitting. Despite the reduction of the dimensionality of the problem using CPLS or PCA, we have to be cautious in order to avoid the over-fitting problem. Therefore, is apparent that some sort of regularized classifier has to be used in order to avoid such problems. Different types of classifiers have been implemented for such cases. A regularized logistic regression algorithm [188] is used in order to test the two methods. The logistic regression method uses the features of the data in order to make the prediction as:

$$y' = g(\theta^T \chi) \tag{25}$$

where the function $g()$ is the logistic function defined as:

$$g(z) = \frac{1}{1 + e^{-z}} \tag{26}$$

The cost function used for the logistic regression is:

$$J(\theta) = \frac{1}{2m}\sum_{i=1}^{m}(g(x) - y)^2 + \frac{\lambda}{2m}(\sum_{j=1}^{n}\theta_j{}^2) \tag{27}$$

where m is the sample size and n the number of features used. The main reason for choosing logistic regression for the classification is that is a simple well studied technique and the estimated result can be directly interpreted as probability. The penalty value λ was chosen by running the following procedure for different values of λ and keeping the value that provided the best results in terms of accuracy.

A Leave one out subject procedure is used for the evaluation of the classification performance. For each left out subject we have two positive and one negative example on which we test the

learned classifier. For CPLS, the projection to the common subspace shared by EEG and fMRI features is used as input to the classifier, while the projection of the EEG features in a lower subspace defined by the principal axis is used for the PCA case. The metrics used for the evaluation of the classification performance are defined bellow:

$$Precision = \frac{tp}{(tp + fp)} \tag{28}$$

$$Recall = \frac{tp}{(tp + fn)} \tag{29}$$

$$Accuracy = \frac{(tp + tn)}{(tp + tn + fp + fn)} \tag{30}$$

$$F1 = 2 * \frac{\text{precision} * \text{recall}}{\text{precision} + \text{recall}} \tag{31}$$

The results can be seen in Figure 5.5. The Receiver operator characteristic (ROC) curves and the accuracy of the classifier for different number of components can be observed. We can see that the results between PCA and CPLS are comparable. In some cases CPLS presents better accuracy than the PCA procedure. The metrics for the best case of each method are presented in Table V.

Table V

	PCA – 20 components	**CPLS – 20 components**
Accuracy	0.8333	0.854
F1	F1(positive) = 0.875 F1(negative) = 0.75 Mean F1 = 0.8125	F1(positive) = 0.888 F1(negative) = 0.787 Mean F1 = 0.838

These results confirm that the CPLS is able to capture significant variations between the different tasks in a meaningful way. Therefore, it allows us to take advantage of the spatial localization of the fMRI on the one hand, while on the other transform the data into a lower

dimension space that retains most of the information of the PCA. Another point that can be observed in the ROC curves for the different components of the CPLS is the fact that it presents better results early on, while on the PCA case the classifier presents significantly lower performance when we retain only a few components and catches up as we add components/ information to the system. This indicates that CPLS manages to preserve relevant information more effectively, by using EEG and fMRI.

5.2. Future directions and extensions using classification fusion

An interesting extension of this study is the use of both modalities in a multiple classifier system. Ensembles of classifiers provide a different framework for classification that recently has been employed for the analysis of neuroimaging data [186]. In the case of EEG and fMRI, CPLS provides a framework for building and testing different architectures for the fusion of the results of multiple classifiers. There exist many works that exploit for example CCA for the purpose of classification fusion, at different levels [183], [187].

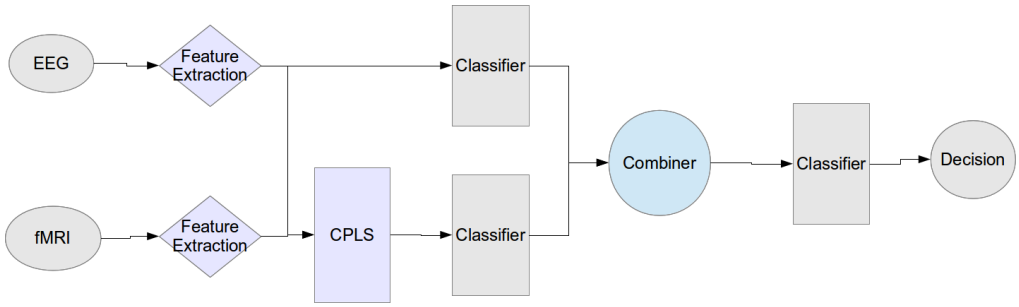

Figure 5.4: The architecture for the hybrid fusion of EEG and fMRI. In this case, fusion is performed in the features using CPLS and the result is used for classification along with the starting dataset. The classification scores of both sets are then combined for the final decision.

Hybrid methods that combine feature level fusion and score level fusion have drawn a lot of attention lately. In our case the feature fusion is provided by the CPLS methodology. An initial experiment towards this direction was performed using the EEG reduced features and the CPLS fused features in order to build a simple hybrid classifier. The idea is to use the CPLS features to support the decision based on the EEG features. This strategy can be seen in Figure 5.4.

The main idea is to use the features of EEG for classification as in an ordinary unimodal classification scenario. The additional decision support comes from the use of fMRI in order to borrow information and generate the CPLS features of the EEG. The reduced dataset using CPLS is fed in a second classifier. The score estimates of each classifier are combined for the final decision level fusion. In essence, what we construct here is a hybrid classifier system that combines fusion in the feature and the decision level.

The scenario that corresponds to such a system can be described as follows: We consider that EEG and fMRI data are recorded from the subjects during the training phase. Using CPLS the two modalities are fused and the projection is used for training. The main problems of using fMRI for such systems is that it is expensive and time consuming to collect the data and therefore, is used only in the training phase. In the test phase only the EEG is used for classification. The PCA reduced features of the EEG and their projection using the CPLS weights learned during the test phase.

This study serves a twofold goal. It explores whether classification fusion using this setting can provide a feasible and efficient alternative and if it is worth to further explore. The second goal is that it will allow us to extract information regarding the type of activity captured by CPLS. Considering the model of EEG-fMRI fusion of Figure 2.4, we expect CPLS to capture information corresponding to variance explained by the union of the two modalities. On the other hand using

the PCA method we expect to capture information that globally characterizes EEG. This experiment will is expected to shed light in this hypothesis using a multivariate data-driven approach.

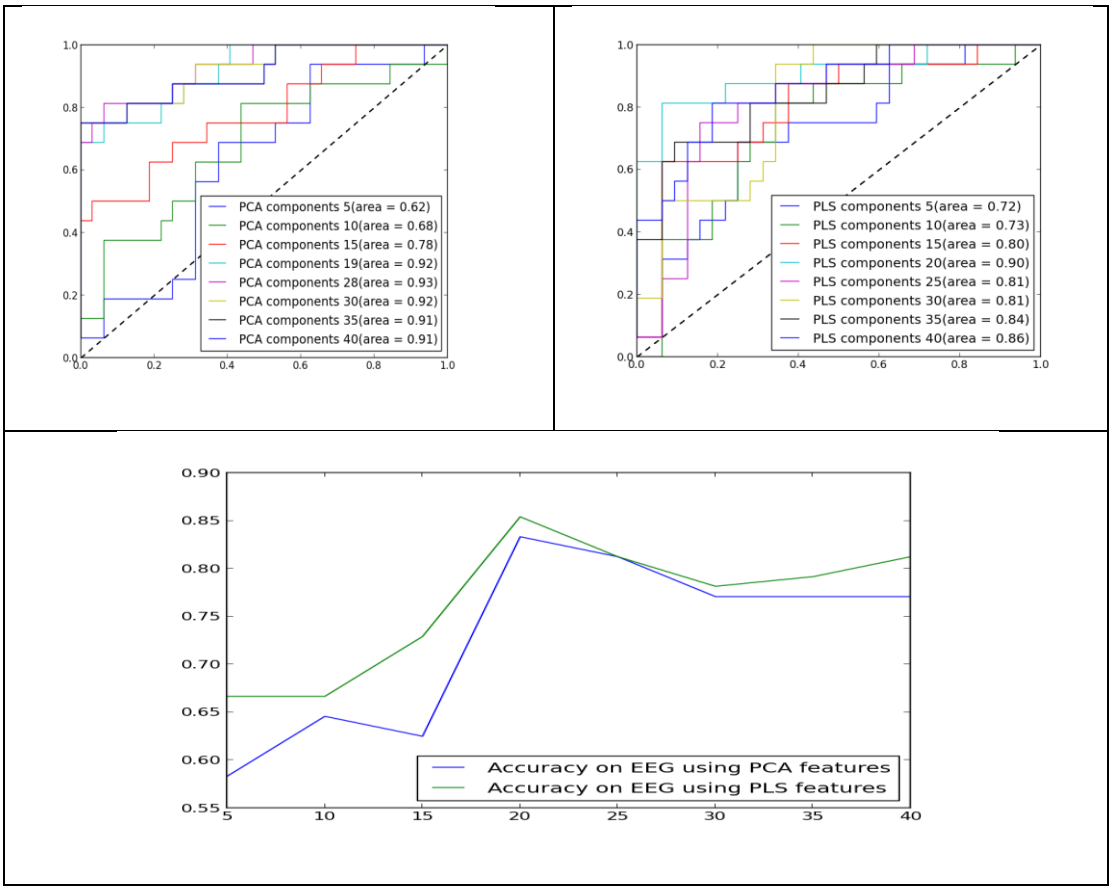

Figure 5.5: Classification results using the PCA and CPLS derived features, respectively. First row displays the ROC curves for the leave one subject procedure for the PCA and CPLS for different numbers of components. Second row displays the accuracy of each case for different number of components

Table VI. The functions used for the combination of classification scores.

Sum	$C = argmax \sum_{i=1}^{R} P(w_j \mid x_i)$
Prod	$C = argmax \prod_{i=1}^{R} P(w_j \mid x_i)$
Mean	$C = argmax \frac{1}{R} \sum_{i=1}^{R} P(w_j \mid x_i)$
Concatenation	$P(w_j \mid [x_i, x_j])$

Table VII. Results of classification for the fusion case

20 components	**PCA**	**CPLS**	**Fusion - Sum**	**Fusion - Product**	**Fusion - Mean**	**Fusion - Concatenated**
Accuracy	0.8333	0.854	0.875	0.854	0.875	0.833
F1(positive)	0.875	0.888	0.909	0.895	0.909	0.875
F1(negative)	0.75	0.787	0.800	0.758	0.800	0.750
Mean F1	0.8125	0.838	0.854	0.827	0.854	0.8125

The functions used for the combination of scores are the sum of scores, the product of scores, the mean of scores and the concatenated case where the two scores are used to construct a new feature vector. These functions are well studied and have been used extensively in previous works [189]. For the final decision a Support Vector Machine (SVM) classifier is used. SVM are well known classifiers that are trying to maximize the margin between two classes. In this case the feature space that the SVM will operate is small compared to the sample size and we can take

advantage of the properties of the SVM, mainly the good regularization properties of the algorithm [190].

Given the estimation from the two classifiers and using the functions defined above we calculate for each sample the corresponding scores and use them as input to the final classifier. The product function assumes independence between the observations of the two classifiers. The sum and mean rules assume that the inputs are independent and that the posteriori probabilities calculated by the classifiers are similar to the prior probabilities. The final meta-classifier takes as input the results of these functions in order to make the final decision.

5.2.1. Support vector machines

In this section a short introduction to SVM is given along with the motivation for using them as a meta-classifier. SVMs try to find the hyperplane that maximizes the margin between the two classes. In the case of the linear SVM two hyperplanes that separate the two classes and allow no points to lie inside the margin created, can be defined as:

$$x_i w - b \geq 1 \; for \; y_i = 1 \tag{32}$$

and

$$x_i w - b \; \leq -1 \; for \; y_i = \; -1 \tag{33}$$

the combined constrain can be written as:

$$y_i(x_i w + b) \geq 1 - \xi_i \tag{34}$$

Where $\xi_i > 0$ are the so-called slack variables controlling the margin and thus allowing a point to be either in the margin $0 < \xi_i < 1$ or misclassified $\xi_i > 1$.

Considering that w is a normal vector to these hyperplanes, we seek to minimize the norm$\|w\|$, under the constraint that no points fall inside the margin as imposed by equations 32 and 33. The optimization becomes:

$$\begin{aligned} &minimize(w,b)\ \ \frac{1}{2}\|w\|^2 + C\sum_{i=1}^{n}\xi_i \\ &subject\ to\ Eq.34. \end{aligned} \tag{35}$$

In this case C is a cost variable that determines the relation between maximizing the margin and minimizing the slack [191]. This optimization problem is solved using Lagrange multipliers but the details of the SVM algorithm are beyond the scope of this study. For an in depth description of the SVM algorithm, refer to [191].

The main reason for using SVM as the meta-classifier is partly due to its good generalization properties, a fact that makes SVM a popular choice and many studies in the classification fusion field are using them as meta-classifiers [187]. An advantage of the SVM is that is we can use different kernels and easily explore the effect of non-linear transformations. For simple cases, a simple naïve Bayes classifier is sufficient for the final decision. Nevertheless, we used SVMs since they have the advantage of projecting the data to a higher dimensional space where the chances of our data being separable are higher.

5.2.2. Results and discussion

The results of this approach can be seen in

Table VII. The functions used for the fusion of the classifiers are described in Table VI. The results indicate that a multiple classifier system is indeed capable to provide better results than the unimodal case using an initial naïve approach to fusion. Thus, it is expected that extending towards more complex fusion schemes will provide better results. An interesting observation that can be

made regarding the fusion results is that the fusion approach seems to achieve very good accuracy at the beginning of the process by using only a small number of features. In order to make sure that the results are not affected significantly by the choice of algorithm we are also tested a Naive Bayes classifier and a penalized logistic regression one. The results were identical to the SVM approach with no significant differences and it is safe to assume that the selection of the fusion classifier does not significantly affect the analysis of the results that follows.

This behavior leads to an important implication regarding the information captured by the PCA and the CPLS procedures. Taking as starting point that the ensemble classification idea is based on the independence and the diversity of the used classifiers, then the fact that the ensemble method presents significantly better results early on, is an indication that the reduced PCA dataset and the reduced CPLS dataset capture different types of information. This diversity of the information is being used by the fusion/ensemble method to achieve better results.

Considering the CPLS approach as a projection method to a common EEG-fMRI subspace we can interpret the EEG and fMRI components as the projection of the EEG and fMRI data respectively to this common subspace, so that the EEG and fMRI component pairs are as close as possible (in a least squares sense) in this new space. This idea is illustrated in Figure 5.6.

5.3. Conclusions

In this study, we introduced a new feature based on the concept of the Fisher score. We used this novel modeling of the EEG to fuse together information from EEG and fMRI. We use HMMs in order to characterize the topography and the temporal evolution of the average ERP. Based on the trained HMM, for each sequence we calculate the Fisher of each parameter for that sequence.

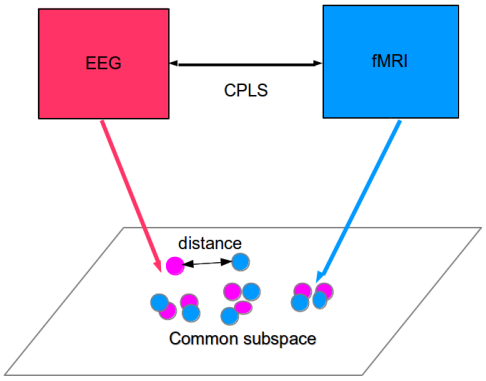

Figure 5.6: Illustration of the CPLS interpretation of the projected components.

The transformation to the Fisher score space, allows bridging the descriptive power of generative models with the efficiency of discriminative approaches. The derived score describes how the parameters of the model must change in order to adapt to the new sequence. Using the derived feature vectors we can use standard discriminative techniques for the decoding of the EEG.

We apply this technique in a multimodal dataset of 16 subjects performing a visual task and use the derived results for fusing EEG information with fMRI using CPLS. We evaluated the effectiveness of CPLS in describing the cross-covariance between the EEG and fMRI datasets, by applying it of the average ERP and the fMRI features. CPLS successfully recovered the two prominent peaks of the average ERP in different components and the corresponding fMRI component localizes the activation in regions that are related to the corresponding peak, as expected from the literature.

Using the same technique between the Fisher score features of the EEG and the fMRI, the results show that using CPLS it is possible to relate the hidden states described by the HMM model to fMRI activations. Using this descriptor we were able to recover components that are significantly different between states. These results indicate that the Fisher score can be used for the decoding

the EEG activation patterns of different tasks. On top of that CPLS can be used to combine and fuse information between modalities and use the results for multimodal classification and decoding. This direction was explored in the last part of this study. The CPLS and Fisher score methodology was used for discrimination of the two type of stimuli. This approach was compared with PCA as a way to perform of dimensionality reduction. CPLS methodology provides comparable results with PCA, a result that confirms the previous analysis. CPLS extracts information relevant to the presented stimulus in part guided by fMRI.

The last part is devoted in the construction of a hybrid classifier that performs fusion in the feature and the decision level. We tested well known functions that have been used extensively for the combination of the scores of multiple classifiers. The significant increase in the classification performance when a low number of components is used for CPLS and PCA provides insight on the type of features that each methodology focuses on. It is apparent that CPLS takes advantage of the common variability with the fMRI. On the other hand PCA uses EEG information only and when a small number of components is used the classification results are not so good. The significant increase in the performance when a small number of components is used, is in line with the model of the explained EEG and fMRI activity presented in Section 2.5. CPLS targets the variability common to both modalities initially, while PCA explains the global EEG variance which includes additional information. The combination of these two modalities provides better classification results since we introduce complemented information from the two methods. This is an important observation that could lead to better analysis techniques that combine these techniques together.

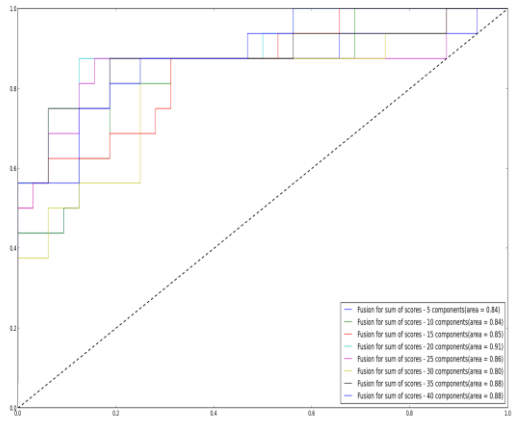

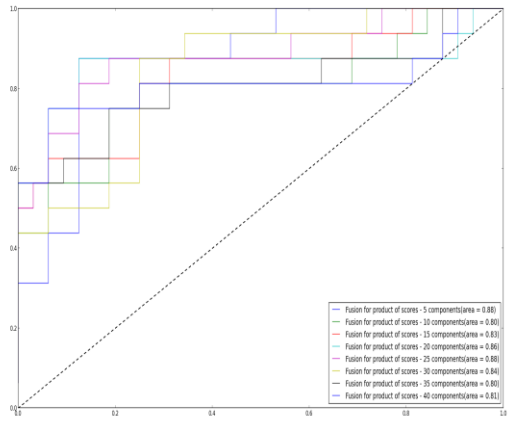

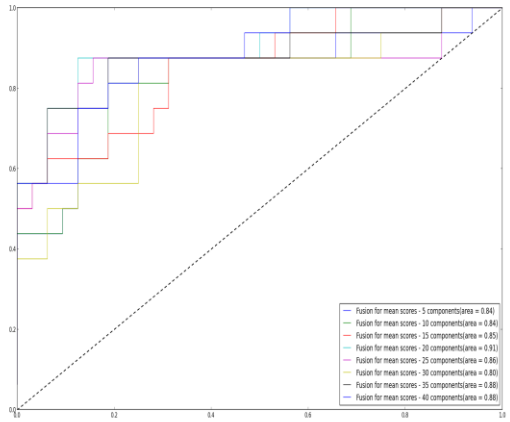

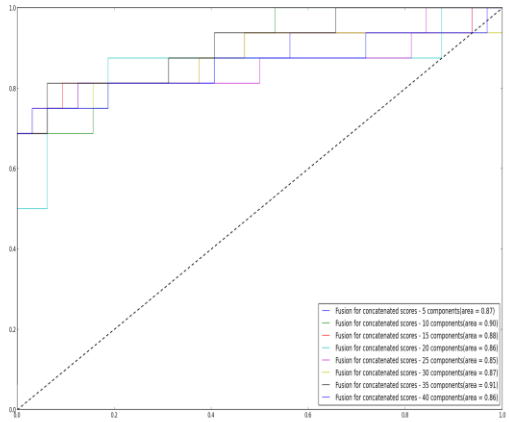

Figure 5.7: ROC curves for each of the combiner functions for different number of components. All functions present similar behavior.

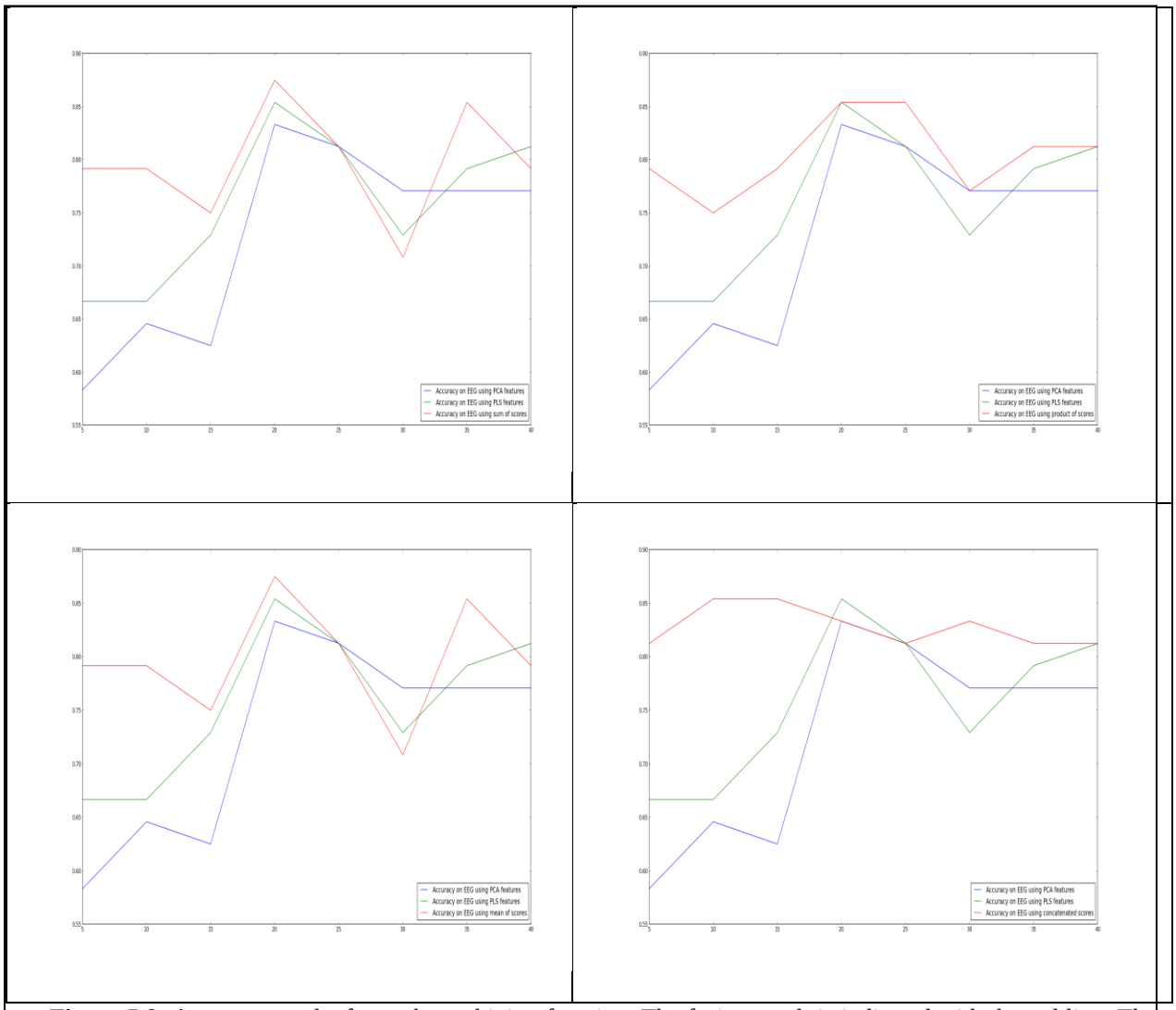

Figure 5.8: Accuracy results for each combining function. The fusion result is indicated with the red line. The fusion result remains almost stable at the same level for different number of components.

CHAPTER 6: **Extending the microstate model using Dynamic Bayesian Networks**

Different methods and techniques have been developed in order to extract features from electroencephalography (EEG) that are capable to characterize pathologies or discriminate different functional states. For the first case, we are interested in the extraction of features that characterize the different groups and are able to distinguish between normal and abnormal EEG. For the latter case we are more interested in the identification of features that characterize the brain response during a certain task. The EEG brain response specific to the given stimulus or event, is known as Event Related Potential (ERP). Approaches that try to extract features from Event related recordings have many applications for the development of brain computer interfaces and a lot of effort has been devoted towards this direction [192].

A lot of studies have focused in the analysis of time and frequency characteristics of the EEG signals. As we noticed in the previous chapters, this approach usually entails the selection of a single channel and extraction of signal features on this particular electrode [170] and this selection of electrodes of interest is usually based on the experimental setup. Various techniques have been developed in order to extract the most informative electrodes for each case [179]. A limitation of the single channel analysis approach is that due to volume conduction, the recorded electrical

activity is the result of the summation of multiple sources activated in coordination [4] and therefore limiting the analysis on a single electrode discards information by disregarding the fact that different aspects of the underlying brain activity are manifested in multiple locations in parallel. Multivariate techniques as Principal Component Analysis (PCA) and Independent Component Analysis (ICA) have been employed in an effort to alleviate this problem [4], [122], [162]. Different methodologies have been used in order to extract features able to discriminate the brain responses to different tasks. Such features include the power of the different bands, auto-regressive parameters and information theoretical measures as Mutual Information and entropy [192]. Time-frequency methods have also been used for studying the temporal behavior of frequency specific features.

In contrast to the analysis that is focused on the temporal features of the multichannel EEG signal, the microstate model considers the spatial distribution of the electric field in the scalp also known as topographic map. In the previous chapters, we extensively explored the use of this EEG feature for group analysis. We used it and displayed its usefulness for the discrimination of pathology and for the discrimination between tasks. The discrimination between tasks was applied for the average ERP and it was performed in a group level. In order to test the usefulness of the newly introduced spatiotemporal modeling of the EEG, we have to test the methodology in the single trial level in a within subject study. In this chapter, we extend the HMM model in order to incorporate the frequency information carried in the EEG signal.

Considering the traditional microstate analysis, it usually considers the wideband EEG signal or is restricted to a single band of interest. The main assumption is that the underlying microstates remain the same throughout the different bands and subsequently the different bands activate in a synchronous and coherent manner [126], [193]. Features regarding the occurrence and duration of

the identified microstates have been used for discriminating different pathologies. Recently, a classification method using HMMs was used for the classification of tasks in Electrocorticography data with promising results [159].

Regarding the band specific evolution of the topographic maps, results from the analysis of temporal features of the EEG and especially from the application of ICA, indicate that activity attributed to a certain band arises in certain electrodes in conjunction or as a response to other band activations in different locations [122], [194]. The ensemble of these activations constitutes an interacting network that characterizes the functional processing that takes place. We use DBNs to model the interaction of the different bands in terms of the temporal evolution of their topographies using DBNs [195] that generalize the concept of Hidden Markov Models and can model the interaction of multiple variables.

In this work we use the spatio-temporal features of the EEG as defined by the microstate model for the classification of single trials between tasks. To our knowledge little effort has been devoted regarding the use of the microstate model towards the classification of single trial responses. We evaluate this approach in a classification scenario where we try to distinguish among target and non-target trials, using the modeled temporal evolution of the topography map in the single trial level. Using different DBNs we are going to study the effect of the coupling between the modeled bands.

6.1. Methods

6.1.1. Modeling of the EEG topography.

As we have noted in the previous chapters, the approaches used for the identification of the dominant microstates are based on clustering techniques and variants of k-means and hierarchical agglomerative algorithm have been developed [170]. The main problem with the application of the microstate approach in the single trial level is that the single-trial recordings contain many more active sources than the average ERP. The signal to noise ratio on the single trial data is also very low, constituting the single trial analysis a difficult task in general.

In this case, the LG graph modeling technique is used for the modeling of the single trial topographies. The main advantage of this approach is that using the LG graph we are able to filter out the noise in the topography and work only with the salient features of the topography map. The additional advantage comes for the discretization of the topographies. The clustering step needed for the creation of the codebook acts as a filtering step, smoothing out noisy topographies and working only with the centroids of the clusters.

6.1.2. Spatio-Temporal modeling of the topography

The next step is to model the temporal evolution of the topography in the scalp. The clustering approach [170] has been used in order to represent the multichannel signal using a set of representative topographies that explain a sufficient amount of the data variance. The clustering approach disregards the temporal dependencies between adjacent topographies and considers that the samples are identically and independently distributed. The basic methodology that has been used so far, also applies in this case.

We are again considering the EEG signals as time series of topographies with temporal dependencies. The main difference with the previous approaches is that we are using Dynamic Bayesian Networks (DBNs) [195] in order to model the temporal evolution of the EEG topography.

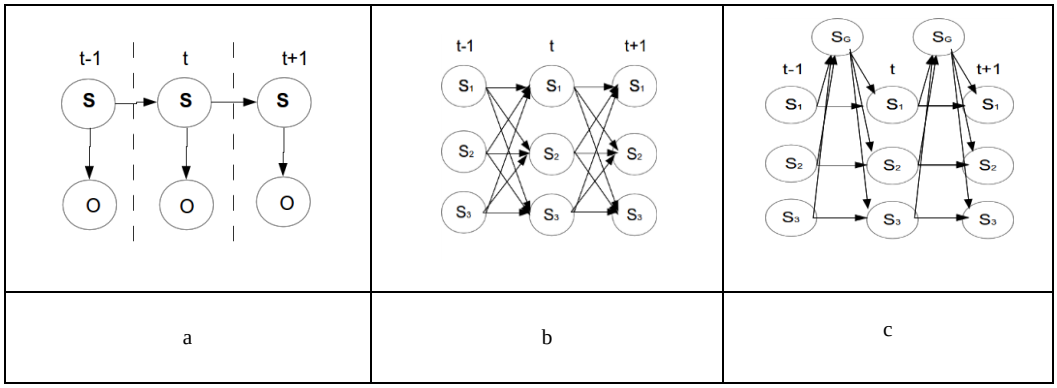

Figure 6.1: Graphical representation for the HMM(a), CHMM(b) and the two level influence model.(c) In models (b) and (c) the observed nodes are not shown for simplicity.

Under this formulation, the modeled stable microstates are represented by hidden states in the Bayesian Network and form a Markov chain while the different topographies represent the observations. A Hidden Markov Model (HMM) can be considered a simple DBN and we can observe it in Figure 6.1.

The assumption that all the bands display the same topography is seriously challenged by findings based on other studies [122], [194]. In our case we want to take under consideration the relationships between the different bands and use this information for better modeling of the data. For this reason we apply three different models to evaluate the interaction between the bands and their effect on the classification result.

Coupled Hidden Markov Models (CHMMs) [195] have been used in order to evaluate the coupling and dependencies between Markov chains. In our case we are considering each band a different Markov Chain and model the ensemble of the bands using CHMM. The graphical model of the CHMM can be seen in Figure 6.1.

Removing the coupling between the chains results in a Parallel Hidden Markov model (PHMM) [196], where each chain follows its own dynamics independently. Using the PHMM we

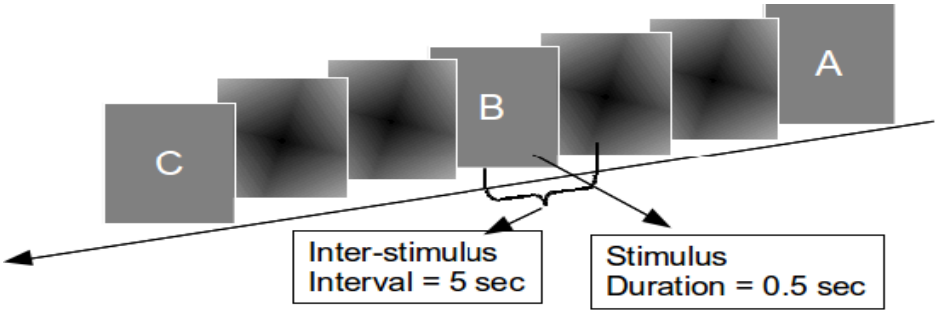

Figure 6.2: Illustration of the experiment used for evaluation of the three models. The target trials are displayed as boxes with letters.

want to assess the importance of the interaction between the bands. The idea is that if the classification results of the PHMM are comparable to those of the CHMM then we cannot justify the extra computational complexity introduced by the CHMM model.

A different model that can represent the influence between Markov Chains was proposed in [197]. Under this model, there exists an extra node, which represents the global state of the system and depends on the states of the individual chains. The next state of each chain depends on the current state and the global system state. The graphical representation of this model can be seen in Figure 1c and is adapted from [197]. Under this model we have the individual chains of the different bands and in contrast to the CHMM the influence of each node to the other is indirectly modeled through the global node. A hidden switching node Q (not shown) is used to simplify the model and represents the individual influence of each band to the global state.

Overall for all models, we consider that each band is characterized by a Markov chain with hidden states. The observed topographies are conditionally independent given the hidden state. We assume that the number of hidden states are discrete and the same for each band. We are also considering that the observations are discrete. This choice allows for a non-parametric modeling of the conditional distribution of the observations on the one hand and on the other it is easier to work

with the LG graph modeling. All the models were evaluated using the Bayes Net Toolbox for Matlab. In the next section we describe the steps used for discretization of the dataset and the construction of the resulting codebook.

6.1.3. Discretization and codebook generation

We apply the single-link hierarchical agglomerative algorithm in the data using the LG graph distance defined before. The single link algorithm provides compact clusters and has been used for vector quantization successfully before [160]. We are using a distance threshold depending on the fidelity of the quantization procedure and the desired number of clusters. We apply this procedure for each band separately. At a second level we are using the same strategy on the centrotypes of the clusters in order to merge similar topographies among bands together. Using the same codebook for all bands we encode the single trials by selecting the symbol (LG graph) that presents the minimum distance from the original topography. In this study we ignore the effect of the discretization error and we assume that it equally affects the training and test procedure of the classification.

6.2. Experiments

6.2.1. Data Description and preprocessing

The dataset used was provided by Clinical Neurophysiology and Neuroimaging Unit, University Hospitals of Geneva. We used all trials from a detection task in our analysis. We used only the period 1000ms after the stimulus where we expect the main response.

Subjects were seated and watched a computer screen. We used the trials from a detection task, where the subjects were asked to press a button with their right index finger as soon as a target appeared [163]. In the detection task background patches and patches containing letters were sequentially displayed in the screen. The later were considered as targets and required motor response from the subject. When background patches without letter were displayed no motor action was required. EEG data were recorded using 20 surface electrodes, according to the 10–20 international system. The stimulus duration was 0.5 sec and the inter-stimulus interval was 5 sec. In total for each subject we have 20 target trials and 69 non target trials.

The data were examined for artifacts and only artifact-free trials were used. We used 8 subjects in the current study. The data were band-pass filtered in the range of delta(0.5 to 3Hz), theta(3 to 8Hz) and alpha band(8 to 13Hz) using a linear Finite Impulse response filter. For the classification procedure only a window of one second after the stimulus was used, where the main response component is expected [163].

6.2.2. Results

We treated each subject separately and for each, a separate codebook was constructed. For the construction of the codebook we considered twenty clusters, as many as the number of electrodes. The error introduced by the quantization procedure is going to be transferred and affect the classification step. At this point though, we are not interested in the quantization procedure itself and since we used all the train and test trials for the codebook construction we assume that the quantization error is a common factor for both training and testing.

An important part of the procedure is the model selection. We tried different numbers of parameters for each model. For all models we assumed that all the chains have the same number of

states and for the influence model we assumed that the global node also has the same number of states as the individual chains. As the number of hidden states increased so did the classification accuracy of the model. We tried different models ranging from four to ten hidden states but the difference in the classification result was not significant when using more than six hidden states. For the influence model the number of hidden states of the individual chains does not play an important role in the classification or the behavior of the model as reported in [197]. We report the results from using six states for all hidden nodes.

We used a repeated random sub-sampling validation procedure in order to evaluate the performance of each model. Each model was trained using a train set of 10 target and 10 non-target trials selected from the dataset without replacement. The remaining 10 target trials and 10 random non-target trials were used for the test set. The train dataset and the test dataset were shuffled 10 times producing different sets and the results were averaged over all repetitions. The average results of this procedure are reported in Table VIII. The measures of performance are defined as:

$$Precision = \frac{tp}{(tp + fp)} \tag{36}$$

$$Recall = \frac{tp}{(tp + fn)} \tag{37}$$

$$Accuracy = \frac{(tp + tn)}{(tp + tn + fp + fn)} \tag{38}$$

In equations (36) to (38) by $\mathrm{tp}, \mathrm{tn}, \mathrm{fp}, \mathrm{fn}$ we denote the number of true positive, the number of true negative, the number of false positive and the number of false negative predictions respectively. We can see that the PHMM model clearly has the worst performance out of the other two models. The CHMM model provides the highest accuracy over all models. This can be partly attributed to the fact that it is the most complex allowing direct interactions among bands. On the

other hand the two-level influence model has fewer parameters to be computed and therefore is more computationally tractable but presents reduced accuracy compared to CHMM.

In order to evaluate whether the reduced performance of the PHMM model can be attributed to the lack of coupling between the bands or the model selection, we run multiple trials using models of different orders, up to ten hidden states. In any case, the performance of the model remained lower than the CHMM and influence model. This result indicates that interactions between the different bands play an important role in the classification result and contribute to the increased performance of the two models that take them under consideration

6.1. Conclusion

We presented a study for the classification of target and non-target single trials from a visual experiment. We modeled the evolution of the EEG topography using dynamic Bayesian nets in an

Table VIII: Mean Results over Subjects

	Classification results		
	Precision	**Recall**	**Accuracy**
PHMM	0.833	0.75	0.790
CHMM	0.901	0.949	0.925
Influence Model	0.88	0.80	0.85

effort to evaluate it as a feature capable to discriminate among tasks. Based on the concept of microstates we are using the hidden states of the Bayesian network to represent the temporal evolution of the EEG topography. We acquired good classification results although we took under

consideration only the spatial configuration of the electric field in the scalp. Since we used only the normalized maps our analysis did not account for differences in the amplitude of the topographic response.

We are extending the microstate notion by modeling the interaction of the states among three bands. Using two DBNs capable to represent the interactions between Markov chains, the CHMMs and a two level influence model, we were able to capture the dependencies and interactions between the topographic activations in different bands. This aspect of the microstate model is often neglected. The results indicate that using this information allowed to capture the dynamics among the bands and improved the classification results. The models that capture the coupling between the different bands provide more information and better results that the PHMM which ignores any interaction between the chains.

In future work we intend to incorporate more features in our analysis, taking advantage of the flexibility provided by the DBNs. An interesting extension is to explore the relation between topographic and time-frequency features using DBNs. Using this methodology we can explore the dynamic interaction between bands and derive useful features that can be used for the discrimination of different pathologies and can also be used for Brain Computer Interface applications.

CHAPTER 7: **Conclusion and Contributions**

In this work, a synergistic methodology for the modeling of the EEG topography using LG graphs and HMMs was presented. The new modeling of the EEG activity was used for fusing EEG and fMRI features for the development of a multimodal classifier system. The Fisher score was introduced as a descriptive feature of the derived HMM. Using the Fisher score we move from the generative HMM model to discriminative techniques that allow the multivariate analysis and assessment of significance of the derived features.

This novel modeling scheme was successfully applied for the classification among single trials of control subjects and subjects diagnosed with Progressive Mild Cognitive Impairment. The results indicate that this methodology can effectively characterize the differences between the two groups and the derived properties of the HMM model were consistent and displayed common behavior with well-studied time-frequency activity of the average ERP. The results are significant and indicate that further study on the neural mechanisms reflected in the topographic patterns could reveal important aspects regarding the MCI and normal aging.

Using the Fisher score, a novel feature-based description of the average ERP was introduced that allows the fusion with features of the fMRI. Canonical Partial Least squares is well known technique that has been used in many applications. It is closely related to Canonical Correlation analysis, although it presents certain advantages that make it suitable for use with classification

applications. We demonstrated that CPLS can effectively separate the different ERP peaks into separate components, along with their fMRI counterparts. We use the Fisher score features in conjunction with CPLS in order to derive the associated localized fMRI activity. The results show that the Fisher score of the transition matrix can effectively describe the temporal associations of the EEG topography and relate these features with meaningful fMRI activity. The classifications results show that the CPLS method reduces the dimensionality of the data effectively and it achieve classification results comparable to those of PCA. The main advantage of CPLS though, is the learning of the common subspace underlying the data that allows borrowing information from one modality in order to improve the classification performance of the other. The results of this methodology to a dataset where the task was to respond to the presence of faces of persons demonstrate this advantage.

From this dissertation, a series of publications were produced and this work was presented in notable conferences:

- Michalopoulos, Konstantinos, Michail Tsakalakis, and Nikolaos Bourbakis. "An Architectural Hardware Scheme for the Generation of LG Graphs for Real-Time Image Analysis." Digital Signal Processing (DSP), 2013 18th International Conference on. IEEE, 2013. 1–6. Print.
- Michalopoulos, Kostas, and Nikolaos Bourbakis. "Microstate Analysis of the EEG Using Local Global Graphs." Bioinformatics and Bioengineering (BIBE), 2013 IEEE 13th International Conference on. IEEE, 2013. 1–5. Print.

- Fusion of EEG topograhic features and fMRI using Canonical Partial Least Squares Bioinformatics and Bioengineering (BIBE), 2014 IEEE 14th International Conference on. IEEE, 2014
- Using Dynamic Bayesian Networks for modeling EEG topographic sequences. Engineering in Medicine and Biology Society, 2014. EMBC 2014. Annual International Conference of the IEEE.
- Michalopoulos, K, M Zervakis, and N Bourbakis. "Current Trends in ERP Analysis Using EEG and EEG/fMRI Synergistic Methods." (2013).

7.1. Future Work

For future work, an extension of the current work in simultaneously acquired datasets of EEG and fMRI is planned. Using simultaneously acquired EEG and fMRI will allow the integration of the two modalities in the single trial level. This will also allow to test the HMM methodology presented in Chapter 4 for building Hybrid classifier systems for the effective decoding of the brain activity.

An interesting extension of the current work has to do with information regarding the connectivity of the different regions. The topography models the distribution of the electrical field on the scalp and does not take under consideration the phase content of the signal. The degree of connectivity between different regions carries significant information that it is important to be taken under consideration. Under this context, it would be interesting to study connectivity measures along with the topographic organization of the electrical field.

Finally, following the results of Chapter 5 and 6, an important future direction involves the in depth study of the HMM and Fisher score modeling for BCI applications. The fusion of EEG and

fMRI is also a promising direction for improving such systems. An important finding from this work is that using our methodology we are able to use fMRI to train the system offline and this information is sufficient to improve the classification results using only the EEG recordings online. We plan to use this approach in brain computer interface applications for reducing the calibration time and improve the performance. Further investigation towards the direction of information and classification fusion using multiple EEG features and classifiers will provide more in depth evaluation of this approach.

References

[1] H. J. Heinze, T. F. Münte, and G. R. Mangun, *Cognitive electrophysiology*. Boston: Birkhäuser, 1994.

[2] V. Sakkalis, "Applied strategies towards EEG/MEG biomarker identification in clinical and cognitive research," *Biomarkers*, vol. 5, no. 1, pp. 93–105, 2011.

[3] S. Ogawa, T. Lee, A. Kay, and D. Tank, "Brain magnetic resonance imaging with contrast dependent on blood oxygenation," *Proc. Natl. Acad. Sci.*, vol. 87, no. 24, pp. 9868–9872, 1990.

[4] S. Makeig, S. Debener, J. Onton, and A. Delorme, "Mining event-related brain dynamics," *Trends Cogn. Sci.*, vol. 8, no. 5, pp. 204–210, 2004.

[5] E. M. Bernat, S. M. Malone, W. J. Williams, C. J. Patrick, and W. G. Iacono, "Decomposing delta, theta, and alpha time-frequency ERP activity from a visual oddball task using PCA," *Int. J. Psychophysiol.*, vol. 64, no. 1, pp. 62–74, 2007.

[6] T. Koenig, L. Prichep, D. Lehmann, P. V. Sosa, E. Braeker, H. Kleinlogel, R. Isenhart, and E. R. John, "Millisecond by Millisecond, Year by Year: Normative EEG Microstates and Developmental Stages," *NeuroImage*, vol. 16, no. 1, pp. 41–48, May 2002.

[7] M. M. Murray, D. Brunet, and C. M. Michel, "Topographic ERP Analyses: A Step-by-Step Tutorial Review," *Brain Topogr.*, vol. 20, no. 4, pp. 249–264, Jun. 2008.

[8] M. J. Rosa, J. Daunizeau, and K. J. Friston, "EEG-fMRI INTEGRATION: A CRITICAL REVIEW OF BIOPHYSICAL MODELING AND DATA ANALYSIS APPROACHES," *J. Integr. Neurosci.*, vol. 09, no. 04, p. 453, 2010.

[9] J. A. Detre, J. S. Leigh, D. S. Williams, and A. P. Koretsky, "Perfusion imaging," *Magn. Reson. Med.*, vol. 23, no. 1, pp. 37–45, 2005.

[10] N. Blockley, S. Francis, and P. Gowland, “Perturbation of the BOLD response by a contrast agent and interpretation through a modified balloon model,” *Neuroimage*, vol. 48, no. 1, pp. 84–93, 2009.

[11] P. L. Nunez and R. Srinivasan, *Electric fields of the brain: the neurophysics of EEG*. Oxford University Press, USA, 2005.

[12] S. Baillet, J. C. Mosher, and R. M. Leahy, “Electromagnetic brain mapping,” *IEEE Signal Process. Mag.*, vol. 18, no. 6, pp. 14 –30, Nov. 2001.

[13] C. Tallon-Baudry and O. Bertrand, “Oscillatory gamma activity in humans and its role in object representation,” *Trends Cogn. Sci.*, vol. 3, no. 4, pp. 151–162, 1999.

[14] G. Pfurtscheller and F. H. Lopes da Silva, “Event-related EEG/MEG synchronization and desynchronization: basic principles,” *Clin. Neurophysiol.*, vol. 110, no. 11, pp. 1842–1857, 1999.

[15] W. Klimesch, “EEG alpha and theta oscillations reflect cognitive and memory performance: a review and analysis,” *Brain Res. Rev.*, vol. 29, no. 2–3, pp. 169–195, 1999.

[16] J. C. de Munck, S. I. Gonçalves, R. Mammoliti, R. M. Heethaar, and F. H. Lopes da Silva, “Interactions between different EEG frequency bands and their effect on alpha–fMRI correlations,” *NeuroImage*, vol. 47, no. 1, pp. 69–76, Aug. 2009.

[17] J. Yordanova, V. Kolev, and J. Polich, “P300 and alpha event-related desynchronization (ERD),” *Psychophysiology*, vol. 38, no. 1, pp. 143–152, 2001.

[18] T.-P. Jung, S. Makeig, M. Westerfield, J. Townsend, E. Courchesne, and T. J. Sejnowski, “Analysis and visualization of single-trial event-related potentials,” *Hum. Brain Mapp.*, vol. 14, no. 3, pp. 166–185, 2001.

[19] F. Miwakeichi, E. Martínez-Montes, P. A. Valdés-Sosa, N. Nishiyama, H. Mizuhara, and Y. Yamaguchi, “Decomposing EEG data into space–time–frequency components using Parallel Factor Analysis,” *NeuroImage*, vol. 22, no. 3, pp. 1035–1045, Jul. 2004.

[20] M. Zervakis, K. Michalopoulos, V. Iordanidou, and V. Sakkalis, “Intertrial coherence and causal interaction among independent EEG components,” *J. Neurosci. Methods*, vol. 197, no. 2, pp. 302–314, Apr. 2011.

[21] T. Demiralp, A. Ademoglu, M. Comerchero, and J. Polich, “Wavelet Analysis of P3a and P3b,” *Brain Topogr.*, vol. 13, no. 4, pp. 251–267, 2001.

[22] C. Tallon-Baudry, O. Bertrand, C. Delpuech, and J. Pernier, “Stimulus Specificity of Phase-Locked and Non-Phase-Locked 40 Hz Visual Responses in Human,” *J. Neurosci.*, vol. 16, no. 13, pp. 4240–4249, 1996.

[23] A. J. Bell and T. J. Sejnowski, “The ‘independent components’ of natural scenes are edge filters,” *Vision Res.*, vol. 37, no. 23, p. 3327, 1997.

[24] T. D. Lagerlund, F. W. Sharbrough, and N. E. Busacker, “Spatial filtering of multichannel electroencephalographic recordings through principal component analysis by singular value decomposition,” *J. Clin. Neurophysiol.*, vol. 14, no. 1, pp. 73–82, 1997.

[25] O. G. Lins, T. W. Picton, P. Berg, and M. Scherg, “Ocular artifacts in EEG and event-related potentials I: Scalp topography,” *Brain Topogr.*, vol. 6, no. 1, pp. 51–63, 1993.

[26] T.-P. Jung, C. Humphries, T. Lee, S. Makeig, M. J. Mckeown, V. Iragui, and T. J. Sejnowski, *Removing Electroencephalographic Artifacts: Comparison between ICA and PCA*. 1998.

[27] K. Michalopoulos, V. Iordanidou, M. Zervakis, P. M. Pardalos, and P. Xanthopoulos, “Application of Decomposition methods in the Filtering of Event-Related Potentials.,” in *Data Mining for Biomarker Discovery*, vol. 65, P. M. Pardalos, P. Xanthopoulos, and M. Zervakis, Eds. Boston, MA: Springer US, 2012.

[28] N. Lazar, *The statistical analysis of functional MRI data*. Springer-Verlag New York, 2008.

[29] M. Skup, “Longitudinal fMRI analysis: A review of methods,” *Stat. Interface*, vol. 3, no. 2, pp. 235–252, 2010.

[30] M. A. Lindquist, “The Statistical Analysis of fMRI Data,” *arXiv:0906.3662*, Jun. 2009.

[31] S. C. Strother, “Evaluating fMRI preprocessing pipelines,” *Eng. Med. Biol. Mag. IEEE*, vol. 25, no. 2, pp. 27 – 41, Apr. 2006.

[32] N. Lazar and N. A. Lazar, “Statistical Issues in fMRI Data Analysis,” in *The Statistical Analysis of Functional MRI Data*, Springer New York, 2008, pp. 1–11.

[33] X. Hu, T. H. Le, T. Parrish, and P. Erhard, “Retrospective estimation and correction of physiological fluctuation in functional MRI,” *Magn. Reson. Med.*, vol. 34, no. 2, pp. 201–212, 2005.

[34] S. Smith, “Preparing fMRI data for statistical analysis,” *Funct. MRI Introd. Methods*, pp. 229–241, 2001.

[35] R. Sladky, K. J. Friston, J. Tröstl, R. Cunnington, E. Moser, and C. Windischberger, “Slice-timing effects and their correction in functional MRI,” *NeuroImage*, vol. 58, no. 2, pp. 588–594, Sep. 2011.

[36] J. Ashburner and K. Friston, “Multimodal image coregistration and partitioning—a unified framework,” *Neuroimage*, vol. 6, no. 3, pp. 209–217, 1997.

[37] R. W. Cox, A. Jesmanowicz, and others, “Real-time 3D image registration for functional MRI,” *Magn. Reson. Med.*, vol. 42, no. 6, pp. 1014–1018, 1999.

[38] M. Jenkinson, P. Bannister, M. Brady, S. Smith, and others, “Improved optimization for the robust and accurate linear registration and motion correction of brain images,” *Neuroimage*, vol. 17, no. 2, pp. 825–841, 2002.

[39] R. P. Woods, M. Dapretto, N. L. Sicotte, A. W. Toga, and J. C. Mazziotta, “Creation and use of a Talairach-compatible atlas for accurate, automated, nonlinear intersubject registration, and analysis of functional imaging data,” *Hum. Brain Mapp.*, vol. 8, no. 2–3, pp. 73–79, 1999.

[40] N. A. Lazar, B. Luna, J. A. Sweeney, and W. F. Eddy, “Combining brains: a survey of methods for statistical pooling of information,” *Neuroimage*, vol. 16, no. 2, pp. 538–550, 2002.

[41] S. M. Smith, M. Jenkinson, M. W. Woolrich, C. F. Beckmann, T. E. J. Behrens, H. Johansen-Berg, P. R. Bannister, M. De Luca, I. Drobnjak, D. E. Flitney, R. K. Niazy, J. Saunders, J. Vickers, Y. Zhang, N. De Stefano, J. M. Brady, and P. M. Matthews, “Advances in functional and structural MR image analysis and implementation as FSL,” *NeuroImage*, vol. 23, Supplement 1, no. 0, pp. S208–S219, 2004.

[42] M. S. Cohen, “Parametric Analysis of fMRI Data Using Linear Systems Methods,” *NeuroImage*, vol. 6, no. 2, pp. 93–103, Aug. 1997.

[43] M. S. Cohen, S. Kosslyn, H. Breiter, G. J. DiGirolamo, W. Thompson, A. Anderson, S. Bookheimer, B. Rosen, and J. Belliveau, “Changes in cortical activity during mental rotation A mapping study using functional MRI,” *Brain*, vol. 119, no. 1, pp. 89–100, 1996.

[44] R. T. Constable, P. Skudlarski, and J. C. Gore, “An roc approach for evaluating functional brain mr imaging and postprocessing protocols,” *Magn. Reson. Med.*, vol. 34, no. 1, pp. 57–64, 1995.

[45] K. J. Friston, A. P. Holmes, J.-B. Poline, P. J. Grasby, S. C. R. Williams, R. S. J. Frackowiak, and R. Turner, “Analysis of fMRI Time-Series Revisited,” *NeuroImage*, vol. 2, no. 1, pp. 45–53, Mar. 1995.

[46] K. J. Worsley and K. J. Friston, “Analysis of fMRI Time-Series Revisited—Again,” *NeuroImage*, vol. 2, no. 3, pp. 173–181, Sep. 1995.

[47] R. B. Buxton, E. C. Wong, and L. R. Frank, “Dynamics of blood flow and oxygenation changes during brain activation: The balloon model,” *Magn. Reson. Med.*, vol. 39, no. 6, pp. 855–864, 1998.

[48] V. D. Calhoun, T. Adali, G. D. Pearlson, and J. J. Pekar, “Spatial and temporal independent component analysis of functional MRI data containing a pair of task-related waveforms,” *Hum. Brain Mapp.*, vol. 13, no. 1, pp. 43–53, May 2001.

[49] J. Himberg and A. Hyv, “Validating the independent components of neuroimaging time-series via clustering and visualization,” *Computer*, 2003.

[50] M. J. McKeown and T. J. Sejnowski, “Independent component analysis of fMRI data: Examining the assumptions,” *Hum. Brain Mapp.*, vol. 6, no. 5–6, pp. 368–372, 1998.

[51] K. Arfanakis, D. Cordes, V. M. Haughton, C. H. Moritz, M. A. Quigley, and M. E. Meyerand, “Combining independent component analysis and correlation analysis to probe interregional connectivity in fMRI task activation datasets,” *Magn. Reson. Imaging*, vol. 18, no. 8, pp. 921–930, Oct. 2000.

[52] O. Friman, J. Cedefamn, P. Lundberg, M. Borga, and H. Knutsson, “Detection of neural activity in functional MRI using canonical correlation analysis,” *Magn. Reson. Med.*, vol. 45, no. 2, pp. 323–330, 2001.

[53] V. d. Calhoun, T. Adali, G. d. Pearlson, and J. j. Pekar, “A method for making group inferences from functional MRI data using independent component analysis,” *Hum. Brain Mapp.*, vol. 14, no. 3, pp. 140–151, 2001.

[54] V. Calhoun, R. Silva, and J. Liu, “Identification of Multimodal MRI and EEG Biomarkers using Joint-ICA and Divergence Criteria,” in *2007 IEEE Workshop on Machine Learning for Signal Processing*, 2007, pp. 151 – 156.

[55] J. V. Haxby, E. A. Hoffman, and M. I. Gobbini, “The distributed human neural system for face perception,” *Trends Cogn. Sci.*, vol. 4, no. 6, pp. 223–233, Jun. 2000.

[56] M. Hanke, Y. O. Halchenko, P. B. Sederberg, E. Olivetti, I. Fründ, J. W. Rieger, C. S. Herrmann, J. V. Haxby, S. J. Hanson, S. Pollmann, M. Hanke, Y. O. Halchenko, P. B. Sederberg, E. Olivetti, I. Fründ, J. W. Rieger, C. S. Herrmann, J. V. Haxby, S. J. Hanson, and S. Pollmann, “PyMVPA: a unifying approach to the analysis of neuroscientific data,” *Front. Neuroinformatics*, vol. 3, p. 3, 2009.

[57] N. K. Logothetis, J. Pauls, M. Augath, T. Trinath, A. Oeltermann, and others, “Neurophysiological investigation of the basis of the fMRI signal,” *Nature*, vol. 412, no. 6843, pp. 150–157, 2001.

[58] G. McCarthy, “Event-related potentials and functional MRI: a comparison of localization in sensory, perceptual and cognitive tasks,” *Electroencephalogr. Clin. Neurophysiol. Suppl.*, vol. 49, pp. 3–12, 1999.

[59] M. g. Woldorff, M. Matzke, F. Zamarripa and, and P. t. Fox, “Hemodynamic and electrophysiological study of the role of the anterior cingulate in target-related processing and selection for action,” *Hum. Brain Mapp.*, vol. 8, no. 2–3, pp. 121–127, 1999.

[60] S. Makeig, T.-P. Jung, and T. J. Sejnowski, “Having your voxels and timing them too?,” in *Exploratory analysis and data modeling in functional neuroimaging*, F. T. Sommer and A. Wichert, Eds. Cambridge, MA, USA: MIT Press, 2003, pp. 195–207.

[61] A. K. Liu, J. W. Belliveau, and A. M. Dale, “Spatiotemporal imaging of human brain activity using functional MRI constrained magnetoencephalography data: Monte Carlo simulations,” *Proc. Natl. Acad. Sci.*, vol. 95, no. 15, pp. 8945–8950, Jul. 1998.

[62] F. Babiloni, C. Babiloni, F. Carducci, G. L. Romani, P. M. Rossini, L. M. Angelone, and F. Cincotti, “Multimodal integration of high-resolution EEG and functional magnetic resonance imaging data: a simulation study,” *NeuroImage*, vol. 19, no. 1, pp. 1–15, May 2003.

[63] B. Opitz, A. Mecklinger, D. Y. Von Cramon, and F. Kruggel, “Combining electrophysiological and hemodynamic measures of the auditory oddball,” *Psychophysiology*, vol. 36, no. 1, pp. 142–147, Jan. 1999.

[64] D. Vitacco, D. Brandeis, R. Pascual-Marqui, and E. Martin, “Correspondence of event-related potential tomography and functional magnetic resonance imaging during language processing,” *Hum. Brain Mapp.*, vol. 17, no. 1, pp. 4–12, Sep. 2002.

[65] R. Pascual-Marqui, M. Esslen, K. Kochi, D. Lehmann, and others, “Functional imaging with low-resolution brain electromagnetic tomography (LORETA): a review,” *Methods Find. Exp. Clin. Pharmacol.*, vol. 24, no. suppl C, pp. 91–95, 2002.

[66] F. Babiloni, F. Cincotti, C. Babiloni, F. Carducci, D. Mattia, L. Astolfi, A. Basilisco, P. M. Rossini, L. Ding, Y. Ni, J. Cheng, K. Christine, J. Sweeney, and B. He, “Estimation of the cortical functional connectivity with the multimodal integration of high-resolution EEG and fMRI data by directed transfer function,” *NeuroImage*, vol. 24, no. 1, pp. 118–131, Jan. 2005.

[67] F.-H. Lin, T. Witzel, M. S. Hämäläinen, A. M. Dale, J. W. Belliveau, and S. M. Stufflebeam, “Spectral spatiotemporal imaging of cortical oscillations and interactions in the human brain,” *NeuroImage*, vol. 23, no. 2, pp. 582–595, Oct. 2004.

[68] R. I. Goldman, J. M. Stern, J. Engel Jr, and M. S. Cohen, “Acquiring simultaneous EEG and functional MRI,” *Clin. Neurophysiol.*, vol. 111, no. 11, pp. 1974–1980, Nov. 2000.

[69] S. P. Koch, J. Steinbrink, A. Villringer, and H. Obrig, “Synchronization between background activity and visually evoked potential is not mirrored by focal hyperoxygenation: implications for the interpretation of vascular brain imaging,” *J. Neurosci.*, vol. 26, no. 18, pp. 4940–4948, 2006.

[70] L. M. Parkes, M. Bastiaansen, D. G. Norris, and others, “Combining EEG and fMRI to investigate the post-movement beta rebound.,” *Neuroimage*, vol. 29, no. 3, p. 685, 2006.

[71] L. Elshoff, K. Groening, F. Grouiller, G. Wiegand, S. Wolff, C. Michel, U. Stephani, and M. Siniatchkin, “The value of EEG-fMRI and EEG source analysis in the presurgical setup of children with refractory focal epilepsy,” *Epilepsia*, vol. 53, no. 9, pp. 1597–1606, 2012.

[72] E. Kobayashi, C. Hawco, C. Grova, F. Dubeau, and J. Gotman, “Widespread and intense BOLD changes during brief focal electrographic seizures,” *Neurology*, vol. 66, no. 7, pp. 1049–1055, 2006.

[73] A. Salek-Haddadi, M. Merschhemke, L. Lemieux, and D. R. Fish, “Simultaneous EEG-correlated ictal fMRI,” *Neuroimage*, vol. 16, no. 1, pp. 32–40, 2002.

[74] K. Blinowska, G. Müller-Putz, V. Kaiser, L. Astolfi, K. Vanderperren, S. Van Huffel, and L. Lemieux, “Multimodal Imaging of Human Brain Activity: Rational, Biophysical Aspects and Modes of Integration,” *Comput. Intell. Neurosci.*, vol. 2009, pp. 1–10, 2009.

[75] S. Debener, M. Ullsperger, M. Siegel, and A. K. Engel, “Single-trial EEG–fMRI reveals the dynamics of cognitive function,” *Trends Cogn. Sci.*, vol. 10, no. 12, pp. 558–563, Dec. 2006.

[76] T. Eichele, K. Specht, M. Moosmann, M. L. A. Jongsma, R. Q. Quiroga, H. Nordby, and K. Hugdahl, “Assessing the spatiotemporal evolution of neuronal activation with single-trial event-related potentials and functional MRI,” *Proc. Natl. Acad. Sci. U. S. A.*, vol. 102, no. 49, pp. 17798–17803, Dec. 2005.

[77] D. Ostwald, “An information theoretic approach to EEG-fMRI integration,” Dec-2010. [Online]. Available: http://etheses.bham.ac.uk/1100/. [Accessed: 22-Jul-2012].

[78] N. Trujillo-Barreto, E. Martinez-Montes, L. Melie-Garcia, and P. Valdés-Sosa, “A symmetrical Bayesian model for fMRI and EEG/MEG neuroimage fusion,” *Int J Bioelectromagn*, vol. 3, no. 1, 2001.

[79] P. A. Valdes-Sosa, J. M. Sanchez-Bornot, R. C. Sotero, Y. Iturria-Medina, Y. Aleman-Gomez, J. Bosch-Bayard, F. Carbonell, and T. Ozaki, "Model driven EEG/fMRI fusion of brain oscillations," *Hum. Brain Mapp.*, vol. 30, no. 9, pp. 2701–2721, 2009.

[80] J. Liu and V. Calhoun, "PARALLEL INDEPENDENT COMPONENT ANALYSIS FOR MULTIMODAL ANALYSIS: APPLICATION TO FMRI AND EEG DATA," in *4th IEEE International Symposium on Biomedical Imaging: From Nano to Macro, 2007. ISBI 2007*, 2007, pp. 1028 –1031.

[81] N. M. Correa, T. Eichele, T. Adalı, Y.-O. Li, and V. D. Calhoun, "Multi-set canonical correlation analysis for the fusion of concurrent single trial ERP and functional MRI," *NeuroImage*, vol. 50, no. 4, pp. 1438–1445, May 2010.

[82] N. M. Correa, Y.-O. Li, T. Adali, and V. D. Calhoun, "Canonical Correlation Analysis for Feature-Based Fusion of Biomedical Imaging Modalities and Its Application to Detection of Associative Networks in Schizophrenia," *IEEE J. Sel. Top. Signal Process.*, vol. 2, no. 6, pp. 998 –1007, Dec. 2008.

[83] C.-G. Benar, R. N. Gunn, C. Grova, B. Champagne, and J. Gotman, "Statistical maps for EEG dipolar source localization," *IEEE Trans. Biomed. Eng.*, vol. 52, no. 3, pp. 401 –413, Mar. 2005.

[84] D. Mantini, L. Marzetti, M. Corbetta, G. Romani, and C. Del Gratta, "Multimodal Integration of fMRI and EEG Data for High Spatial and Temporal Resolution Analysis of Brain Networks," *Brain Topogr.*, vol. 23, no. 2, pp. 150–158, 2010.

[85] V. d. Calhoun, T. Adali, N. r. Giuliani, J. j. Pekar, K. a. Kiehl, and G. d. Pearlson, "Method for multimodal analysis of independent source differences in schizophrenia: Combining gray matter structural and auditory oddball functional data," *Hum. Brain Mapp.*, vol. 27, no. 1, pp. 47–62, 2006.

[86] S. a Meda, B. Narayanan, J. Liu, N. I. Perrone-Bizzozero, M. C. Stevens, V. D. Calhoun, D. C. Glahn, L. Shen, S. L. Risacher, A. J. Saykin, and G. D. Pearlson, "A large scale multivariate parallel ICA method reveals novel imaging-genetic relationships for Alzheimer's disease in the ADNI cohort.," *NeuroImage*, vol. 60, no. 3, pp. 1608–21, Apr. 2012.

[87] E. Martínez-Montes, P. A. Valdés-Sosa, F. Miwakeichi, R. I. Goldman, and M. S. Cohen, "Concurrent EEG/fMRI analysis by multiway Partial Least Squares," *NeuroImage*, vol. 22, no. 3, pp. 1023–1034, Jul. 2004.

[88] R. Bro, "Multiway calibration. Multilinear PLS," *J. Chemom.*, vol. 10, no. 1, pp. 47–61, 1996.

[89] J. Sui, T. Adali, Q. Yu, J. Chen, and V. D. Calhoun, "A review of multivariate methods for multimodal fusion of brain imaging data," *J. Neurosci. Methods*, vol. 204, no. 1, pp. 68–81, Feb. 2012.

[90] G. K. Aguirre, E. Zarahn, and M. D'Esposito, "The Variability of Human, BOLD Hemodynamic Responses," *NeuroImage*, vol. 8, no. 4, pp. 360–369, Nov. 1998.

[91] D. A. Handwerker, J. M. Ollinger, and M. D'Esposito, "Variation of BOLD hemodynamic responses across subjects and brain regions and their effects on statistical analyses," *NeuroImage*, vol. 21, no. 4, pp. 1639–1651, Apr. 2004.

[92] L. Wu, T. Eichele, and V. Calhoun, "Parallel independent component analysis using an optimized neurovascular coupling for concurrent EEG-fMRI sources," in *2011 Annual International Conference of the IEEE Engineering in Medicine and Biology Society,EMBC*, 2011, pp. 2542 –2545.

[93] K. J. Friston, "Modalities, Modes, and Models in Functional Neuroimaging," *Science*, vol. 326, no. 5951, pp. 399–403, Oct. 2009.

[94] K. J. Friston, "Functional and effective connectivity in neuroimaging: A synthesis," *Hum. Brain Mapp.*, vol. 2, no. 1–2, pp. 56–78, Jan. 1994.

[95] E. Bullmore and O. Sporns, "Complex brain networks: graph theoretical analysis of structural and functional systems," *Nat. Rev. Neurosci.*, vol. 10, no. 3, pp. 186–198, Mar. 2009.

[96] V. Sakkalis, "Review of advanced techniques for the estimation of brain connectivity measured with EEG/MEG," *Comput. Biol. Med.*, vol. 41, no. 12, pp. 1110–1117, Dec. 2011.

[97] G. Deshpande, S. LaConte, G. A. James, S. Peltier, and X. Hu, "Multivariate Granger causality analysis of fMRI data," *Hum. Brain Mapp.*, vol. 30, no. 4, pp. 1361–1373, 2009.

[98] S. Micheloyannis, E. Pachou, C. J. Stam, M. Breakspear, P. Bitsios, M. Vourkas, S. Erimaki, and M. Zervakis, "Small-world networks and disturbed functional connectivity in schizophrenia," *Schizophr. Res.*, vol. 87, no. 1–3, pp. 60–66, Oct. 2006.

[99] V. Sakkalis, T. Oikonomou, E. Pachou, I. Tollis, S. Micheloyannis, and M. Zervakis, "Time-significant Wavelet Coherence for the Evaluation of Schizophrenic Brain Activity using a Graph theory approach," in *28th Annual International Conference of the IEEE Engineering in Medicine and Biology Society, 2006. EMBS '06*, 2006, pp. 4265 –4268.

[100] C. J. Stam, G. Nolte, and A. Daffertshofer, “Phase lag index: Assessment of functional connectivity from multi channel EEG and MEG with diminished bias from common sources,” *Hum. Brain Mapp.*, vol. 28, no. 11, pp. 1178–1193, 2007.

[101] W. R. Adey, D. O. Walter, and C. Hendrix, “Computer techniques in correlation and spectral analyses of cerebral slow waves during discriminative behavior,” *Exp. Neurol.*, vol. 3, no. 6, pp. 501–524, 1961.

[102] M. Ding, S. L. Bressler, W. Yang, and H. Liang, “Short-window spectral analysis of cortical event-related potentials by adaptive multivariate autoregressive modeling: data preprocessing, model validation, and variability assessment,” *Biol. Cybern.*, vol. 83, no. 1, pp. 35–45, 2000.

[103] E. Pereda, R. Q. Quiroga, and J. Bhattacharya, “Nonlinear multivariate analysis of neurophysiological signals,” *Prog. Neurobiol.*, vol. 77, no. 1–2, pp. 1 – 37, 2005.

[104] J. Arnhold, P. Grassberger, K. Lehnertz, and C. E. Elger, “A robust method for detecting interdependences: application to intracranially recorded {EEG},” *Phys. Nonlinear Phenom.*, vol. 134, no. 4, pp. 419 – 430, 1999.

[105] B. B. Biswal, J. V. Kylen, and J. S. Hyde, “Simultaneous assessment of flow and BOLD signals in resting-state functional connectivity maps,” *NMR Biomed.*, vol. 10, no. 4–5, pp. 165–170, 1997.

[106] D. Cordes, V. M. Haughton, K. Arfanakis, J. D. Carew, P. A. Turski, C. H. Moritz, M. A. Quigley, and M. E. Meyerand, “Frequencies Contributing to Functional Connectivity in the Cerebral Cortex in ‘Resting-state’ Data,” *Am. J. Neuroradiol.*, vol. 22, no. 7, pp. 1326–1333, Aug. 2001.

[107] V. G. van de Ven, E. Formisano, D. Prvulovic, C. H. Roeder, and D. E. J. Linden, “Functional connectivity as revealed by spatial independent component analysis of fMRI measurements during rest,” *Hum. Brain Mapp.*, vol. 22, no. 3, pp. 165–178, 2004.

[108] M. J. Jafri, G. D. Pearlson, M. Stevens, and V. D. Calhoun, “A Method for Functional Network Connectivity Among Spatially Independent Resting-State Components in Schizophrenia,” *NeuroImage*, vol. 39, no. 4, pp. 1666–1681, Feb. 2008.

[109] K. J. Friston, L. Harrison, and W. Penny, “Dynamic causal modelling,” *NeuroImage*, vol. 19, no. 4, pp. 1273–1302, Aug. 2003.

[110] C. W. J. Granger, “Investigating Causal Relations by Econometric Models and Cross-Spectral Methods,” *Econometrica*, vol. 37, no. 3, pp. 424–438, 1969.

[111] O. David, S. J. Kiebel, L. M. Harrison, J. Mattout, J. M. Kilner, and K. J. Friston, "Dynamic causal modeling of evoked responses in EEG and MEG," *NeuroImage*, vol. 30, no. 4, pp. 1255–1272, May 2006.

[112] M. Kaminski and K. Blinowska, "A new method of the description of the information flow in the brain structures," *Biol. Cybern.*, vol. 65, no. 3, pp. 203–210, 1991.

[113] K. Sameshima and L. A. Baccalá, "Using partial directed coherence to describe neuronal ensemble interactions," *J. Neurosci. Methods*, vol. 94, no. 1, pp. 93–103, 1999.

[114] G. Lohmann, K. Erfurth, K. Müller, and R. Turner, "Critical comments on dynamic causal modelling," *NeuroImage*, vol. 59, no. 3, pp. 2322–2329, Feb. 2012.

[115] R. Goebel, A. Roebroeck, D.-S. Kim, and E. Formisano, "Investigating directed cortical interactions in time-resolved fMRI data using vector autoregressive modeling and Granger causality mapping," *Magn. Reson. Imaging*, vol. 21, no. 10, pp. 1251–1261, Dec. 2003.

[116] A. Roebroeck, E. Formisano, R. Goebel, and others, "Mapping directed influence over the brain using Granger causality and fMRI," *Neuroimage*, vol. 25, no. 1, pp. 230–242, 2005.

[117] O. Demirci, M. C. Stevens, N. C. Andreasen, A. Michael, J. Liu, T. White, G. D. Pearlson, V. P. Clark, and V. D. Calhoun, "Investigation of relationships between fMRI brain networks in the spectral domain using ICA and Granger causality reveals distinct differences between schizophrenia patients and healthy controls," *NeuroImage*, vol. 46, no. 2, pp. 419–431, Jun. 2009.

[118] X. Lei, D. Ostwald, J. Hu, C. Qiu, C. Porcaro, A. P. Bagshaw, and D. Yao, "Multimodal Functional Network Connectivity: An EEG-fMRI Fusion in Network Space," *PLoS ONE*, vol. 6, no. 9, p. e24642, 2011.

[119] L. Dipietro, M. Plank, H. Poizner, and H. I. Krebs, "EEG microstate analysis in human motor corrections," in *2012 4th IEEE RAS EMBS International Conference on Biomedical Robotics and Biomechatronics (BioRob)*, 2012, pp. 1727–1732.

[120] B. W. Jervis, S. Belal, T. Cassar, M. Besleaga, C. Bigan, K. Michalopoulos, M. Zervakis, K. Camilleri, and S. Fabri, "Waveform Analysis of Non-Oscillatory Independent Components in Single-Trial Auditory Event-Related Activity in Healthy Subjects and Alzheimer's Disease Patients," *Curr. Alzheimer Res.*, vol. 7, no. 4, p. 14, 2010.

[121] S. Makeig, M. Westerfield, T.-P. Jung, S. Enghoff, J. Townsend, E. Courchesne, and T. J. Sejnowski, "Dynamic Brain Sources of Visual Evoked Responses," *Science*, vol. 295, no. 5555, pp. 690–694, Jan. 2002.

[122] M. Zervakis, K. Michalopoulos, V. Iordanidou, and V. Sakkalis, “Intertrial coherence and causal interaction among independent EEG components,” *J. Neurosci. Methods*, vol. 197, no. 2, pp. 302–314, Apr. 2011.

[123] R. Palaniappan, P. Raveendran, and S. Omatu, “VEP optimal channel selection using genetic algorithm for neural network classification of alcoholics,” *Neural Netw. IEEE Trans. On*, vol. 13, no. 2, pp. 486–491, 2002.

[124] D. Lehmann, H. Ozaki, and I. Pal, “EEG alpha map series: brain micro-states by space-oriented adaptive segmentation,” *Electroencephalogr. Clin. Neurophysiol.*, vol. 67, no. 3, pp. 271–288, Sep. 1987.

[125] J. Wackermann, D. Lehmann, C. M. Michel, and W. K. Strik, “Adaptive segmentation of spontaneous EEG map series into spatially defined microstates,” *Int. J. Psychophysiol.*, vol. 14, no. 3, pp. 269–283, May 1993.

[126] C. M. Michel and M. M. Murray, “Towards the utilization of EEG as a brain imaging tool,” *NeuroImage*, vol. 61, no. 2, pp. 371–385, Jun. 2012.

[127] R. D. Pascual-Marqui, C. M. Michel, and D. Lehmann, “Segmentation of brain electrical activity into microstates: model estimation and validation,” *IEEE Trans. Biomed. Eng.*, vol. 42, no. 7, pp. 658–665, 1995.

[128] G. Pourtois, S. Delplanque, C. Michel, and P. Vuilleumier, “Beyond Conventional Event-related Brain Potential (ERP): Exploring the Time-course of Visual Emotion Processing Using Topographic and Principal Component Analyses,” *Brain Topogr.*, vol. 20, no. 4, pp. 265–277, Jun. 2008.

[129] T. Koenig, M. Kottlow, M. Stein, and L. Melie-García, “Ragu: A free tool for the analysis of EEG and MEG event-related scalp field data using global randomization statistics,” *Comput. Intell. Neurosci.*, vol. 2011, p. 4, 2011.

[130] D. Brunet, M. M. Murray, and C. M. Michel, “Spatiotemporal analysis of multichannel EEG: CARTOOL,” *Intell Neurosci.*, vol. 2011, pp. 2:1–2:15, Jan. 2011.

[131] X. Tian, D. Poeppel, and D. E. Huber, “TopoToolbox: using sensor topography to calculate psychologically meaningful measures from event-related EEG/MEG,” *Intell Neurosci.*, vol. 2011, pp. 7:1–7:8, Jan. 2011.

[132] J. Britz, D. Van De Ville, and C. M. Michel, “BOLD correlates of EEG topography reveal rapid resting-state network dynamics,” *NeuroImage*, vol. 52, no. 4, pp. 1162–1170, Oct. 2010.

[133] V. Brodbeck, A. Kuhn, F. von Wegner, A. Morzelewski, E. Tagliazucchi, S. Borisov, C. M. Michel, and H. Laufs, “EEG microstates of wakefulness and NREM sleep,” *NeuroImage*, vol. 62, no. 3, pp. 2129–2139, Sep. 2012.

[134] T. Koenig, D. Lehmann, M. C. Merlo, K. Kochi, D. Hell, and M. Koukkou, “A deviant EEG brain microstate in acute, neuroleptic-naive schizophrenics at rest,” *Eur. Arch. Psychiatry Clin. Neurosci.*, vol. 249, no. 4, pp. 205–211, 1999.

[135] D. Lehmann, P. L. Faber, S. Galderisi, W. M. Herrmann, T. Kinoshita, M. Koukkou, A. Mucci, R. D. Pascual-Marqui, N. Saito, J. Wackermann, G. Winterer, and T. Koenig, “EEG microstate duration and syntax in acute, medication-naïve, first-episode schizophrenia: a multi-center study,” *Psychiatry Res. Neuroimaging*, vol. 138, no. 2, pp. 141–156, Feb. 2005.

[136] J. Kindler, D. Hubl, W. K. Strik, T. Dierks, and T. Koenig, “Resting-state EEG in schizophrenia: Auditory verbal hallucinations are related to shortening of specific microstates,” *Clin. Neurophysiol.*, vol. 122, no. 6, pp. 1179–1182, Jun. 2011.

[137] N. Ahuja, “Dot pattern processing using Voronoi neighborhoods,” *Pattern Anal. Mach. Intell. IEEE Trans. On*, no. 3, pp. 336–343, 1982.

[138] N. Ahuja, B. An, and B. Schachter, “Image representation using Voronoi tessellation,” *Comput. Vis. Graph. Image Process.*, vol. 29, no. 3, pp. 286–295, 1985.

[139] J. Shi and J. Malik, “Normalized cuts and image segmentation,” *Pattern Anal. Mach. Intell. IEEE Trans. On*, vol. 22, no. 8, pp. 888–905, 2000.

[140] N. Bourbakis, P. Yuan, and P. Kakumanu, “A graph based object description and recognition methodology,” *Int. J. Artif. Intell. Tools*, vol. 17, no. 06, pp. 1161–1194, 2008.

[141] J.-D. Boissonnat and F. Cazals, “Smooth surface reconstruction via natural neighbour interpolation of distance functions,” presented at the Proceedings of the sixteenth annual symposium on Computational geometry, 2000, pp. 223–232.

[142] F. Meyer, “Topographic distance and watershed lines,” *Signal Process*, vol. 38, no. 1, pp. 113–125, Jul. 1994.

[143] N. G. Bourbakis, “Emulating human visual perception for measuring difference in images using an SPN graph approach,” *IEEE Trans. Syst. Man Cybern. Part B Cybern.*, vol. 32, no. 2, pp. 191 –201, Apr. 2002.

[144] A. C. K. Soong, J. C. Lind, G. R. Shaw, and Z. J. Koles, “Systematic comparisons of interpolation techniques in topographic brain mapping,” *Electroencephalogr. Clin. Neurophysiol.*, vol. 87, no. 4, pp. 185–195, Oct. 1993.

[145] A. Delorme and S. Makeig, “EEGLAB: an open source toolbox for analysis of single-trial EEG dynamics including independent component analysis,” *J. Neurosci. Methods*, vol. 134, no. 1, pp. 9–21, 2004.

[146] S. Beucher, “Watershed, hierarchical segmentation and waterfall algorithm,” in *Mathematical morphology and its applications to image processing*, Springer, 1994, pp. 69–76.

[147] L. Vincent and P. Soille, “Watersheds in digital spaces: an efficient algorithm based on immersion simulations,” *IEEE Trans. Pattern Anal. Mach. Intell.*, vol. 13, no. 6, pp. 583–598, 1991.

[148] T. P. Jung, S. Makeig, M. J. McKeown, A. J. Bell, T. W. Lee, and T. J. Sejnowski, “Imaging brain dynamics using independent component analysis,” *Proc. IEEE*, vol. 89, no. 7, pp. 1107–1122, 2001.

[149] J. Barrie, B. Suliman, C. Kenneth, C. Tracey, B. Cristin, E. J. L. David, M. Kostas, Z. Michalis, B. Mircea, F. Simon, and M. Joseph, “The independent components of auditory P300 and CNV evoked potentials derived from single-trial recordings,” *Physiol. Meas.*, vol. 28, no. 8, p. 745, 2007.

[150] I. Kondakor, D. Lehmann, C. M. Michel, D. Brandeis, K. Kochi, and T. Koenig, “Prestimulus EEG microstates influence visual event-related potential microstates in field maps with 47 channels,” *J. Neural Transm.*, vol. 104, no. 2–3, pp. 161–173, Feb. 1997.

[151] M. De Lucia, C. M. Michel, S. Clarke, and M. M. Murray, “Single-trial topographic analysis of human EEG: A new `image’ of event-related potentials,” in *6th International Special Topic Conference on Information Technology Applications in Biomedicine, 2007. ITAB 2007*, 2007, pp. 95–98.

[152] M. D. Lucia, C. M. Michel, and M. M. Murray, “Comparing ICA-based and Single-Trial Topographic ERP Analyses,” *Brain Topogr.*, vol. 23, no. 2, pp. 119–127, Jun. 2010.

[153] K. Nishida, Y. Morishima, M. Yoshimura, T. Isotani, S. Irisawa, K. Jann, T. Dierks, W. Strik, T. Kinoshita, and T. Koenig, “EEG microstates associated with salience and frontoparietal networks in frontotemporal dementia, schizophrenia and Alzheimer’s disease,” *Clin. Neurophysiol.*, vol. 124, no. 6, pp. 1106–1114, Jun. 2013.

[154] J. Britz and C. M. Michel, “State-Dependent Visual Processing,” *Front. Psychol.*, vol. 2, Dec. 2011.

[155] L. R. Rabiner, “A tutorial on hidden Markov models and selected applications in speech recognition,” *Proc. IEEE*, vol. 77, no. 2, pp. 257–286, 1989.

[156] A. Sundaresan, A. RoyChowdhury, and R. Chellappa, “A hidden markov model based framework for recognition of humans from gait sequences,” in *Image Processing, 2003. ICIP 2003. Proceedings. 2003 International Conference on*, 2003, vol. 2, pp. II–93.

[157] A. Schliep, A. Schönhuth, and C. Steinhoff, “Using hidden Markov models to analyze gene expression time course data,” *Bioinformatics*, vol. 19, no. suppl 1, pp. i255–i263, 2003.

[158] F. Cincotti, A. Scipione, A. Timperi, D. Mattia, A. Marciani, J. Millan, S. Salinari, L. Bianchi, and F. Bablioni, “Comparison of different feature classifiers for brain computer interfaces,” in *Neural Engineering, 2003. Conference Proceedings. First International IEEE EMBS Conference on*, 2003, pp. 645–647.

[159] M. De Lucia, I. Constantinescu, V. Sterpenich, G. Pourtois, M. Seeck, and S. Schwartz, “Decoding Sequence Learning from Single-Trial Intracranial EEG in Humans,” *PLoS ONE*, vol. 6, no. 12, p. e28630, Dec. 2011.

[160] W. H. Equitz, “A new vector quantization clustering algorithm,” *Acoust. Speech Signal Process. IEEE Trans. On*, vol. 37, no. 10, pp. 1568–1575, 1989.

[161] M.-P. Deiber, V. Ibañez, P. Missonnier, F. Herrmann, L. Fazio-Costa, G. Gold, and P. Giannakopoulos, “Abnormal-induced theta activity supports early directed-attention network deficits in progressive MCI,” *Neurobiol. Aging*, vol. 30, no. 9, pp. 1444–1452, 2009.

[162] K. Michalopoulos, M. Zervakis, N. Bourbakis, P. Giannakopoulos, and M.-P. Deiber, “Decomposition and evaluation of activity in multiple event-related trials,” in *2012 IEEE 12th International Conference on Bioinformatics Bioengineering (BIBE)*, 2012, pp. 374–379.

[163] M.-P. Deiber, P. Missonnier, O. Bertrand, G. Gold, L. Fazio-Costa, V. Ibañez, and P. Giannakopoulos, “Distinction between Perceptual and Attentional Processing in Working Memory Tasks: A Study of Phase-locked and Induced Oscillatory Brain Dynamics,” *J. Cogn. Neurosci.*, vol. 19, no. 1, pp. 158–172, Jan. 2007.

[164] K. Michalopoulos, M. Zervakis, and N. Bourbakis, “Current Trends in ERP Analysis Using EEG and EEG/fMRI Synergistic Methods,” Humana Press, 2013, pp. 1–28.

[165] T. Eichele, V. D. Calhoun, M. Moosmann, K. Specht, M. L. A. Jongsma, R. Q. Quiroga, H. Nordby, and K. Hugdahl, “Unmixing concurrent EEG-fMRI with parallel independent component analysis,” *Int. J. Psychophysiol.*, vol. 67, no. 3, pp. 222–234, Mar. 2008.

[166] B. He and Z. Liu, “Multimodal Functional Neuroimaging: Integrating Functional MRI and EEG/MEG,” *IEEE Rev. Biomed. Eng.*, vol. 1, no. 2008, pp. 23–40, Nov. 2008.

[167] C. Grova, J. Daunizeau, E. Kobayashi, A. P. Bagshaw, J.-M. Lina, F. Dubeau, and J. Gotman, "Concordance between distributed EEG source localization and simultaneous EEG-fMRI studies of epileptic spikes," *NeuroImage*, vol. 39, no. 2, pp. 755–774, Jan. 2008.

[168] F. Babiloni, F. De Vico Fallani, and F. Cincotti, "Multimodal Integration of EEG, MEG, and Functional MRI in the Study Of Human Brain Activity," in *Advanced Methods of Biomedical Signal Processing*, S. Cerutti and Carlorchesi, Eds. John Wiley & Sons, Inc., 2011, pp. 153–167.

[169] A. Tzovara, M. M. Murray, G. Plomp, M. H. Herzog, C. M. Michel, and M. De Lucia, "Decoding stimulus-related information from single-trial EEG responses based on voltage topographies," *Pattern Recognit.*, vol. 45, no. 6, pp. 2109–2122, Jun. 2012.

[170] K. Michalopoulos and N. Bourbakis, "Microstate analysis of the EEG using local global graphs," in *Bioinformatics and Bioengineering (BIBE), 2013 IEEE 13th International Conference on*, 2013, pp. 1–5.

[171] K. Michalopoulos, V. Sakkalis, V. Iordanidou, and M. Zervakis, "Activity detection and causal interaction analysis among independent EEG components from memory related tasks," in *Engineering in Medicine and Biology Society, 2009. EMBC 2009. Annual International Conference of the IEEE*, 2009, pp. 2070 –2073.

[172] T. Jaakkola, M. Diekhans, and D. Haussler, "A Discriminative Framework for Detecting Remote Protein Homologies," *J. Comput. Biol.*, vol. 7, no. 1–2, pp. 95–114, Feb. 2000.

[173] A. Velivelli, T. Huang, and A. Hauptmann, "Video shot retrieval using a kernel derived from a continuous HMM," *Proc SPIE*, p. 607311, Jan. 2006.

[174] R. A. Johnson and D. W. Wichern, *Applied multivariate statistical analysis*. Prentice Hall, 1992.

[175] A. Krishnan, L. J. Williams, A. R. McIntosh, and H. Abdi, "Partial Least Squares (PLS) methods for neuroimaging: A tutorial and review," *NeuroImage*, vol. 56, no. 2, pp. 455–475, May 2011.

[176] H. Su and G. Zheng, "A Partial Least Squares Regression-Based Fusion Model for Predicting the Trend in Drowsiness," *IEEE Trans. Syst. Man Cybern. Part Syst. Hum.*, vol. 38, no. 5, pp. 1085–1092, Sep. 2008.

[177] J. A. Wegelin, "A Survey of Partial Least Squares (PLS) Methods, with Emphasis on the Two-Block Case," 2000.

[178] R. N. Henson, D. G. Wakeman, V. Litvak, and K. J. Friston, "A Parametric Empirical Bayesian Framework for the EEG/MEG Inverse Problem: Generative Models for Multi-Subject and Multi-Modal Integration," *Front. Hum. Neurosci.*, vol. 5, Aug. 2011.

[179] V. Litvak, J. Mattout, r&#233, mie, S. Kiebel, C. Phillips, R. Henson, J. Kilner, G. Barnes, R. Oostenveld, J. Daunizeau, G. Flandin, W. Penny, and K. Friston, "EEG and MEG Data Analysis in SPM8," *Comput. Intell. Neurosci.*, vol. 2011, Mar. 2011.

[180] J. Wirsich, C. Bénar, J.-P. Ranjeva, M. Descoins, E. Soulier, A. Le Troter, S. Confort-Gouny, C. Liégeois-Chauvel, and M. Guye, "Single-trial EEG-informed fMRI reveals spatial dependency of BOLD signal on early and late IC-ERP amplitudes during face recognition," *NeuroImage*, vol. 100, pp. 325–336, Oct. 2014.

[181] A. Cichocki, Y. Washizawa, T. Rutkowski, H. Bakardjian, A.-H. Phan, S. Choi, H. Lee, Q. Zhao, L. Zhang, and Y. Li, "Noninvasive BCIs: Multiway Signal-Processing Array Decompositions," *Computer*, vol. 41, no. 10, pp. 34–42, Oct. 2008.

[182] L. F. Nicolas-Alonso and J. Gomez-Gil, "Brain Computer Interfaces, a Review," *Sensors*, vol. 12, no. 2, pp. 1211–1279, Jan. 2012.

[183] F. Castanedo, "A Review of Data Fusion Techniques," *Sci. World J.*, vol. 2013, p. e704504, Oct. 2013.

[184] B. Jeon and D. . Landgrebe, "Decision fusion approach for multitemporal classification," *IEEE Trans. Geosci. Remote Sens.*, vol. 37, no. 3, pp. 1227–1233, May 1999.

[185] F. Moreno-Seco, J. M. Iñesta, P. J. P. de León, and L. Micó, "Comparison of Classifier Fusion Methods for Classification in Pattern Recognition Tasks," in *Structural, Syntactic, and Statistical Pattern Recognition*, D.-Y. Yeung, J. T. Kwok, A. Fred, F. Roli, and D. de Ridder, Eds. Springer Berlin Heidelberg, 2006, pp. 705–713.

[186] L. . Kuncheva, J. J. Rodriguez, C. O. Plumpton, D. E. J. Linden, and S. J. Johnston, "Random Subspace Ensembles for fMRI Classification," *IEEE Trans. Med. Imaging*, vol. 29, no. 2, pp. 531–542, Feb. 2010.

[187] F. Lotte, M. Congedo, A. Lécuyer, F. Lamarche, and B. Arnaldi, "A review of classification algorithms for EEG-based brain-computer interfaces," *J. Neural Eng.*, vol. 4, no. 2, pp. R1–R13, Jun. 2007.

[188] T. Koenig, M. Stein, M. Grieder, and M. Kottlow, "A Tutorial on Data-Driven Methods for Statistically Assessing ERP Topographies," *Brain Topogr.*, pp. 1–12.

[189] W. Klimesch, M. Doppelmayr, D. Röhm, D. Pöllhuber, and W. Stadler, "Simultaneous desynchronization and synchronization of different alpha responses in the human electroencephalograph: a neglected paradox?," *Neurosci. Lett.*, vol. 284, no. 1–2, pp. 97–100, 2000.

[190] K. P. Murphy, “Dynamic bayesian networks: representation, inference and learning,” University of California, 2002.

[191] C. Vogler and D. Metaxas, “Parallel hidden Markov models for American sign language recognition,” in *The Proceedings of the Seventh IEEE International Conference on Computer Vision, 1999*, 1999, vol. 1, pp. 116–122 vol.1.

[192] D. Zhang, D. Gatica-Perez, S. Bengio, and D. Roy, “Learning influence among interacting Markov chains,” in *NIPS*, 2005.

Konstantinos Michalopoulos Curriculum Vitae

Konstantinos Michalopoulos is a PhD candidate in the Computer Engineering department of Wright State University, Dayton, OH under the supervision of Professor Bourbakis. He holds a bachelor's and Master's degree in Electronics and Computer Engineering from Technical University of Crete, Greece. His research interests include analysis of and modeling of brain activities. He will start his professional career at the University of Rochester, School of Medicine this fall 2014.